UC Davis
UC Davis Electronic Theses and Dissertations

Title

The Implementation of Tissue Engineering, Gene Editing, Biomaterials Science, and Immunology for Tissue Regeneration

Permalink

https://escholarship.org/uc/item/1659409x

Author

Garrity, Carissa Rayann

Publication Date

2024

Peer reviewed|Thesis/dissertation

eScholarship.org Powered by the California Digital Library
University of California

The Implementation of Tissue Engineering, Gene Editing, Biomaterials Science, and Immunology for Tissue Regeneration

By

CARISSA GARRITY

DISSERTATION

Submitted in partial satisfaction of the requirements for the degree of

DOCTOR OF PHILOSOPHY

In

Integrative Pathobiology

In the

OFFICE OF GRADUATE STUDIES

of the

UNIVERSITY OF CALIFORNIA

DAVIS

Approved:

_____

Natalia Vapniarsky, Chair

_____

Jeroen Saeij

_____

Ala Moshiri

Committee in Charge

2024

Acknowledgements

This dissertation represents a remarkable and eye-opening journey filled with testing yet fulfilling science and life-based lessons. This journey was filled with lessons that challenged me professionally, scientifically, and personally. This journey, although, represents one of my greatest accomplishments and proudest moments. The completion of this mission would not be possible without the contribution from many individuals that deserve their own award in itself for their support, guidance, and patience along the way.

First and foremost, I would like to thank my mentor Dr. Natalia Vapniarsky-Arzi for her support, wisdom, compassion, and exceptionally strong patience as I developed professionally and personally. I admire her guidance and support throughout my entire journey, especially when I attempted to maneuver the rocky paths of professionalism. Thank you for being my biggest cheerleader, I would not be who I am today without you. Likewise, I would like to thank my appreciation to Dr. Jeroen Saeij, who contributed immensely to my growth in scientific communication and contributed towards the development of several projects.

The completion of the second chapter of this dissertation would not have been possible without Dr. Luis Diego Castillo Charpentier. Diego joined our lab to offer another pair of eyes to troubleshoot one of the biggest hurdles of my Ph.D. Diego not only assisted in overcoming our experimental hurdles, he contributed immensely to teaching me how to be a better scientist. Diego taught me the importance of being meticulous and concise with guidance and constructive criticism.

I would like to acknowledge the funding sources that made this work come through. These include the Cal Vet tuition waiver, graduate student support program (GSSP), Advancing Science in America Foundation,

and of course my mentor Dr. Natalia Vapniarsky. I would also like to thank Dr. Erin Kent for her help and support on all aspects of graduate studies and cheerful advice.

This work would not have been possible without the contribution to all the professionals who helped with data collection, late night cell passaging, figure construction, emotional support, and so much more. Specifically, thank you Dr. Alice Wong for your patience in the early days of my Ph.D when I was still learning the basics of holding a pipette. Thank you, Dr. Tanya Garcia, for sitting down and coaching me through material science and statistical questions that were by no means my field of expertise. Thank you, Justine Irvin, for the fun lab laughs and keeping things jolly around the holidays when we are too serious about work. Thank you, Heather McEligot, for contributing to the development of my second chapter and your patience while I navigated the final year of my graduate studies. Thank you, Nicole Gonzales, for contributing and writing one of the chapters of this dissertation. Also, thank you for the many laughs and late-night dances when lab work became too much. Nicole Cox thank you for allowing me to mentor you and serving as a role model to me by reminding me to keep my head up when science doesn't work.

The completion of my Ph.D. would not have been near as joyful or bearable without Enmian Chang and Iris Rivas. These two individuals stayed at lab late, got up early, held a smile when I asked the most grueling/tedious tasks, and wiped many tears of mine. I am humbled to say that without these two individuals, I would have taken much longer to finish. I am honored to call Iris and Enmian some of my closest friends. You both contributed towards my graduate career and my life more than you know.

Finally, I thank my family members: my mom, step-dad, dad, and boyfriend- Ryan for their unconditional love, support, and patience through my many successes and failures. Ryan, thank you for your unwavering support and love as I told you that I signed up for another 4 years of college after undergrad. Dad, without

your service and sacrifice in the navy, my entire undergraduate career and half of graduate school would not have been funded. I probably would have never attended graduate school without your contribution. Thank you for constructive criticism, support, inspiration, and contribution to my projects with your engineering mindset. My success thus far is because of you.

Table of Contents

Abstract vii

The Implementation of Tissue Engineering, Gene Editing, Biomaterials Science, and Immunology for Tissue Regeneration vii

Chapter 1

A Fresh Glimpse into Cartilage Immune Privilege 1
Abstract 1
Introduction 2
MHC as a Major Player in Transplantation 4
Immune Characteristics of Cartilage 9
Evidence Supporting Immune Privilege 9
Evidence Confronting Immune Privilege 12
Lessons from Other Immune-Privileged Tissues 16
Methods to Manipulate Immunity 18
Conclusions 21
References 22

Chapter 2

Tissue-Engineered Scaffold-Free Immuno-Universal Cartilage 30
Abstract 30
Introduction 31
Materials and Methods 33
Results 47
Discussion 55
References 60

Chapter 3

Exploration of Auricular Chondrocytes as a Cell Source for Cartilage Tissue Engineering for Temporomandibular Joint Disc Using a Porcine Model 62
Abstract 62
Introduction 63
Materials and Methods 66
Experiment 67
Results 72
Discussion 76
References 79

Chapter 4

Biomechanical Ageing of Cartilage in a Canine Model 82
Abstract 82

Introduction 83
Materials and Methods 86
Results 93
Discussion 100
References 106

Chapter 5

Tilapia Fish Skin Treatment of Third-Degree Skin Burns in Murine Model 114
Abstract 114
Introduction 115
Materials and Methods 117
Results 125
Discussion 142
References 149

Abstract

The Implementation of Tissue Engineering, Gene Editing, Biomaterials Science, and Immunology for Tissue Regeneration

By

Carissa Garrity

Tissue regeneration, once a dream or a fantasy, is now becoming a reality. Science has advanced so much that cells can be cryopreserved and expanded into millions under laboratory conditions. Cells can be manipulated to become something they were not before and can be coerced into forming actual tissues. The discovery of powerful growth factors and the ability to synthesize them, helps to achieve these goals. Our understanding of pathologic processes and aging also plays an essential role in our ability to regenerate tissues. Laboratory methods have advanced immensely, allowing more efficient and rapid progress in regenerative medicine. This thesis addresses the regenerative efforts of two types of tissues: cartilage and skin. These tissues have an essential function in our bodies, but their structure and biology are dramatically different. Yet the common denominator is that people can benefit greatly from learning more about the regeneration of these tissues.

Cartilage is a shock-absorbing tissue lining the ends of diarthrodial joints that aims to provide a frictionless surface for joint articulation. In disease, damage of articular cartilage is often accompanied by tissue thinning and an irreversible yet progressive degeneration. Cartilage's innately poor regenerative capacity and progressively increasing demand for its regeneration have resulted in astonishing developments and achievements in the field of tissue engineering (TE) and regenerative therapies. However, despite advancements in cartilage tissue engineering and current clinical transplantation practices, the ability to replace deficient or damaged cartilage remains limited. In response, researchers are urgently trying to develop novel and clinically applicable solutions for the treatment of cartilage degenerative disorders.

The translation of cartilage tissue engineering practices is hindered by the lack of suitable cell sources and implant integration with surrounding native tissue. The lack of implant integration is further heightened within the joint environment, where constant motion and loading generate tensile, compressive, and shear forces. The lack of native tissue-graft integration and long-term efficacious cartilage implantation suggest that further exploration is needed to see if immunology is playing a role in the lack of tissue integration. In addition, the quality of cartilage tissue generated varies greatly with different cell sources. Cartilage replacement therapies primarily utilize chondrocytes (cartilage cells) as their main cell source for generating cartilage tissue. Moreover, the chondrocytes can be sourced from multiple anatomical locations. The current harvesting procedure to extract chondrocytes for cartilage tissue engineering can be quite limited and invasive. Therefore, the exploration of different cell sources or chondrocyte harvesting locations would be beneficial for improving cartilage tissue engineering techniques.

Another indicator of cartilage tissue quality is the mechanical durability of the tissue to withstand daily forces. A current limitation of cartilage tissue engineering practices is the inability to generate tissues of sufficient biomimicry to that of native tissue. Previous attempts in our laboratory have shown that tissue engineered cartilage is inferior to native tissue in terms biochemical composition and mechanical durability. Our laboratory has explored several applications and interventions to improve the quality of tissue engineered cartilage. This discrepancy between native tissue and tissue engineered cartilage is also due to our lack of understanding of cartilage biomechanics and limiting testing modalities.

Tissue regeneration is not limited to cartilage tissue. The demand for skin regeneration primarily aims to repair wounds caused from burns, infections, or other reconstructive surgeries. However, skin regenerative therapies are limited in the availability of sufficient autograft tissue. In addition, facilitating internal regeneration is difficult due to deficient vascularity within the wound. With this approach, wound

closure may be delayed or improper healing. Improper healing could lead to scarring or deformity which could lead to mental adversities. Researchers may have found a speedy and miraculous therapy to facilitate wound closure and wound vascularization: fish skin bandages. The science of this therapy has yet to be explored in a comprehensive fashion until now.

Chapter 1 of this dissertation provides a concise review of cartilage immunology at the tissue and cellular level as it relates to immune privilege. It covers the current cartilage replacement therapies and how the lack of efficacy of each one could be explained by chondrocyte expression of the major histocompatibility complex. The chapter summarizes the current arguments and evidence supporting and refuting the immune privilege status of cartilage. The chapter also outlines the immunomodulatory mechanisms seen in other immune-privileged tissues and cancer. It concludes with a provision of how current methodologies to manipulate immune recognition could be beneficial to cartilage replacement therapies.

Chapter 2 presents a comprehensive study that accomplishes the following: 1) It explores the immunogenicity of chondrocytes. 2) It explores a novel strategy for evading immune detection of allogeneic chondrocytes through genetic editing. 3) It constructs genetically engineered immune-universal tissue-engineered cartilage constructs. 4) It evaluates the safety and efficacy of genetically engineered chondrocytes as a cell source for tissue-engineered cartilage implants.

Chapter 3 explores auricular chondrocytes as a cell source for cartilage tissue engineering. This chapter first outlines the current sources of cartilage tissue engineering and the disadvantages. It next uses previously published methods to construct cartilage tissue constructs from auricular chondrocytes. Upon completion, the tissue was evaluated mechanically and biochemically to determine its credibility as a sufficient as a cell source to construct durable cartilage tissue.

Chapter 4 explores the biomechanical properties of canine articular cartilage across age using an *in-situ* testing model. It provides extensive characterization of biochemical composition-mechanical function relationships of canine articular surfaces and presents a comparison of these values across different joints. Specifically, it reports the instantaneous modulus at 15% strain, thickness, collagen content, glycosaminoglycan content, cellularity, and histological changes across age. Also, this chapter provides an innovative, quantitative, and visual assessment of regional distribution of mechanical properties of cartilage using 3D mapping of each surface. This chapter suggests that additional unknown factors may play a role in influencing cartilage's mechanical properties.

Chapter 5 explored the feasibility of using fish skin bandages as a therapeutic option for third-degree burns. The study induces third-degree burns on mice and treats the burns with either tilapia-skin or hydrocolloid adhesive bandages. The study explored the therapeutic efficacy of fish-skin bandages vs hydrocolloid adhesive bandages at the histologic, hematologic, molecular, and gross level. This study may seem out of place with the other chapters. However, this chapter reflects on how to induce internal tissue regeneration using external therapeutics. By studying the healing mechanisms behind tilapia skin, perhaps these factors can be applied to cartilage and induce tissue regeneration *in vivo*.

In summary, this dissertation delineates the cumulative progression of studies providing robust techniques methodologies for tissue regeneration and durability following transplantation. This work provides a solid foundation for future assessment directed at full tissue replacement conditions. Furthermore, this platform can be optimized for regeneration of other tissue structures, such as skin.

Chapter 1

A Fresh Glimpse into Cartilage Immune Privilege

Carissa Garrity, Boaz Arzi, Brian Haus, Cassandra A. Lee, and Natalia Vapniarsky

Published in *Cartilage* October 2022

https://doi.org/10.1177/19476035221126349

Abstract

The increasing prevalence of degenerative cartilage disorders in young patients is a growing public concern worldwide. The poor innate regenerative capacity of cartilage has inspired the exploration and development of cartilage replacement treatments such as tissue-engineered cartilages and osteochondral implants as potential solutions to cartilage loss. the clinical application of tissue-engineered implants is hindered by the lack of long-term follow-up demonstrating efficacy, biocompatibility, and bio-integration. The historically reported immunological privilege of cartilage tissue was based on histological and morphological observations pointing out the lack of vascularity and the presence of a tight extracellular matrix. However, clinical studies in humans and animals do not unequivocally support the immune-privilege theory. More in-depth studies on cartilage immunology are needed to make clinical advances such as tissue engineering more applicable. this review analyzes the literature that supports and opposes the concept that cartilage is an immune-privileged tissue and provides insight into mechanisms conferring various degrees of immune privilege to other, more in-depth studied tissues such as testis, eyes, brain, and cancer.

Keywords: cartilage immunology, tissue engineering, MHC, allogenic, immunological rejection, t cell

Introduction

The high prevalence of degenerative articular cartilage disorders among young and adult patients is a public health concern worldwide. Cartilage loss due to trauma or wear leads to osteoarthritis (OA). Clinical symptoms of OA include pain, joint swelling, and restricted range of motion, causing functional disability and reduced quality of life [1]. In the United States alone, 1 in 25 working-age adults from 18 to 64 years are limited to arthritis [2]. Out of this population, almost half experience work limitations, equating to $164 billion in lost wages [2]. It is predicted that by 2040, doctor diagnosed arthritic conditions will equate to 78.4 million people [2]. Cartilage loss in pediatric patients is also increasing in frequency due to a significant rise in sports injuries and is of particular concern given the lifelong disability that subsequently occurs.

Cartilage's innately poor regenerative capacity [3,4] and progressively increasing demand for its regeneration have resulted in astonishing developments and achievements in the field of tissue engineering (TE) and regenerative therapies. However, despite advancements in cartilage TE and current clinical transplantation practices, the ability to replace deficient or damaged cartilage remains limited. Traditional methods such as fresh articular cartilage with bone (osteochondral) autografts and allografts are currently used as cartilage replacements in affected patients [5].

Cartilage autografts are derived from the same individual and are harvested from a non-weightbearing area of the joint. However, the quantity of available cartilage is limited, and autograft collection incurs additional morbidity. Allografts are tissues obtained from a donor of the same species. A common example of allogenic cartilage treatments is allogenic osteochondral implantation (OCI), also called osteochondral allograft transplantation (OAT). The benefits of allografts are in the relative availability of donor tissue and

the possibility of an off-the-shelf implant that can be introduced in a single surgery without inducing second site morbidity in the patient [6,7]. However, allografts present the risk of disease transmission and eliciting immune rejection [8-10]. For instance, despite the average 12-year success rate of osteochondral allografts, up to 25% of allografts are failing, and 36% of patients require additional or revision surgeries [11]. The lack of long-term durability and integration could be due to immunological destruction of the graft. Immunological rejection of a tissue graft is typically prevented by immunologic matching of donor and recipient before transplantation. Surprisingly, unlike solid organ allografts, immunologic matching, also known as major histocompatibility complex (MHC) matching, is not routinely performed with osteochondral allografts [12]. This is due to the historical concept that cartilage is an "immune privileged" tissue [13-15].

Immune privilege is best summarized as a tissue's specific ability to repress an immune response to implanted tissues or antigens [16], while immunogenicity is the ability to provoke the immune response [17]. Mechanisms governing immune privilege in tissues such as brain [18], eye [19], placenta [20], ovary [21], and testis [22] are continuously explored. However, studies addressing the immune status of cartilage are few, and there is a discrepancy between the evidence presented in the literature and how it is translated to clinical practice. For instance, contradicting the immune-privileged claim is the fact that only autologous but not allogenic chondrocytes are used in current cartilage replacement therapies [23-24]. In addition, reports comparing the outcomes of allogenic OCI in immunologically matched and mismatched human patients [8] and in dogs [10] provide evidence that questions the concept of cartilage's immune privilege. Specifically, in humans, the long-term outcomes of massive osteochondral implants were better when recipients and donors were immunologically matched [8]. In dogs, the inflammatory response was much more severe in joints that received an immunologically mismatched allograft [10]. Similarly, a histological study in rabbits comparing the host response to cartilage autografts, allografts, and xenografts

(tissue from another species) reported strong innate and adaptive immune responses to xenografts, mild responses to allografts, and no response to autografts, in osteochondral implants [13].

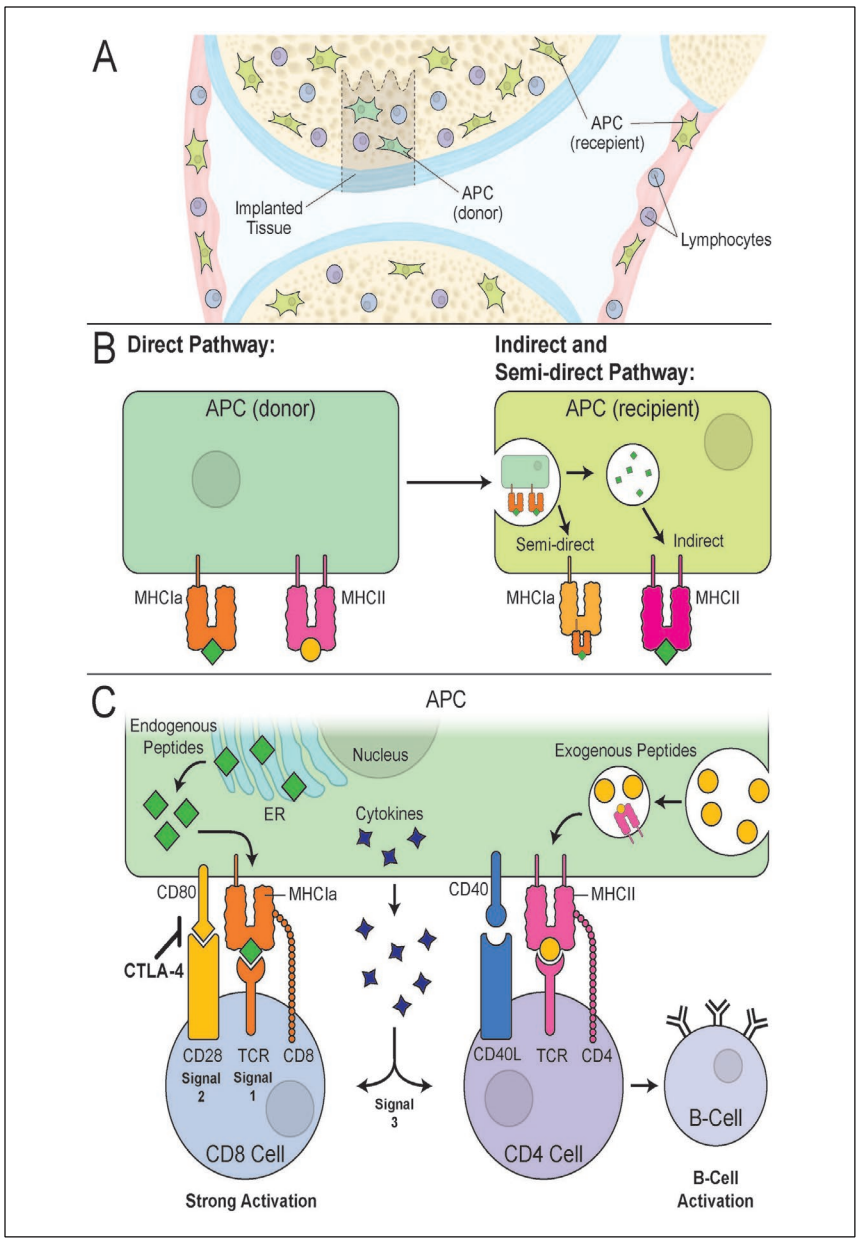
In contrast, there are numerous studies that provide strong evidence of immunosuppressive and potentially immune privileged properties of chondrocytes and engineered cartilage neotissue. For instance, several studies have demonstrated that chondrocytes are not only unable to stimulate immune responses, but they also suppress the proliferation of activated immune cells [14, 25,26]. It is possible that the application of engineered tissue replacements is hindered by our lack of understanding of cartilage immunology and immune privilege. Here, we critically review the literature supporting and confronting the notion that cartilage is an immune-privileged tissue and provide an insight into novel methods that can advance the field of cartilage regeneration.

MHC as a Major Player in Transplantation

The primary role of the MHC molecules is to assist in the maintenance of an organism's health by presenting foreign, self-, or altered self-peptides to immune cells (lymphocytes and, more specifically, T cells). The function of MHC molecules was first discovered in the context of transplantation in mice, hence, the name major histocompatibility complex [27]. However, the primary role of MHC molecules is immunological surveillance and marking of altered or infected cells for the adaptive immune system's elimination and mounting of the humoral and cellular immune response. The terminology for MHC equivalent in humans identifies the same molecules as (human leukocyte antigen) HLA; in swine as SLA; in a dog, DLA, in cat FLA, and so on for any other species. For this review, the MHC acronym will be used regardless of species. The immune response to nonself-MHC molecules and non-self-peptides presented by the MHC complexes are the primary causes of transplant rejection. For the benefit of understanding

the immune status of cartilage tissue, it is imperative first to review the classes and the function of MHC in more detail.

There are 2 classes of MHC molecules. MHC class I molecules fit into 2 categories: classical (MHC Ia) and nonclassical (MHC Ib) [28]. The MHC I molecules are expressed on all nucleated mammalian cells. The class II MHC is expressed by professional antigen-presenting cells (APCs), such as B cell, dendritic cells, and macrophages. As MHC I and MHC II play a critical role in the recognition and activation of immune cells by presenting self-, altered-self-, or non-self-peptides (alloantigens), these molecules are the main drivers of transplant rejection. Analogous to personal identification documents, they are located on the surface of the cells and present intracellular or extracellular components. Specifically, MHC II molecules present extracellular peptides taken up by phagocytosis, while MHC I molecules present intracellular peptides.[28] If the MHC presents foreign or inappropriate peptides, activation and clonal expansion of effector T cells will follow, leading to the destruction of the targeted cells/organs. The peptides MHC molecules present are recognized by T lymphocytes via direct, indirect, and semi-direct pathways (**Fig. 1A** and **B**). For T cells to be properly activated by MHC, 3 signals should be perceived in conjunction: (1) MHC-peptide complex binding the respective T-cell receptor and co-receptor (CD4 or CD8), (2) binding to co-stimulatory receptors (CD28 and CD80/B7 on lymphocytes and APCs, respectively), and (3) cytokine secretion [28] (**Fig. 1C**). Notably, the lack of MHC expression will be interpreted by natural killer (NK) cells as missing self, and cells with no MHC expression will be killed.



The non-classical MHC I molecules (MHC Ib) are far less studied and are thought to play a critical role in regulating immune activation [29]. Specifically, the non-classical MHC I mediate inhibitory or activating stimuli in NK cells (cells of the innate immune system that are capable of killing other cells without the need for specific antibodies) and cytotoxic T cells [30]. MHC Ib molecules function as a shield to ensure that the cells are not incorrectly lysed by immune cells [28]. Non-classical MHC molecules present the leader peptide (or signal peptide, that initiates the process of assembling all the components of MHC I) derived from classical MHC I molecules to lymphocytes [28]. These nonclassical MHC-peptide complexes bind to the inhibitory receptors, NKG2A, KIR2D, and LIR-1 on NK cells or CD8 T cells to prevent the cell lysis [28] (**Fig. 2A**). The expression of non-classical MHC molecules is thought to be associated with evasive immune mechanisms seen in tumors [31], placental trophoblasts [32,33], the eye [34], and testis [35].

Figure 1. MHC antigen presentation pathways in the context of osteochondral implants. (A) in a scenario of osteochondral allograft implantation, aPCs can be either donor or recipient derived. the donor aPC will reside in the implant's bone marrow cavity, while recipient aPC will be present in the synovium and in the recipient's bone marrow. (B) in the direct pathway of antigen presentation, donor aPC will present donor peptides/antigens on MHC class ia and MHC class ii complexes. in the semi-direct pathway, recipient aPC can fuse with donor cell or donor cell exosome membrane to present intact donor MHC ia complexes with associated donor peptides. in the indirect pathway, a recipient aPC presents digested donor peptides (green rectangles) on its MHC class ii complex. as a result, the recipient aPC can present digested donor peptides or whole donor MHC molecules, which will be subsequently recognized by lymphocytes. (C) Peptide presented by MHC class ia will be recognized by a recipient cytotoxic t cell (CD8, t cell) and result in strong activation of the lymphocyte. Peptides presented by MHC class ii complex will be recognized by t-helper lymphocytes (CD4, t cell). Besides MHC class ia or MHC class ii recognition, additional signals are necessary to activate CD4 t-helper cells or CD8 cytotoxic t cells. in addition to MHC class ia with presented endogenous peptide binding to the t-cell receptor (tCr) (Signal 1), there should be an additional binding of co-receptor CD8 with MHC complex and CD28 (t cell) binding with CD80/B7 (aPC) (Signal 2). Stimulation with appropriate cytokines secreted by the aPC will further aid in the activation of the CD8 t cell (Signal 3). to keep activation in balance, the cytotoxic t-lymphocyte-associated protein 4 (Ctla-4) expression by CD8 t cell will inhibit activation of this cell. a similar mode of 3-signal activation will be needed upon engagement of tCr on the CD4 t-helper cells with exogenous peptides presented by the MHC class ii complexes. Upon sufficient activation of CD4 t cells, B cells are activated by recognizing peptides bound to its B-cell receptor and presented by MHC ii from CD4 t cells. Once B cells are activated, they will generate antibodies against the peptide recognized by B-cell receptors. MHC = major histocompatibility complex; aPC = antigen-presenting cell.

When MHC I complexes present a non-self- or altered peptide, cytotoxic T cells recognize the mismatch and destroy the immuno-incompatible cell (**Fig. 2B**). Although cartilage is considered an immune-privileged tissue, it is unclear if cartilage MHC expression levels and functionality is different compared with other tissues. For example, it would be essential to understand if the immune privilege of cartilage is due to non-classical MHC I components. Based on our knowledge, it is currently unknown if chondrocytes express non-classical MHC molecules. Many aspects of cartilage immunology still need to be explored before the status of cartilage's immune privilege can be confirmed and fully understood. In the following sections of the review, we will discuss additional aspects of current knowledge of cartilage immunology.

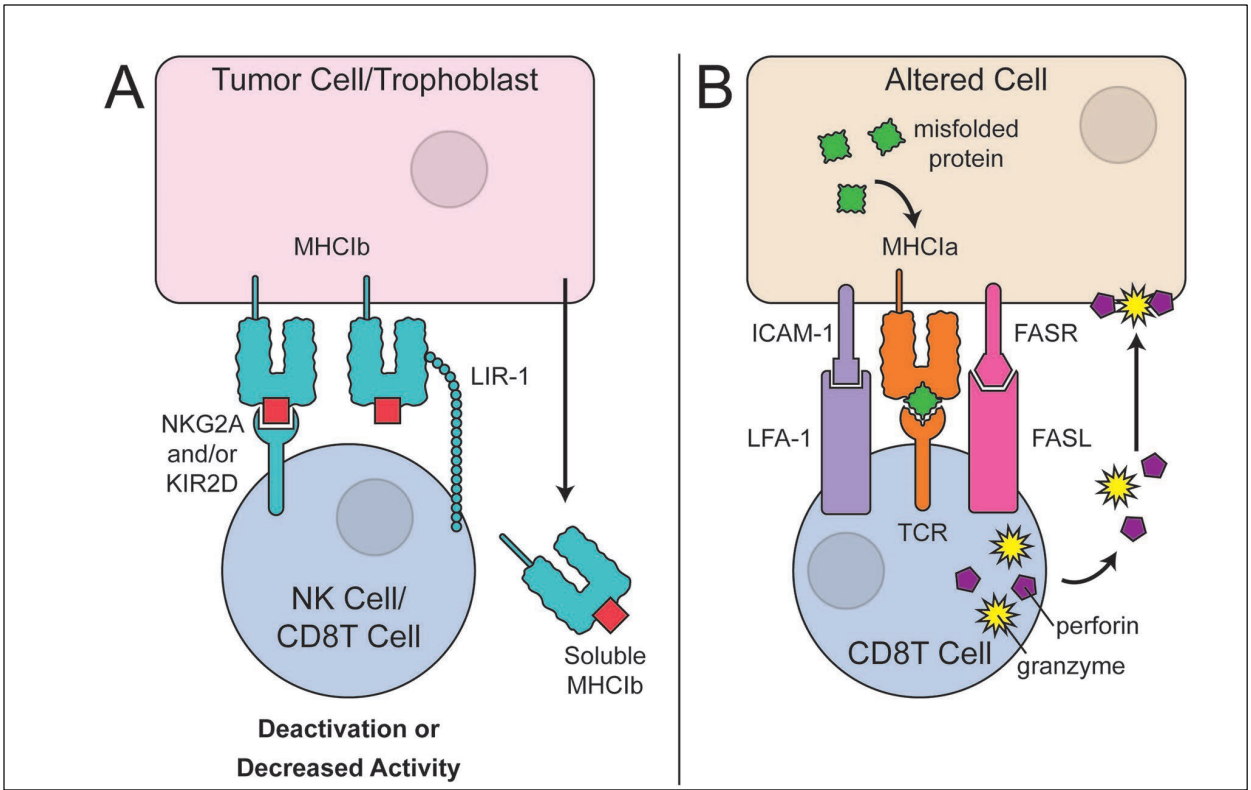


Figure 2. Non-classical MHC and altered-self recognition via classical MHC class i. (A) tumor cells and trophoblasts are known to express the non-classical, MHC class 1b molecules that lead to deactivation and decreased activity of CD8 t cells and NK cells. the binding of minor MHC class 1b complexes is via Kir2D, NKg2a, and lir-1 receptors. (B) in case of neoplastic transformation or other alteration of cells, the signal protein peptide for MHC i synthesis will be altered or mutated which will be readily recognized by CD8 t cells. the binding and subsequent activation of cytotoxic CD8 t cell will result in the release of granzyme and perforin enzymesmediated destruction of the altered cell. the binding of additional co-receptors such as Fas ligand (Fasl) with Fas receptor (Fasr) and lFa-1 with iCaM-1 on the CD8 t cell and the altered cell, respectively, will further activate the cytotoxic cell. MHC =m ajor histocompatibility complex; NK = natural killer.

MHC I matching prevents the recognition of donor MHC as an alloantigen (peptide derived from a different individual) and prevents rejection. MHC molecules are highly polymorphic and diverse across individuals. This diversity allows the host's immune system to recognize a broad range of pathogens (viruses and bacteria). Still, unfortunately, as a side effect, recognition of non-self-MHC results in the mounting of the immune response following transplantation. Determining the degree of similarity of MHC molecules (MHC

matching) between donor and recipient before transplantation helps to select individuals with similar MHC phenotypes [28]. It is done by comparing the blood type and evaluating anti-MHC antibodies in the recipient's serum [36]. However, even in MHC identical individuals, rejection can still be facilitated by MHC presentation of other alloantigens. Therefore, recipients may require lifelong immunosuppressive therapy to prevent immunological rejection of the transplant [28]. Consequently, it is not surprising to find down-regulation of MHC on tumors [37] or the trophoblast [38], tissues that typically avoid immune recognition and subsequent destruction.

Immune Characteristics of Cartilage

Evidence supporting Immune Privilege

Numerous studies have suggested that chondrocytes are immune evasive [14,25,26,39]. Adkisson *et al.* [14] showed that isolated chondrocytes inhibit T-cell proliferation *in vitro* through 3 main mechanisms: expression of CD80/B7 inhibitors, chondromodulin I, and secretion of indoleamine 2,3-dioxygenase (IDO). B7 inhibitors, such as PD-L1, directly bind to CD28/PD-1, hence preventing the co-stimulation needed for effector and naïve T-cell activation [28]. Chondromodulin-I is a glycoprotein that promotes chondrogenesis [40] and inhibits CD4 T-cell activation by downregulating the production of IL-2 [41]. IDO is an enzyme involved in tryptophan catabolism [42]. By depleting the extracellular environment from tryptophan, IDO prevents T effector cell proliferation and induces cellular arrest in these cells [43]. In addition, the metabolites of IDO are toxic to CD8 T cells and Th1 cells, while IDO itself is reported to promote T regulatory cell differentiation [43]. IDO has been found in immune-privileged tissues such as the testis [44] and has been shown to play a role in preventing allogenic rejection of fetuses during pregnancy [45]. However, IDO has also been detected in non-privileged tissues such as the spleen and skin in mice [46].

Due to IDO expression in both privileged and non-privileged tissue, it would be inaccurate to argue that the presence of IDO alone is sufficient to induce immune privilege (**Fig. 3A**).

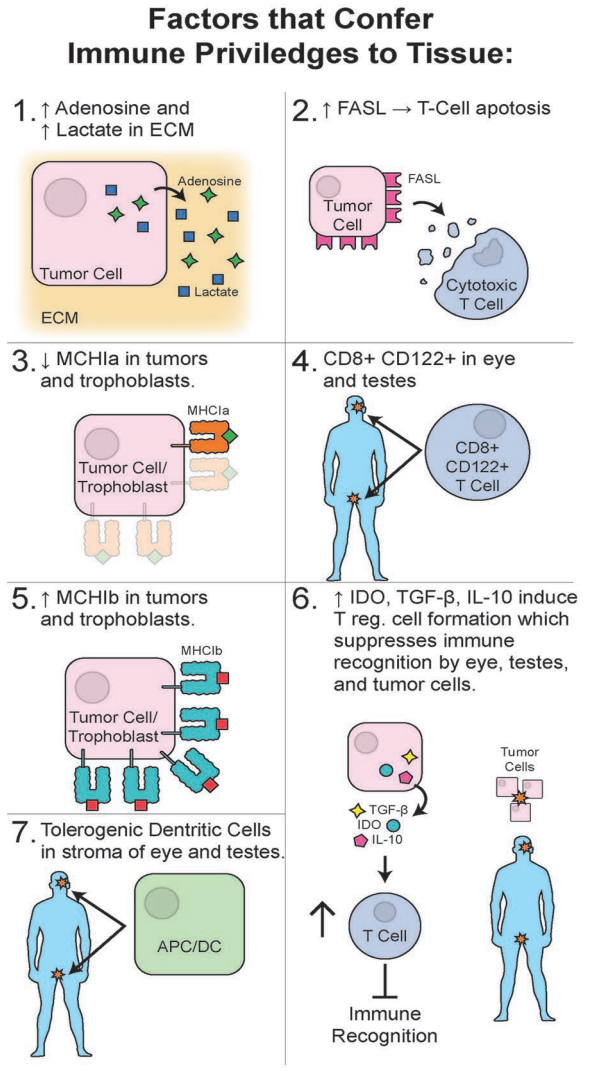


Figure 3. Concepts supporting and refuting cartilage's immune privilege. (A) the left side of the scheme presents factors supporting the privilege. eCM shielding is probably the most common argument. the presence of immunomodulatory molecules such as tgF-β in the eCM is another possibility. Some groups demonstrated expression of Fas ligand (Fasl), CD80/B7 inhibitors, such as PD-l1/l2, and secretion of iDO by chondrocytes. (B) the right side presents factors disputing the immune privilege of cartilage. Chondrocytes, just like any other somatic cells, express MHC class 1a molecules and may express MHC class ii upon inflammatory cytokines stimulation. aPC and lymphocytes are present in the synovium of all synovial joints and will be able to detect non-self-antigens. Histological examination of not-matched osteochondral allografts determined the presence of pannus tissue. Pannus formation is usually induced by antigenic stimulation in cases of rheumatoid arthritis or bacterial infections. eCM = extracellular matrix; MHC = major histocompatibility complex; aPC = antigen-presenting cell; iDO = indoleamine 2,3-dioxygenase.

An additional argument is that immune-evasive properties of chondrocytes are linked to their mesenchymal lineage [47-49]. Mesenchymal stromal cells (MSCs) are the progenitor cells to chondrocytes with well-documented immunomodulatory properties [50]. MSCs inhibit T-cell proliferation [50-52] through the expression of non-classical MHC molecules and the secretion of soluble mediators such as TGF-β, IL-10, and IDO [53-56]. Chondrocytes also secrete TGF-β and IDO. Despite the shared lineage

between chondrocytes and MSCs, terminal chondrogenic differentiation can alter chondrocytes' immune characteristics, making them more immunogenic [57]. For example, rat MSC-derived chondrocytes were shown to acquire the surface expression of CD80/B7 and CD86/CD28, which rendered them more immunogenic than the parent MSCs lacking expression of these molecules [57]. With that said, human articular chondrocytes have no expression of CD80 or CD86 at either protein or RNA levels [26]. Species differences could explain the latter. While direct contact between lymphocytes and chondrocytes is possible *in vitro*, in reality, chondrocytes *in situ* are surrounded by a dense network of extracellular matrix (ECM). Thus, the third postulate for chondrocyte immune privilege claims that ECM sequesters antigens and shields against immune detection [25,58,59].

The composition and density of ECM are essential for the function of the tissue but may also shield chondrocytes from direct contact with lymphocytes. A lymphocyte has an average diameter of 6 to 7 µm [60]. Wolf *et al.* [61] have shown that T cells can migrate through multicomponent synthetic lattices by amoeboid shape changes as long as the gap size remains below 1 to 2 µm. During transplant rejection of solid organs, lymphocytes must traverse the basement membrane (a type of ECM) [62]. The pore size of basement membrane is 0.75 to 3.85 µm [63], about half the diameter of a lymphocyte. The average pore size of cartilage ECM is 6 nm in diameter [64], a thousand times smaller than lymphocyte diameter. The latter suggests that the density of cartilage's ECM may protect allogenic chondrocytes from lymphocyte detection. It remains to be determined what happens in case of ECM degradation and if lymphocytes can "find" allogenic chondrocytes upon even the slightest ECM breakage.

It is possible that, in addition to the structural barrier, the ECM contributes to the immune privilege of cartilage by harboring non-cellular immune modulators. For example, active and latent forms of TGF-β1 were reported to be present in the ECM [65]. TGF-β is important in chondrogenesis [66], ECM synthesis

[67], and inducing tolerance through the induction of T regulatory cell differentiation [28]. High molecular weight hyaluronic acid, a major glycosaminoglycan of cartilage ECM, was reported to induce the expression of regulatory genes such as IL-10 in macrophages [68]. Therefore, it is reasonable to assume that ECM density, entrapped bioactive proteins, and structural components directly may contribute to immune privilege of cartilage tissue.

Recently, a significant contribution of $CD8^+$ T regulatory cells to the immune-evasive mechanisms of immune privileged tissues [69-72] was reported. $CD8^+$ T regulatory cells have been found in immune-privileged tissues such as the eye [73] and testis [74]. The $CD8^+CD122^+$ T regulatory cells are naturally occurring regulatory cells that inhibit the proinflammatory cytokine (IFN-gamma) by activated CD8 and CD4 T [75]. If $CD8^+$ T regulatory cells reside in the joint or in the cartilage tissue, it could explain the lack of immune responses seen following cartilage transplantation [76]. Further investigation is needed to determine if $CD8^+$ T regulatory cells are present in cartilage grafts or within other components of the synovial joint.

Evidence Confronting Immune Privilege

While the arguments presented in the previous section support cartilages' immune privilege, they are primarily based on *in vitro* or *ex vivo* experiments. It is unclear if these mechanisms translate to *in vivo* situations where the tissue integrity and joint environment are not controlled experimentally. A 12-year follow-up study of osteochondral transplants in 291 patients reported a 25% failure rate with a 36% rate of revision surgery [11]. This review did not discuss the reasons for the implant failure [11]. The authors do not specify if immunological matching was performed between the donors and recipients, but based on the general trend in the field, it is likely that it was not performed. As osteochondral plugs include cartilage, bone, and bone marrow, elements other than cartilage may compromise the successful

integration of osteochondral transplants. Indeed, it was established a long ago that fresh and frozen bone allografts are highly immunogenic [77]. The bone marrow elements were also proven immunogenic [78]. In support of the latter radiologic and histologic studies investigating the failed osteochondral allografts from the talus reported edema around the implants, progressive cyst formation, irregularities at the subchondral plate, fragmentation, subchondral collapse, and importantly abundance of rejection-associated lymphocytic subsets (**Fig. 3B**) [79].

It is currently recommended practice to pulse lavage the osteochondral allografts to physically remove the residual marrow cells to reduce the potential contribution of immunogenicity by the bone marrow [80,81]. However, a study by Ambra *et al.* [82] investigating pulse lavage in removing bone marrow elements showed little efficiency in this procedure. A report by Friedlaender *et al.* [8] compared the long-term outcomes of large OAT in MHC matched versus mismatched in 29 human patients. This study concluded that there is a benefit in MHC matching, particularly for class II MHC. [8] Specifically, patients who had failed or fair outcomes (some or significant pain, functional limitation, and need for braces) had more anti-MHC antibodies either before or following the transplantation. [8] A study by Hunt *et al.* [12] determined that the presence of anti-MHC class I antibodies in immunologically mismatched recipients of fresh osteochondral allografts was associated with poor graft survival compared with recipients with no such antibodies. Also, allograft size was associated with the outcome [12]. The larger osteochondral allografts were associated with a higher implant failure rate [12]. Cumulatively, it can be deducted from the studies above that the high degree of osteochondral implant failure can be due to immune incompatibility of bone and bone marrow components; correspondingly, immunologic matching may reduce the chance of osteochondral implant failure.

However, it remains unclear if cartilage tissue itself is immunologically inert or if it is too contributing to the immunologic process in failing implants. In addition to a tight ECM (discussed earlier), cartilage's lack of vascularity was proposed to contribute to its privileged immune status. Kandel *et al* [83]. study evaluating failed osteochondral implants from the knee reported pannus formation, fibrillation, degeneration, and erosion of the chondral portions of the grafts. According to the medical dictionary definition, a pannus is a sheet of inflammatory granulation tissue that spreads from the synovial membrane and invades the joint. The synovial membrane is a highly vascularized structure. It is an immunological guardian of the joint containing phagocytic cells capable of antigen presentation and chemical signaling to recruit additional leukocytes from the circulation [84]. A study in rats where chondrocytes suspended in hyaluronan were transplanted between rats of two separate strains found that lymphocyte infiltration was seen not at the articular surface but the deep margin of the implant. The authors suggested that allogenic chondrocytes may have specific surface antigens that may attract leukocytes and NK cells from the bone marrow [85]. Pannus formation was not reported in this study. Still, the lack of vascularity in the cartilage tissue did not protect it from the egress of leukocytes via other vascularized elements of the joint such as synovium or bone marrow. In concert, these observations suggest that cartilage's lack of vascularity is not a sufficient mechanism to protect it from immune cells of the other vascularized compartments of the joint and that cartilage is potentially also immunogenic.

Reports from additional animal studies further subvert cartilage's immune-privilege status. For example, we found no reports on cartilaginous or osteochondral allotransplantation in veterinary surgical clinical practice, despite abundant reports on successful allografting of cartilage under experimental preclinical settings [86,87]. A study in dogs found that the inflammatory response was the most severe in joints implanted with immunologically mismatched osteochondral allografts [10]. Also, pannus formation was typical in cases where fresh mismatched implants were introduced [10]. The same study also reported

that cryopreservation of the osteochondral implants enhanced the deleterious effects on the allografts [10]. Assuming cartilage is immunogenic, it would be essential to analyze what components may potentially contribute to the immunogenicity—cells or ECM.

Studies on the immune response toward decellularized natural biomaterial matrixes that are essentially comprised of ECM molecules indicate that structural molecules can be immunogenic [88]. Similarly, renal transplantation studies report antibodies to ECM components such as perlecan, fibronectin, and collagens in patients with chronic renal rejection [89,90]. More specific to cartilage tissue, it was shown by Klatt *et al.* [91] that nonfibrillar collagen type II enhanced gene expression of proinflammatory mediators and proteolytic enzymes in chondrocytes. Also, hyaluronic acid, a second major ECM component of cartilage, was shown to have differential signaling based on its molecular weight. Specifically, Rayahin *et al.* [68] demonstrated that contrary to high molecular weight hyaluronic acid that has immunomodulatory properties, low molecular weight hyaluronic acid induced proinflammatory genes in macrophages. The latter two studies suggest that cartilage is shielded from immune system surveillance if its matrix is intact. However, the immune system reacts when ECM components and chondrocytes are exposed to immune cell-bearing joint elements such as synovium or bone marrow.

Chondrocyte surface antigens, such as MHC molecules, could further contribute to the aggravation of the immune response. It is well known that chondrocytes constitutively express MHC I and, in some species, also MHC II molecules [25]. Studies by Hunt and Friedlaender (mentioned above) documented the presence of anti-MHC antibodies in patients with poor osteochondral transplantation outcomes [8,12]. However, it remains to be determined if these antibodies were developed in response to MHC molecular presentation by chondrocytes or other elements of the osteochondral implant. Furthermore, it remains to be determined if and how antibodies contribute to implant failure or negative outcomes. Indeed,

Williams *et al.* [92] describe a mechanism known as accommodation, where the transplant can remain uninjured despite the presence of anti-MHC antibodies directed against it. Several studies confirm this phenomenon may be true in renal [93] and heart [94] transplantation. Dehoux and Gianello [95] suggest that there may be a "delicate balance" between the production of neutralizing and non-neutralizing antibodies to prevent rejection while inducing accommodation. Identifying factors that would tip the balance in favor of accommodation would be an essential contribution to our understanding of cartilage immunology and the ability to engineer and direct outcomes of allotransplantation [96-98].

Lessons from Other Immune-Privileged Tissues

Two tissues commonly studied for their immune-privilege mechanisms are the testis [99] and the eye [100]. A recent review defined the immune privilege of the testis as a tissue capable of inducing a systemic tolerance of alloantigens, xenoantigens, and immunogenic autoantigens [99]. The Sertoli cell barrier and a specific macrophage phenotype in the interstitium contribute to the testis's immune privilege [99]. A specific phenotype of immunomodulatory interstitial testicular macrophages was identified in rats [101]. These macrophages differed from the circulating cells by their ability to constitutively produce and secrete anti-inflammatory cytokines [101,102]. It remains to be determined if similar macrophages are present in the cartilaginous joint.

The expression of transmembrane molecule Fas ligand (FasL) by ocular [100] and testicular [99] macrophages are additional factors that contribute to the immune privilege of these organs. The Fas receptor (FasR)-FasL interaction is a signal transduction pathway that regulates cell death [103]. The cell bearing the receptor is targeted for death, while the cell bearing the ligand induces death [103]. If a cell expresses the FasR, the cell is capable of being recognized and killed by immune cells. However, if the cell expresses FasL, it can induce apoptosis of immune cells and escape the destruction. While FasR presence

on chondrocytes is unequivocal, FasL expression is controversial and was undetectable in healthy and osteoarthritic human cartilage by the Hashimoto group [104], but was reported by Fujihara *et al.* [76] in human and murine auricular chondrocytes. Interestingly, a significant amount of soluble FasL was found in the synovial fluid of OA and rheumatoid arthritis patients [105]. It remains to be elucidated if the soluble FasL in the synovium contributes to immune-modulatory properties seen in cartilage tissue. Although, the self-perpetuating nature of OA [106] does not support this notion.

Extensive reports exist on cancer immuno-evasion [107,108]. Selected examples of strategies employed by cancer cells to avoid recognition of altered-self include down-regulation of MHC Ia [109], expression of FasL [110], and the presence of tolerogenic tumor-associated APC [111] in the tumor interstitium (**Fig. 4**). To the best of our knowledge, tolerance inducing phenotypes of APCs have not been detected in cartilage tissue or the synovium. Further research is needed to characterize leukocyte populations within synovium and their influence on articular cartilage immunology. In addition, there have been no experiments inducing the systemic tolerance to xenoantigens or alloantigens transplanted directly into cartilage or the joint. Therefore, more studies are necessary to determine if the cartilage is indeed an immune-privileged tissue and what factors contribute to this privilege. Perhaps evaluating cartilage immune privilege in the context of the entire joint considering it an organ, would be insightful.

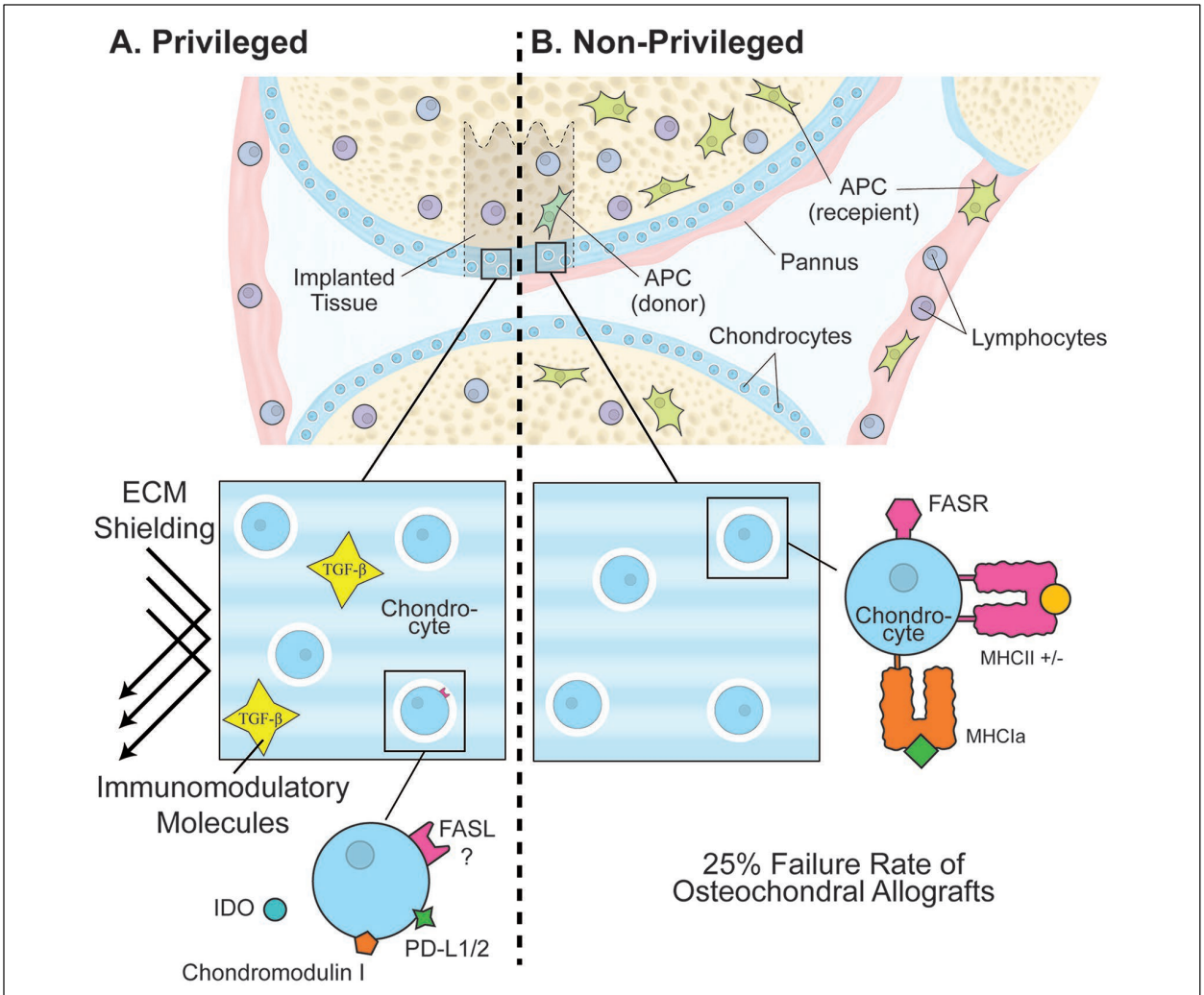


Figure 4. Selected factors known to confer an immune privilege to tissues are shown: (1) Secretion of an increased concentration of adenosine and lactate in the eCM of the tumors; (2) overexpression of Fasl by tumor cells was shown to induce apoptosis in cytotoxic t cells; (3) down-regulation of MHC class 1a was reported in regular and transmissible tumors as well as trophoblasts; (4) presence of stromal regulatory t cells CD8+CD122+ was reported in testis and the eye; (5) overexpression of minor, MHC 1b complexes was reported in trophoblasts and tumor cells; (6) secretion of iDO, tgF-β, and il-10 is a well-documented strategy to induce the t regulatory lymphocytes' formation to suppress the immune recognition by eye, testis, and neoplastic cells; (7) presence of tolerogenic dendritic cells in the stroma of the eye and testis was reported. eCM = extracellular matrix; MHC = major histocompatibility complex; iDO = indoleamine 2,3-dioxygenase.

Methods to Manipulate Immunity

In principle, even with MHC matching for organ transplantation, immunosuppression is still required to avoid rejection [112,113]. Regrettably, immunosuppression may lead to significant complications such as

increased susceptibility to opportunistic infections [114]. Thus, current research efforts are directed at the investigation of methods of masking recognizable antigens or manipulating genes responsible for immune recognition of non-self-antigens to offer a potential solution for manufacturing immunouniversal organs [115].

In this context, beta 2 microglobulin (B2M) gene was knocked out in mice resulting in a complete absence of MHC Ia surface molecule expression, making these animals a universal organ donor [116]. MHC-null pigs [117] and individual specific cell lines such as hematopoietic blood progenitors and endothelial cells [118] were developed using a similar strategy. Along these lines, immuno-engineered MHC-null embryonic stem cells [119] and induced pluripotent stem cells [120] were explored as promising cell sources for regenerative medicine, considering their unlimited proliferation capacity and the ability to differentiate into any functional tissue.

Although elimination of MHC expression renders cells invisible to lymphocyte recognition, NK cells can detect and destroy cells with “missing self.” [28] In addition, slight differences in minor histocompatibility molecules or tissue specific antigens may result in immune rejection [28]. This problem can be solved by the induction of expression of single-chain dimers of non-classical MHC I complex [121]. These single-chain fragments of MHC I proteins bind to inhibitory receptors such as CD94/NGK2A on NK cells and T cytotoxic T cells and prevent the cell from lysis. Indeed, this strategy was applied and proved effective in protecting induced pluripotent human stem cells genetically edited to express no MHC Ia but single-chain non-classical MHC Ib from lysis. This study utilized recombinant adeno-associated virus gene editing [121].

Genetic deletion of MHC I is not the only way to manipulate immunity. Mechanisms that disrupt cytokine gradients and cytokine receptors responsible for effector T cell trafficking can be considered. Expectedly,

nature mastered this approach in the maternal-fetal interface where Ccl5 and Cxcl9/10 genes are epigenetically silenced [122]. As a result of this epigenetic silencing, effector cells cannot reach the fetus, thus preventing its recognition as non-self and subsequent distraction. In the context of cartilage, CCR2 (cytokine receptor) agonist administration to osteoarthritic mice attenuated macrophage accumulation in the synovium, reduced synovitis, and cartilage damage [123]. This same study showed no benefit of blocking CCL5/CCLR5 axis in attenuating OA. These findings imply that T-cell trafficking signals may be specific to tissue types, and cytokine trafficking manipulation for immunomodulation purposes may need to be tailored to specific tissue types.

Inhibition of cytotoxic T-cell activity, induction of T regulatory cell phenotypes, and shift of macrophage and dendritic cells toward tolerogenic phenotypes are additional tactics that were shown success in immunomodulation. As shown in **Figure 1** of this review, CTLA-4 is an inhibitory receptor, also known as CD152, expressed by T regulatory cells or effector T cells after activation that binds to CD80 or CD86 receptors on APC to induce an inhibitory signal. Administration of CTLA-4 immunoglobulins or tetra dimers thereof was shown to be effective in modulating the immune response in patients and animal models of rheumatoid arthritis [124]. To overcome the challenges of delivery of such potent molecules to the implantation site, nanotechnology and nanoengineering have very clever methods to offer [125,126]. For instance, to prevent the rejection of xenogeneic pancreatic islets, encapsulating these islets into a nanobot capable of a sustained release of CTLA-4 peptide was shown to prolong pancreatic islet survival in the xenogeneic transplantation model [127]. CTLA4 bio patterned implant not only survived the transplantation and sustained normoglycemia in the experimental mice but also induced T regulatory differentiation at the implantation site [127].

Induction of T regulatory phenotypes at the implantation site can be a more precise and accurate way to induce tolerance if APCs are given the correct type of antigen to present to T cells and "educate" these cells to be tolerant toward this particular antigen. The antigen is known in instances like pancreatic islet transplantation or autoimmune destruction. Hence, using dual nanoformulation delivery, impressive work has been done on inducing antigen-specific tolerance and preventing autoimmune type I diabetes in mice [128]. Specifically, a delivery system comprised of 4 different nanoparticles was designed. Each particle was loaded with either tolerance-inducing factors (Vitamin D3 or TGF-β1) or dendritic cell colony-stimulating factor (GM-CSF), or insulin (antigen). These particles prevented the development of autoimmune destruction of pancreatic islets in experimental non-obese diabetic mice model, when administered as a cocktail [128]. These particles prevented the development of autoimmune destruction of pancreatic islets in experimental non-obese diabetic mice model, when administered as a cocktail [128]. In the context of cartilage, it is unknown if and which peptides may be immunogenic. Thus, more work needs to be done to identify these potentially antigenic molecules before immunoneutral cartilage tissue can be engineered.

Conclusions

The increasing prevalence of degenerative cartilage diseases is a growing public health concern worldwide. The transplantation of cartilage allografts is regarded as a safe solution due to the historical concept of cartilage being an immune-privileged tissue. However, several studies confront the concept of the immune-privilege status of cartilage by providing evidence of an immune response following allogenic cartilage transplantation. These contradictory findings highlight the need for studies that explore the immunology of cartilage.

The study of immune tissues is highly instructive in developing universal tissues suitable for transplantation. The immune evasion mechanisms discovered thus far have contributed toward engineering immunologically invisible cell lines. The efficacy of MHC engineering and CRISPR multiplexing in various cell lines suggests that this technology could be translated to cartilage tissue. The application of this technology to cartilage tissue could create universal cartilage allografts that could potentially promote the clinical application of tissue-engineered cartilage and help millions of patients.

Declaration of Conflicting Interests

The author(s) declared no potential conflicts of interest with respect to the research, authorship, and/or publication of this article.

References

1. Hunter DJ, McDougall JJ, Keefe FJ. The symptoms of osteoarthritis and the genesis of pain. Rheum Dis Clin North Am. 2008;34(3):623-43.
2. Center for Disease Control and Prevention. Arthritis-related statistics. 2018 Jul 18. Available from: https://www.cdc. gov/arthritis/data_statistics/arthritis-related-stats.htm.
3. Nam Y, Rim YA, Jung SM, Ju JH. Cord blood cell-derived iPSCs as a new candidate for chondrogenic differentiation and cartilage regeneration. Stem Cell Res Ther.2017;8(1):16.
4. Akkiraju H, Nohe A. Role of chondrocytes in cartilage formation, progression of osteoarthritis and cartilage regeneration. J Dev Biol. 2015;3(4):177-92.
5. Martín AR, Patel JM, Zlotnick HM, Carey JL, Mauck RL. Emerging therapies for cartilage regeneration in currently excluded “red knee” populations. NPJ Regen Med. 2019;4:12.
6. Cinque ME, Kennedy NI, Moatshe G, Vinagre G, Chahla J, Hussain ZB, et al. Osteochondral allograft transplants for large trochlear defects. Arthrosc Tech. 2017;6(5):e1703-7.
7. Arzi B, Clark KC, Sundaram A, Spriet M, Verstraete FJM, Walker NJ, et al. Therapeutic efficacy of fresh, allogeneic mesenchymal stem cells for severe refractory feline chronic gingivostomatitis. Stem Cells Transl Med. 2017;6(8):1710-22.
8. Friedlaender GE, Strong DM, Tomford WW, Mankin HJ. Long-term follow-up of patients with osteochondral allografts. A correlation between immunologic responses and clinical outcome. Orthop Clin North Am. 1999;30(4):583-8.
9. Oakeshott RD, Farine I, Pritzker KP, Langer F, Gross AE. A clinical and histologic analysis of failed fresh osteochondral allografts. Clin Orthop Relat Res. 1988;233:283-94.
10. Stevenson S, Dannucci GA, Sharkey NA, Pool RR. The fate of articular cartilage after transplantation of fresh and cryopreserved tissue-antigen-matched and mismatched osteochondral allografts in dogs. J Bone Joint Surg Am. 1989;71(9):1297-307.

11. Assenmacher AT, Pareek A, Reardon PJ, Macalena JA, Stuart MJ, Krych AJ. Long-term outcomes after osteochondral allograft: a systematic review at long-term follow-up of 12.3 years. Arthroscopy. 2016;32(10):2160-8.
12. Hunt HE, Sadr K, Deyoung AJ, Gortz S, Bugbee WD. The role of immunologic response in fresh osteochondral allografting of the knee. Am J Sports Med. 2014;42(4):886-91.
13. Arzi B, DuRaine GD, Lee CA, Huey DJ, Borjesson DL, Murphy BG, et al. Cartilage immunoprivilege depends on donor source and lesion location. Acta Biomater. 2015;23: 72-81.
14. Adkisson HD, Milliman C, Zhang X, Mauch K, Maziarz RT, Streeter PR. Immune evasion by neocartilage-derived chondrocytes: implications for biologic repair of joint articular cartilage. Stem Cell Res. 2010;4(1):57-68.
15. Elattar M, Dhollander A, Verdonk R, Almqvist KF, Verdonk P. Twenty-six years of meniscal allograft transplantation: is it still experimental? A meta-analysis of 44 trials. Knee Surg Sports Traumatol Arthrosc. 2011;19(2):147-57.
16. Forrester JV, Xu H, Lambe T, Cornall R. Immune privilege or privileged immunity? Mucosal Immunol. 2008;1(5): 372-81.
17. Mahanty S, Prigent A, Garraud O. Immunogenicity of infectious pathogens and vaccine antigens. BMC Immunol. 2015;16:31.
18. Wenkel H, Streilein JW, Young MJ. Systemic immune deviation in the brain that does not depend on the integrity of the blood-brain barrier. J Immunol. 2000;164(10):5125-31.
19. Taylor AW. Ocular immune privilege and transplantation. Front Immunol. 2016;7:37.
20. Kanellopoulos-Langevin C, Caucheteux SM, Verbeke P, Ojcius DM. Tolerance of the fetus by the maternal immune system: role of inflammatory mediators at the feto-maternal interface. Reprod Biol Endocrinol. 2003;1:121.
21. Minas V, Rolaki A, Kalantaridou SN, Sidiropoulos J, Mitrou S, Petsas G, et al. Intratumoral CRH modulates immunoescape of ovarian cancer cells through FasL regulation. Br J Cancer. 2007;97(5):637-45.
22. Fijak M, Meinhardt A. The testis in immune privilege. Immunol Rev. 2006;213:66-81.
23. Jacobi M, Villa V, Magnussen RA, Neyret P. MACI—a new era? Sports Med Arthrosc Rehabil Ther Technol. 2011;3(1):10.
24. Ossendorf C, Steinwachs MR, Kreuz PC, Osterhoff G, Lahm A, Ducommun PP, et al. Autologous chondrocyte implantation (ACI) for the treatment of large and complex cartilage lesions of the knee. Sports Med Arthrosc Rehabil Ther Technol. 2011;3:11.
25. Osiecka-Iwan A, Hyc A, Radomska-Lesniewska DM, Rymarczyk A, Skopinski P. Antigenic and immunogenic properties of chondrocytes. Implications for chondrocyte therapeutic transplantation and pathogenesis of inflammatory and degenerative joint diseases. Cent Eur J Immunol. 2018;43(2):209-19.
26. Pereira RC, Martinelli D, Cancedda R, Gentili C, Poggi A. Human articular chondrocytes regulate immune response by affecting directly T cell proliferation and indirectly inhibiting monocyte differentiation to professional antigen-presenting cells. Front Immunol. 2016;7:415.
27. Snell GD, Higgins GF. Alleles at the histocompatibility-2 locus in the mouse as determined by tumor transplantation. Genetics. 1951;36(3):306-10.
28. Murphy K, Weaver C. Janeway's immunobiology. New York: Garland Science, Taylor and Francis Group LLC; 2017. p. 213-371
29. Allen RL. Non-classical immunology. Genome Biol. 2001;2(2):REPORTS4004.

30. Halenius A, Gerke C, Hengel H. Classical and non-classical MHC I molecule manipulation by human cytomegalovirus: so many targets—but how many arrows in the quiver? Cell Mol Immunol. 2015;12(2):139-53.
31. Kochan G, Escors D, Breckpot K, Guerrero-Setas D. Role of non-classical MHC class I molecules in cancer immunosuppression. Oncoimmunology. 2013;2(11):e26491.
32. Tilburgs T, Henry Evans J, Crespo ÂC, Strominger JL. The HLA-G cycle provides for both NK tolerance and immunity at the maternal-fetal interface. Proc Natl Acad Sci U S A. 2015;112(43):13312-7.
33. Rizzo R, Vercammen M, van de Velde H, Horn PA, Rebmann V. The importance of HLA-G expression in embryos, trophoblast cells, and embryonic stem cells. Cell Mol Life Sci. 2011;68(3):341-52.
34. Niederkorn JY, Chiang EY, Ungchusri T, Stroynowski I. Expression of a nonclassical MHC class Ib molecule in the eye. Transplantation. 1999;68(11):1790-9.
35. Fiszer D, Kurpisz M. Major histocompatibility complex expression on human, male germ cells: a review. Am J Reprod Immunol. 1998;40(3):172-6.
36. Berger A. HLA typing. BMJ. 2001;322(7280):218.
37. Bijen CB, Bantema-Joppe EJ, de Jong RA, Leffers N, Mourits MJE, Eggink HF, et al. The prognostic role of classical and nonclassical MHC class I expression in endometrial cancer. Int J Cancer. 2010;126(6):1417-27.
38. Rapacz-Leonard A, Dąbrowska M, Janowski T. Major histocompatibility complex I mediates immunological tolerance of the trophoblast during pregnancy and may mediate rejection during parturition. Mediators Inflamm. 2014;2014:579279.
39. Abe S, Nochi H, Ito H. Alloreactivity and immunosuppressive properties of articular chondrocytes from osteoarthritic cartilage. J Orthop Surg (Hong Kong). 2016;24(2):232-9.
40. Klinger P, Surmann-Schmitt C, Brem M, Swoboda B, Distler JH, Carl HD, et al. Chondromodulin 1 stabilizes the chondrocyte phenotype and inhibits endochondral ossification of porcine cartilage repair tissue. Arthritis Rheum. 2011;63(9):2721-31.
41. Setoguchi K, Misaki Y, Kawahata K, Shimada K, Juji T, Tanaka S, et al. Suppression of T cell responses by chondromodulin I, a cartilage-derived angiogenesis inhibitory factor: therapeutic potential in rheumatoid arthritis. Arthritis Rheum. 2004;50(3):828-39.
42. Soliman H, Mediavilla-Varela M, Antonia S. Indoleamine 2,3-dioxygenase: is it an immune suppressor? Cancer J. 2010;16(4):354-9.
43. Wu H, Gong J, Liu Y. Indoleamine 2, 3-dioxygenase regulation of immune response (Review). Mol Med Rep. 2018;17(4):4867-73.
44. Gualdoni GS, Jacobo PV, Sobarzo CM, Pérez CV, Matzkin ME, Höcht C, et al. Role of indoleamine 2,3-dioxygenase in testicular immune-privilege. Sci Rep. 2019;9(1):15919.
45. Munn DH, Zhou M, Attwood JT, Bondarev I, Conway SJ, Marshall B, et al. Prevention of allogeneic fetal rejection by tryptophan catabolism. Science. 1998;281(5380):1191-3.
46. Dai X, Zhu BT. Indoleamine 2,3-dioxygenase tissue distribution and cellular localization in mice: implications for its biological functions. J Histochem Cytochem. 2010;58(1):17-28.
47. Du WJ, Reppel L, Leger L, Schenowitz C, Huselstein C, Bensoussan D, et al. Mesenchymal stem cells derived from human bone marrow and adipose tissue maintain their immunosuppressive properties after chondrogenic differentiation: role of HLA-G. Stem Cells Dev. 2016;25(19):1454-69.
48. Le Blanc K, Tammik C, Rosendahl K, Zetterberg E, Ringdén O. HLA expression and immunologic properties of differentiated and undifferentiated mesenchymal stem cells. Exp Hematol. 2003;31(10):890-6.

49. Zheng ZH, Li XY, Ding J, Jia JF, Zhu P. Allogeneic mesenchymal stem cell and mesenchymal stem cell-differentiated chondrocyte suppress the responses of type II collagen-reactive T cells in rheumatoid arthritis. Rheumatology (Oxford). 2008;47(1):22-30.
50. Peroni JF, Borjesson DL. Anti-inflammatory and immu-nomodulatory activities of stem cells. Vet Clin North Am Equine Pract. 2011;27(2):351-62.
51. Corcione A, Benvenuto F, Ferretti E, Giunti D, Cappiello V, Cazzanti F, et al. Human mesenchymal stem cells modulate B-cell functions. Blood. 2006;107(1):367-72.
52. Ben-Ami E, Berrih-Aknin S, Miller A. Mesenchymal stem cells as an immunomodulatory therapeutic strategy for autoimmune diseases. Autoimmun Rev. 2011;10(7):410-5.
53. DelaRosa O, Lombardo E, Beraza A, Mancheño-Corvo P, Ramirez C, Menta R, et al. Requirement of IFN-gammamediated indoleamine 2,3-dioxygenase expression in the modulation of lymphocyte proliferation by human adiposederived stem cells. Tissue Eng Part A. 2009;15(10):2795806.
54. Ge W, Jiang J, Arp J, Liu W, Garcia B, Wang H. Regulatory T-cell generation and kidney allograft tolerance induced by mesenchymal stem cells associated with indoleamine 2,3-dioxygenase expression. Transplantation. 2010;90(12):1312-20.
55. Nasef A, Chapel A, Mazurier C, Bouchet S, Lopez M, Mathieu N, et al. Identification of IL-10 and TGF-beta transcripts involved in the inhibition of T-lymphocyte proliferation during cell contact with human mesenchymal stem cells. Gene Expr. 2007;13(4-5):217-26.
56. Selmani Z, Naji A, Zidi I, Favier B, Gaiffe E, Obert L, et al. Human leukocyte antigen-G5 secretion by human mesenchymal stem cells is required to suppress T lymphocyte and natural killer function and to induce CD4+CD25highFOXP3+ regulatory T cells. Stem Cells. 2008;26(1):212-22.
57. Ryan AE, Lohan P, O'Flynn L, Treacy O, Chen X, Coleman C, et al. Chondrogenic differentiation increases antidonor immune response to allogeneic mesenchymal stem cell transplantation. Mol Ther. 2014;22(3):655-67.
58. Chen CT. Cartilage extracellular matrix and integrity and OA. In: Bruce M. Rothschild, editor. Principles of osteoarthritis: its definition, character derivation and modalityrelated recognition. IntechOpen; 2012.
59. Mow VC, Wang CC, Hung CT. The extracellular matrix, interstitial fluid and ions as a mechanical signal transducer in articular cartilage. Osteoarthritis Cartilage. 1999;7(1):41-58.
60. Kuse R, Schuster S, Schübbe H, Dix S, Hausmann K. Blood lymphocyte volumes and diameters in patients with chronic lymphocytic leukemia and normal controls. Blut. 1985;50(4):243-8.
61. Wolf K, Müller R, Borgmann S, Bröcker E-B, Friedl P. Amoeboid shape change and contact guidance: T-lymphocyte crawling through fibrillar collagen is independent of matrix remodeling by MMPs and other proteases. Blood. 2003;102(9):3262-9.
62. Wiradjaja F, DiTommaso T, Smyth I. Basement membranes in development and disease. Birth Defects Res C Embryo Today. 2010;90(1):8-31.
63. Howat WJ, Holmes JA, Holgate ST, Lackie PM. Basement membrane pores in human bronchial epithelium: a conduit for infiltrating cells? Am J Pathol. 2001;158(2):673-80.
64. Linn FC, Sokoloff L. Movement and composition of interstitial fluid of cartilage. Arthritis Rheum. 1965;8:481-94.
65. Pedrozo HA, Schwartz Z, Gomez R, Ornoy A, Xin-Sheng W, Dallas SL, et al. Growth plate chondrocytes store latent transforming growth factor (TGF)-beta 1 in their matrix through latent TGF-beta 1 binding protein-1. J Cell Physiol. 1998;177(2):343-54.
66. Fortier LA, Barker JU, Strauss EJ, McCarrel TM, Cole BJ. The role of growth factors in cartilage repair. Clin Orthop Relat Res. 2011;469(10):2706-15.

67. Gharravi AM, Orazizadeh M, Hashemitabar M. Direct expansion of chondrocytes in a dynamic three-dimensional culture system: overcoming dedifferentiation effects in monolayer culture. Artif Organs. 2014;38(12):1053-8.
68. Rayahin JE, Buhrman JS, Zhang Y, Koh TJ, Gemeinhart RA. High and low molecular weight hyaluronic acid differentially influence macrophage activation. ACS Biomater Sci Eng. 2015;1(7):481-93.
69. Niederkorn JY. Emerging concepts in CD8(+) T regulatory cells. Curr Opin Immunol. 2008;20(3):327-31.
70. Cone RE, Li X, Sharafieh R, O'Rourke J, Vella AT. The suppression of delayed-type hypersensitivity by CD8+ regulatory T cells requires interferon-gamma. Immunology. 2007;120(1):112-9.
71. Papatriantafyllou M, Moldenhauer G, Ludwig J, Tafuri A, Garbi N, Hollmann G, et al. Dickkopf-3, an immune modulator in peripheral CD8 T-cell tolerance. Proc Natl Acad Sci U S A. 2012;109(5):1631-6.
72. Kezuka T, Streilein JW. In vitro generation of regulatory CD8+ T cells similar to those found in mice with anterior chamber-associated immune deviation. Invest Ophthalmol Vis Sci. 2000;41(7):1803-11.
73. Wilbanks GA, Streilein JW. Characterization of suppres-sor cells in anterior chamber-associated immune deviation (ACAID) induced by soluble antigen. Evidence of two functionally and phenotypically distinct T-suppressor cell populations. Immunology. 1990;71(3):383-9.
74. Cong L, Wang SF, Zhao ZL, Yang RY. Donor-antigen inoculation in the testis promotes skin allograft acceptance induced by conventional costimulatory blockade via induction of CD8 + CD122+ and CD4 + CD25+ regulatory T cells. Transplantation. 2016;100(4):763-71.
75. Rifa'i M, Shi Z, Zhang SY, Lee YH, Shiku H, Isobe K, et al. CD8+CD122+ regulatory T cells recognize activated T cells via conventional MHC class I-alphabetaTCR interaction and become IL-10-producing active regulatory cells. Int Immunol. 2008;20(7):937-47.
76. Fujihara Y, Takato T, Hoshi K. Macrophage-inducing FasL on chondrocytes forms immune privilege in cartilage tissue engineering, enhancing in vivo regeneration. Stem Cells. 2014;32(5):1208-19.
77. Langer F, Czitrom A, Pritzker KP, Gross AE. The immunogenicity of fresh and frozen allogeneic bone. J Bone Joint Surg Am. 1975;57(2):216-20.
78. Stevenson S, Shaffer JW, Goldberg VM. The humoral response to vascular and nonvascular allografts of bone. Clin Orthop Relat Res. 1996;326:86-95.
79. Pomajzl RJ, Baker EA, Baker KC, Fleischer MM, Salisbury MR, Phillips DM, et al. Case series with histopathologic and radiographic analyses following failure of fresh osteochondral allografts of the talus. Foot Ankle Int. 2016;37(9): 958-67.
80. Gortz S, Bugbee WD. Fresh osteochondral allografts: graft processing and clinical applications. J Knee Surg. 2006;19(3):23140.
81. Lewandrowski KU, Rebmann V, Pässler M, Schollmeier G, Ekkernkamp A, Grosse-Wilde H, et al. Immune response to perforated and partially demineralized bone allografts. J Orthop Sci. 2001;6(6):545-55.
82. Ambra LF, de Girolamo L, Gomoll AH. Pulse lavage fails to significantly reduce bone marrow content in osteochondral allografts: a histological and DNA quantification study. Am J Sports Med. 2019;47(11):2723-8.
83. Kandel RA, Gross AE, Ganel A, McDermott AG, Langer F, Pritzker KP. Histopathology of failed osteoarticular shell allografts. Clin Orthop Relat Res. 1985;197:103-10.
84. Kemble S, Croft AP. Critical role of synovial tissue-resident macrophage and fibroblast subsets in the persistence of joint inflammation. Front Immunol. 2021;12:715894.

85. Moskalewski S, Hyc A, Osiecka-Iwan A. Immune response by host after allogeneic chondrocyte transplant to the cartilage. Microsc Res Tech. 2002;58(1):3-13.
86. McCarty EC, Fader RR, Mitchell JJ, Glenn RE Jr, Potter HG, Spindler KP. Fresh osteochondral allograft versus autograft: twelve-month results in isolated canine knee defects. Am J Sports Med. 2016;44(9):2354-65.
87. Crist BD, Stoker AM, Pfeiffer FM, Kuroki K, Cook CR, Franklin SP, et al. Optimising femoral-head osteochondral allograft transplantation in a preclinical model. J Orthop Translat. 2016;5:48-56.
88. Morris AH, Stamer DK, Kyriakides TR. The host response to naturally-derived extracellular matrix biomaterials. Semin Immunol. 2017;29:72-91.
89. Cravedi P, Farouk S, Angeletti A, Edgar L, Tamburrini R, Duisit J, et al. Regenerative immunology: the immunological reaction to biomaterials. Transpl Int. 2017;30(12):1199208.
90. Filippone EJ, McCue PA, Farber JL. Transplant glomerulopathy. Mod Pathol. 2018;31(2):235-52.
91. Klatt AR, Paul-Klausch B, Klinger G, Kühn G, Renno JH, Banerjee M, et al. A critical role for collagen II in cartilage matrix degradation: collagen II induces pro-inflammatory cytokines and MMPs in primary human chondrocytes. J Orthop Res. 2009;27(1):65-70.
92. Williams JM, Holzknecht ZE, Plummer TB, Lin SS, Brunn GJ, Platt JL. Acute vascular rejection and accommodation: divergent outcomes of the humoral response to organ transplantation. Transplantation. 2004;78(10):1471-8.
93. Salama AD, Delikouras A, Pusey CD, Cook HT, Bhangal G, Lechler RI, et al. Transplant accommodation in highly sensitized patients: a potential role for Bcl-xL and alloantibody. Am J Transplant. 2001;1(3):260-9.
94. Jindra PT, Hsueh A, Hong L, Gjertson D, Shen X-D, Gao F, et al. Anti-MHC class I antibody activation of proliferation and survival signaling in murine cardiac allografts. J Immunol. 2008;180(4):2214-24.
95. Dehoux J-P, Gianello P. Accommodation and antibodies. Transplant Immunology. 2009;21(2):106-10.
96. Lewandowska K, Choi HU, Rosenberg LC, Zardi L, Culp LA. Fibronectin-mediated adhesion of fibroblasts: inhibition by dermatan sulfate proteoglycan and evidence for a cryptic glycosaminoglycan-binding domain. J Cell Biol. 1987;105(3):1443-54.
97. Schmidt G, Robenek H, Harrach B, Glössl J, Nolte V, Hörmann H, et al. Interaction of small dermatan sulfate proteoglycan from fibroblasts with fibronectin. J Cell Biol. 1987;104(6):1683-91.
98. Hunziker EB, Rosenberg LC. Repair of partial-thickness defects in articular cartilage: cell recruitment from the synovial membrane. J Bone Joint Surg Am. 1996;78(5):721-33.
99. Zhao S, Zhu W, Xue S, Han D. Testicular defense systems: immune privilege and innate immunity. Cell Mol Immunol. 2014;11(5):428-37.
100. Taylor AW. Ocular immune privilege. Eye. 2009;23(10): 1885-9.
101. Winnall WR, Muir JA, Hedger MP. Rat resident testicular macrophages have an alternatively activated phenotype and constitutively produce interleukin-10 in vitro. J Leukoc Biol. 2011;90(1):133-43.
102. Bhushan S, Hossain H, Lu Y, Geisler A, Tchatalbachev S, Mikulski Z, et al. Uropathogenic E. coli induce different immune response in testicular and peritoneal macrophages: implications for testicular immune privilege. Plos One. 2011;6(12):e28452.
103. Yamada A, Arakaki R, Saito M, Kudo Y, Ishimaru N. Dual role of Fas/FasL-mediated signal in peripheral immune tolerance. Front Immunol. 2017;8:403.
104. Hashimoto S, Setareh M, Ochs RL, Lotz M. Fas/Fas ligand expression and induction of apoptosis in chondrocytes. Arthritis Rheum. 1997;40(10):1749-55.

105. Hashimoto H, Tanaka M, Suda T, Tomita T, Hayashida K, Takeuchi E, et al. Soluble Fas ligand in the joints of patients with rheumatoid arthritis and osteoarthritis. Arthritis Rheum. 1998;41(4):657-62.
106. Maldonado M, Nam J. The role of changes in extracellular matrix of cartilage in the presence of inflammation on the pathology of osteoarthritis. Biomed Res Int. 2013;2013:284873.
107. Medema JP, de Jong J, Peltenburg LT, Verdegaal EM, Gorter A, Bres SA, et al. Blockade of the granzyme B/perforin pathway through overexpression of the serine protease inhibitor PI-9/SPI-6 constitutes a mechanism for immune escape by tumors. Proc Natl Acad Sci U S A. 2001;98(20):11515-20.
108. Seliger B. Strategies of tumor immune evasion. Biodrugs. 2005;19(6):347-54.
109. BubenÃ-k J. Tumour MHC class I downregulation and immunotherapy (Review). Oncol Rep. 2003;10(6):2005-8.
110. Wada A, Tada Y, Kawamura K, Takiguchi Y, Tatsumi K, Kuriyama T, et al. The effects of FasL on inflammation and tumor survival are dependent on its expression levels. Cancer Gene Ther. 2007;14(3):262-7.
111. Gur-Wahnon D, Borovsky Z, Liebergall M, Rachmilewitz J. The induction of APC with a distinct tolerogenic phenotype via contact-dependent STAT3 activation. Plos One. 2009;4(8):e6846.
112. Gabardi S, Martin ST, Roberts KL, Grafals M. Induction immunosuppressive therapies in renal transplantation. Am J Health Syst Pharm. 2011;68(3):211-8.
113. Sasazuki T, Juji T, Morishima Y, Kinukawa N, Kashiwabara H, Inoko H, et al. Effect of matching of class I HLA alleles on clinical outcome after transplantation of hematopoietic stem cells from an unrelated donor. Japan Marrow Donor Program. N Engl J Med. 1998;339(17):1177-85.
114. Min DI, Monaco AP. Complications associated with immunosuppressive therapy and their management. Pharmacotherapy. 1991;11(5):119S-125S.
115. Lanza R, Russell DW, Nagy A. Engineering universal cells that evade immune detection. Nat Rev Immunol. 2019;19:723-33.
116. Prange S, Zucker P, Jevnikar AM, Singh B. Transplanted MHC class I-deficient nonobese diabetic mouse islets are protected from autoimmune injury in diabetic nonobese recipients. Transplantation. 2001;71(7):982-5.
117. Sake HJ, Frenzel A, Lucas-Hahn A, Nowak-Imialek M, Hassel P, Hadeler KG, et al. Possible detrimental effects of beta-2-microglobulin knockout in pigs. Xenotransplantation. 2019;26(6):e12525.
118. Figueiredo C, Blasczyk R. A future with less HLA: potential clinical applications of HLA-universal cells. Tissue Antigens. 2015;85(6):443-9.
119. Deuse T, Seifert M, Phillips N, Fire A, Tyan D, Kay M, et al. Human leukocyte antigen I knockdown human embryonic stem cells induce host ignorance and achieve prolonged xenogeneic survival. Circulation. 2011;124(11 Suppl):S3-9.
120. Mattapally S, Pawlik KM, Fast VG, Zumaquero E, Lund FE, Randall TD, et al. Human leukocyte antigen class I and II knockout human induced pluripotent stem cell-derived cells: universal donor for cell therapy. J Am Heart Assoc. 2018;7(23):e010239.
121. Gornalusse GG, Hirata RK, Funk SE, Riolobos L, Lopes VS, Manske G, et al. HLA-E-expressing pluripotent stem cells escape allogeneic responses and lysis by NK cells. Nat Biotechnol. 2017;35(8):765-72.
122. Nancy P, Tagliani E, Tay C-S, Asp P, Levy DE, Erlebacher A. Chemokine gene silencing in decidual stromal cells limits T cell access to the maternal-fetal interface. Science. 2012;336(6086):1317-21.

123. Raghu H, Lepus CM, Wang Q, Wong HH, Lingampalli N, Oliviero F, et al. CCL2/CCR2, but not CCL5/CCR5, mediates monocyte recruitment, inflammation and cartilage destruction in osteoarthritis. Ann Rheum Dis. 2017;76(5):914-22.
124. Cutolo M, Sulli A, Paolino S, Pizzorni C. CTLA-4 blockade in the treatment of rheumatoid arthritis: an update. Expert Rev Clin Immunol. 2016;12(4):417-25.
125. Conigliaro P, Scrivo R, Valesini G, Perricone R. Emerging role for NK cells in the pathogenesis of inflammatory arthropathies. Autoimmun Rev. 2011;10(10):577-81.
126. Cifuentes-Rius A, Desai A, Yuen D, Johnston APR, Voelcker NH. Inducing immune tolerance with dendritic cell-targeting nanomedicines. Nat Nanotechnol. 2021;16(1):37-46.
127. Zhang W, Gorantla VS, Campbell PG, Li Y, Yang Y, Komatsu C, et al. Biopatterned CTLA4/Fc matrices facilitate local immunomodulation, engraftment, and glucose homeostasis after pancreatic islet transplantation. Diabetes. 2016;65(12):3660-6.
128. Lewis JS, Stewart JM, Marshall GP, Carstens MR, Zhang Y, Dolgova NV, et al. Dual-sized microparticle system for generating suppressive dendritic cells prevents and reverses Type 1 diabetes in the nonobese diabetic mouse model. ACS Biomater Sci Eng. 2019;5(5):2631-46.

Chapter 2

Tissue-Engineered Scaffold-Free Immuno-Universal Cartilage

Authors:

Carissa Garrity[1], Jeroen Saeij[1], Luis Diego Castillo Charpentier[1], Nicole Cox[1], Iris Rivas[1], Heather McEligot[1], Natalia Vapniarsky[1*]

[1]Department of Pathology, Microbiology, and Immunology, University of California, Davis, Davis, CA, United States of America

*Corresponding author

Abstract:

Cartilage has poor regenerative ability and tissue replacement strategies, such as tissue engineering, have been explored as a potential solution. Tissue-engineered cartilage constructs are commonly derived from allogenic cell sources. However, the transplantation of isolated allogeneic chondrocytes is not practiced for immunologic reasons. The main molecule responsible for allograft rejection is the major histocompatibility complex class I (MHC-I). ß-2 microglobulin (β2M) is a structural component of MHC-I conserved across species. In this study, we hypothesized that *β2M* gene knockout (β2M-KO) in porcine chondrocytes would lead to loss of MHC-I expression while retaining cellular function and the ability to form immuno-universal cartilage constructs. *β2M*-KO was achieved by the CRISPR/Cas9 system using plasmid transfection. Positively transfected cell lines were selected and biallelic disruption of the *β2M* gene at the exon 2 locus in chondrocytes was confirmed with Sanger sequencing. qRT-PCR, and ELISA demonstrated decreased expression of the *β2M* on genetic and protein levels. Flow cytometry showed significant downregulation of MHC-I despite IFNy stimulation. A significant difference in immunological

function was confirmed between the knockout and wild type control cell lines in co-culture with allogeneic lymphocytes. Lymphocyte proliferation was 1.6 times less when co-cultured with β2M-KO chondrocytes in comparison to wildtype chondrocytes. Cartilage constructs derived from β2M-KO and wildtype chondrocytes were assembled using scaffold-free methodology. Constructs were mechanically tested for compressive and tensile strength and analyzed biochemically and histologically. There were no significant differences in either tensile, compressive, biochemical or histological properties between the construct sourced from β2M-KO and wild type chondrocyte. Collectively, our data indicate that immuno-universal cartilage constructs with properties akin to constructs sourced from wild type cells can be tissue engineered from β2M-KO chondrocytes.

Key words: β2M-KO, cartilage immunology and immunogenicity, tissue engineering, MHC I-null, allogenic

1. Introduction

The high prevalence of disorders involving cartilage tissue is a public health concern worldwide. Articular cartilage for instance damaged by trauma initiates the process of osteoarthritis [1]. Other types of cartilages are also in high demand for reconstructive surgery following trauma-related tissue loss or tumor resections. The low regenerative capacity of cartilage and progressive demand for its regeneration, has invited the exploration of new strategies for tissue replacement and regeneration [2]. Despite the advancements and success of cartilage repair therapies, the clinical efficacy remains suboptimal due to several shortcomings. For instance, strategies that utilize autologous tissues (tissues derived from the same individual) are limited in quantity and thus only suitable for repair of small size cartilage defects [3]. In addition, the harvest of autologous cartilage introduces donor site morbidity [4, 5]. Cartilage allografts (tissues derived form a different individual of the same species) resolve these concerns, but introduce

new ones such as disease transmission and immune response [6-8]. The shortcomings of the current treatment options invite the discovery of novel strategies for cartilage replacement therapy.

Scaffold-free cartilage tissue engineering (TE) has been recently explored for its efficacy to produce tissue without introducing exogenous matrix [9]. Allogeneic chondrocytes are an attractive cell source due to the ability to produce “off-the-shelf” tissue. However, TE cartilage derived from allogenic chondrocytes is yet to be proven safe and efficacious for clinical use. Immunological safety aspects of TE allografts have not been explored largely due to the historical assumption that cartilage is immuno-privileged [10]. Recent literature has challenged this paradigm and invited more study into cartilage immunology [11].

Recent advances in genetic editing offer an elegant solution to bypass the immunological rejection [12]. Specifically, engineering cartilage from immuno-universal chondrocytes is an attractive option. One approach for creating such cells involves genetic silencing or deletion of major histocompatibility complex (MHC I) molecule. MHC class I molecules are expressed on all nucleated cells and present foreign, self, or altered self-peptides to T cells [13]. The immune response to non-self MHC molecules and non-self-peptides presented by the MHC complexes are the primary causes of transplant rejection [13]. The disruption of polymorphic and polygenic MHC units of the molecule is difficult, but targeting a conserved β-2-microglobulin (β2M) subunit, which is required for cell surface expression of MHC molecules [13] was successfully done [14-16]. Cellular therapy with β2M knockout (KO) cells improved tissue repair of heart [14] and lung [15], and improved the engraftment of gene-edited peripheral blood mononuclear cells [16].

These studies combined with the changing perspective of cartilage immune privilege inspired this study. Here we show that MHC I expression in chondrocytes is upregulated under inflammatory conditions and

that co-culture of such chondrocytes induces allogenic lymphocyte proliferation. We also report on the immunologic utility of MHC I-null porcine chondrocytes for cartilage tissue engineering.

2. Materials and Methods

2.a. General Study Design **(Figure 1)**

The guide RNAs (sgRNA) were designed targeting exon 2 of porcine β2M. The guide RNAs were: Forward oligo: 5' **CACCG**GAGTAAACCTGAACCTTCGG 3' and reverse oligo: 5' **AAAC**CCGAAGGTTCAGGTTTACTC**C** 3.' The β2M sgRNAs were ligated into a digested CRISPR/Cas9 vector and cloned. Successful ligation was confirmed with standard PCR and Sanger sequencing. Chondrocytes were transfected with the CRISPR/Cas9-β2M constructed plasmid. β2M-KO chondrocytes were purified with antibiotic selection with puromycin. Gene disruption was confirmed with Sanger sequencing of transfected chondrocytes. The knockout was further validated with several assays. We validated MHC-I downregulation with flow cytometry. We confirmed β2M gene downregulation with qPCR, and quantified β2M expression on a protein level with ELISA. We explored the immunogenicity of MHC-1 null chondrocytes by co-culturing them with allogeneic lymphocytes We assessed lymphocyte proliferation and polarization to different lymphocyte subtypes in the co-culture conditions. Finally, we confirmed no off-target effects on chondrogenic potential by tissue-engineering cartilage constructs using scaffold-free technology.

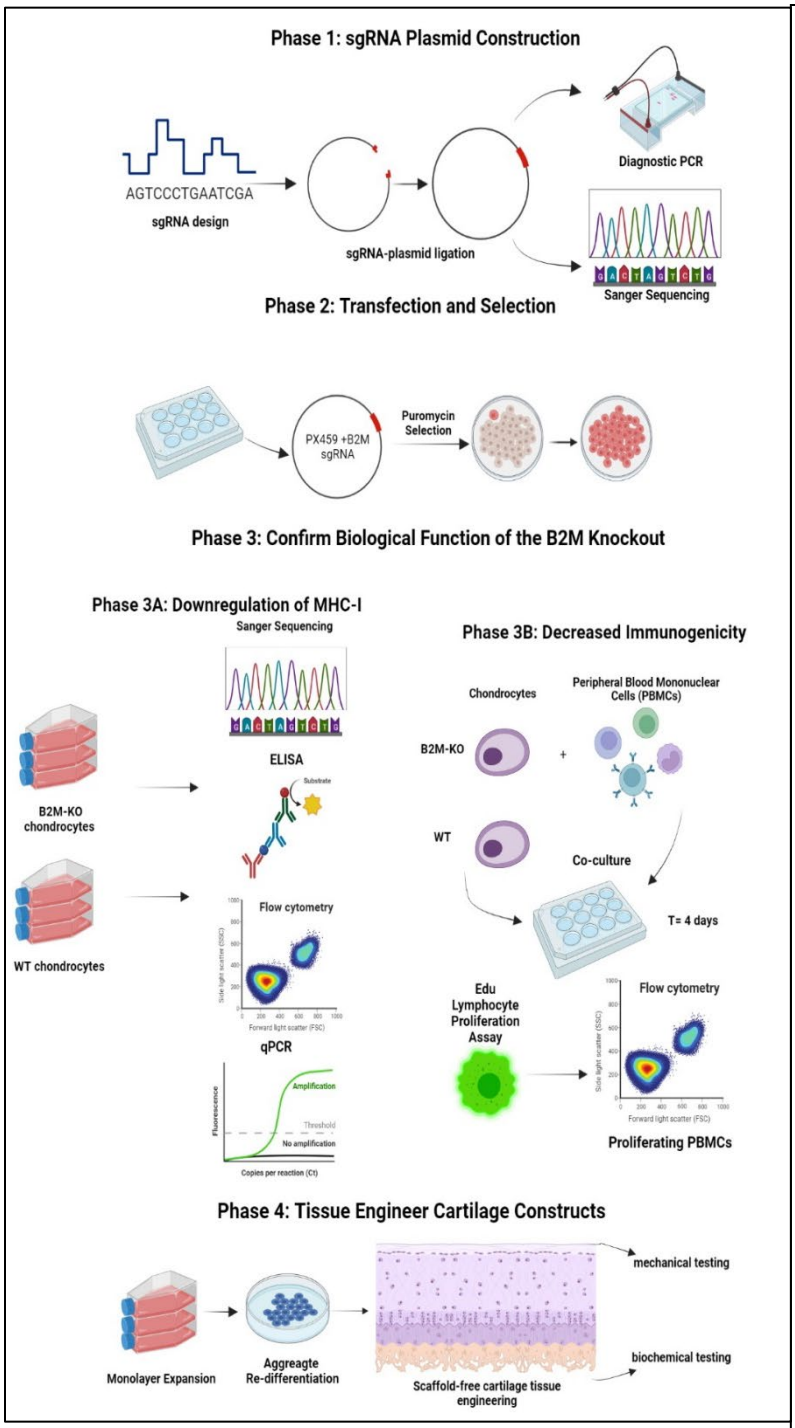


Figure 1: The guide RNAs (sgRNA) were designed targeting exon 2 of porcine β2M. The guide RNAs were: Forward oligo: 5' CACCGGAGTAAACCTGAACCTTCGG 3' and reverse oligo: 5' AAA**C**CCGAAGGTTCAGGTTTACTC**C** 3.' The β2M sgRNAs were ligated into a BBsI digested CRISPR/Cas9 expression plasmid pSpCas9 (BB)-2A- Puro (PX459) and cloned. Successful ligation was confirmed with standard PCR and Sanger sequencing. Chondrocytes were transfected with the CRISPR/Cas9-β2M constructed plasmid. β2M-KO chondrocytes were purified with puromycin. antibiotic selection Gene disruption of transfected chondrocytes was confirmed with Sanger sequencing. The knockout was further validated with several assays. We validated MHC-I downregulation with flow cytometry. We confirmed β2M gene downregulation with qPCR, and quantified β2M expression on a protein level with ELISA. We explored the immunogenicity of MHC-1 null chondrocytes by co-culturing them with allogeneic peripheral blood mononuclear cells (PBMCs). We assessed PBMC proliferation in the co-culture conditions. Finally, we confirmed no off-target effects on chondrogenic potential by tissue-engineering cartilage constructs using scaffold-free technology. Cartilage constructs were tested for biochemical composition and mechanical properties and compared to WT derived cartilage constructs.

2.a.1 Chondrocyte Isolation and Cell Culture

Porcine costal chondrocytes were isolated through enzymatic digestion in 0.2% collagenase solution (Worthington LS004176) supplemented with 3% fetal bovine serum for 18 hours at 37°C and 5% CO_2 with orbital rotation at 60 RPM. Chondrocytes not immediately used were cryopreserved in liquid nitrogen in 90% FBS and 10% Dimethyl Sulfoxide (DMSO) (Corning DMSO Mediatech Inc).

2.a.2 Chondrocyte Monolayer Expansion

Isolated chondrocytes were cultured to confluency in monolayer according to previously published protocol [17]. The culture media composition is provided in Table 1. Cultures were maintained in a humidified atmosphere at 37°C and 5% CO_2. Chondrocytes were passaged 3-4 times until a sufficient number of cells was reached. For passaging, cells were lifted up following 10-minute digestion at 37°C with Trypsin (Gibco 0.05% Trypsin-EDTA 1X, Cat# 25300-054), spun down at 400 G and further digested in 0.2% collagenase (Worthington 285 U/mg) supplemented with 3% FBS for 30 to 45 minutes at 37°C to remove any residual ECM that is produced by chondrocytes during monolayer expansion.

2.a.3 Assessment of MHC I expression in chondrocytes

Porcine chondrocytes (wild type, and β2M KO chondrocytes) were cultured in monolayer as described above in media supplemented with physiological OA concentrations (0.1-10 ng/mL) of IFNγ (Bio-rad PPP022 5ug) concentrations for three days [18]. On the third day, cells were lifted with 0.05% trypsin and labeled with FITC-MHC-I (BioRad MCA2261F) and fixable viability dye (Invitrogen Ref 65-0865-14). Flow cytometry parameters were set to collect 100,000 events or stop after 330 seconds. MHC I expression was measured in three KO donors (N=3) and compared to wild type chondrocytes. The flow cytometry data was analyzed on FlowJo software. The data was gated based on live cell populations prior to gating for MHC-I positive cells. Similarly, the effects of TNFα on MHC I expression were explored.

Table 1: Chondrogenic Expansion Media

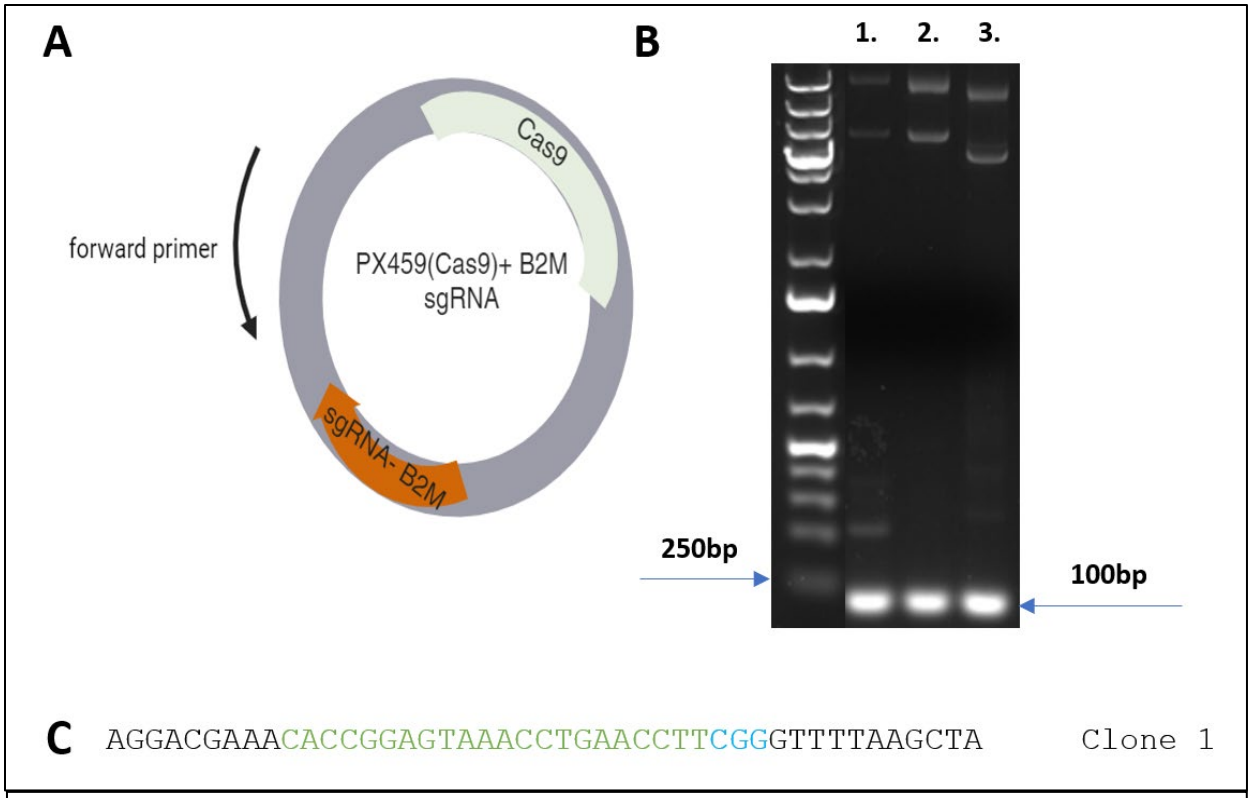
Component	Manufacturer/catalog #	Expansion media	Chondrogenic media
DMEM	Gibco 10566-016	Full strength	Full strength
Pen/strep amphotericin B	BioWhitaker 17-745E	10 mg/mL	10 mg/mL
MEM non-essential amino acids	Gibco 11140-050	10 mg/mL	10 mg/mL
Insulin/human transferrin/selenium (ITS+) premix	Corning 0354352	10 mg/mL	10 mg/mL
Sodium pyruvate	Thermo P2256-25g	100 µg/mL	100 µg/mL
L-Ascorbate-2-phosphate	Sigma Aldrich A8960-5g	50 µg/mL	50 µg/mL
L-proline	Sigma Aldrich P0380-100g	40 µg/mL	40 µg/mL
Dexamethasone	Sigma Aldrich D4902-25mg	0.0104 mg/mL	0.104 mg/mL
Fetal bovine serum	Atlanta biologicals S11550	100 µL/mL	N/A

Human recombinant TGF beta 1	Pepro Tech 100-21 – 10 µg	1 ng/mL	10 ng/mL
Human recombinant FGF	Pepro Tech 100-18B – 100 µg	5 ng/mL	N/A
Human recombinant PDGF	Pepro Tech 100-14B	10 ng/mL	N/A
Human recombinant BMP-2	Pepro tech 120-02-100ug	N/A	30ng/mL

2.b. Engineering of MHC I-null costal chondrocytes.

2b.1sgRNA Design and CRISPR plasmid Construction

The sgRNA target sequence 5' GAGTAAACCTGAACCTTCGG 3' was taken from Sake et al [19]. We further validated the design of the sgRNA using the online tool CHOPCHOP [20]. The final sequences of the sgRNA targeting exon 2 of porcine β2M are as follows with the additional nucleotides (restriction enzyme Bbsl, bolded): Forward oligo: 5' **CACCG**GAGTAAACCTGAACCTTCGG 3' and reverse oligo: 5' **AAAC**CCGAAGGTTCAGGTTTACTC**C** 3.' to assist in ligating to the plasmid. The oligos were annealed to form an oligo duplex with T4 PNK (Biolab M02015) and T4 Ligation Buffer (NEB). The oligo duplex was ligated into the Bbsl cloning site of the CRISPR/Cas9 expression plasmid pSpCas9 (BB)-2A- Puro (PX459) (Addgene plasmid #62988) with Quick Ligase (M2200L) and Quick Buffer (Biolabs B2200S). The plasmid was then cloned, grown, and selected with 100ug/ml Ampicillin in E. coli competent bacteria (Biolabs C2992H) **(Supplemental Figure 1).**

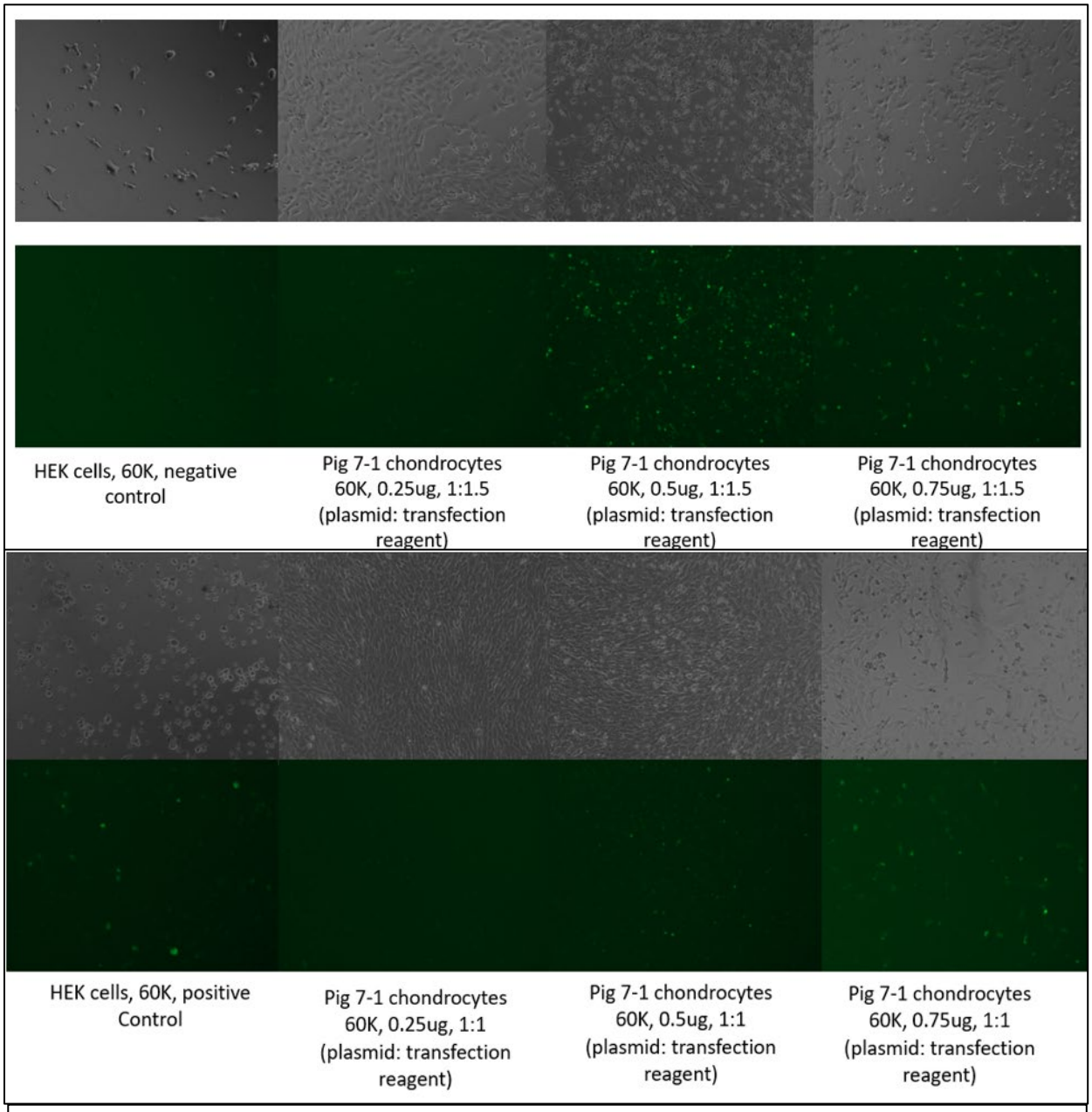


Supplemental Figure 1: Ligation of β2M sgRNA oligos into PX459 CRISPR vector. (A) Gene map and primers used for PCR verification of positive clones. Forward primer (black arrow) is encoded within the plasmid backbone slightly upstream of the guide sequence. The reverse primer used was the sgRNA reverse oligo of β2M (orange arrow). Standard PCR was performed to confirm successful ligation of sgRNA into CRISPR/Cas9 PX459 plasmid. (B) Confirmation of three positive clones with the β2M sgRNA insert within the plasmid with PCR. Positive clones were detected by confirmation of a 100bp amplicon. Additional larger sized bands represent remnant digested PX459 plasmid that did not ligate with β2M sgRNA. PCR cleanup was performed to remove remaining digested plasmid and purify positive clones. (C) Sanger sequencing confirmation of β2M sgRNA sequences ligated into the plasmid. The sgRNA is indicated in green while the PAM sequence is indicated in blue.

2b.2 Transfection, Selection, Cell Culture

Porcine costal chondrocytes were cultured in monolayer, as described above. Transfection was previously optimized using JetOptimus reagents (Polyplus 55-250) and a GFP plasmid (CAG-GFP was a gift from Fred Gage (Addgene plasmid # 16664; http://n2t.net/addgene:16664; RRID: Addgene_16664) During transfection optimization, cells were seeded into a flask and allowed a few days to grow to approximately 60-80% confluency. Cells ($6*10^4$) were transfected at either a 1:1 or a 1: 1.5 ratio of GFP plasmid to

JetOptimus transfection reagent and subjected to puromycin selection at 1µg/ml (Invitrogen Cat# QLL-43-02-ANT-PR) 24 hours after transfection. Transfection efficiency was measured with fluorescent microscopy



Supplemental Figure 2: Transfection optimization with GFP plasmid and JetOptimus Transfection Reagents. Porcine chondrocytes were plated in a 24 well plate at $6*10^4$ cells per well. Cells were transfected with various concentrations of plasmid and 2 different variations of plasmid (µg) to transfection reagent (µl) ratios. Pictures were taken 24 hours after transfection in blind focus and with fluorescence microscopy. Human embryonic kidney cells (HEK) were used as a control. Transfection with a plasmid (µg) to transfection reagent (µl) ratio of 1:1.5 were the most efficient (top two rows). The most efficient transfection conditions used 0.5 µg of GFP plasmid and 0.75 µl of transfection reagent (1:1.5 ratio).

(Supplemental Figure 2).

Subsequently, costal chondrocytes were transfected and selected using similar methodology but with the pSpCas9-2A- Puro (PX459)- β2M oligo duplex vector. The media was replaced every 3-4 days over 2 cycles where selection media containing 1μg/ml of puromycin (Invitrogen- QLL-43-02) was alternated with regular expansion media until no decrease in number of chondrocytes was observed following selection media exposure. The β2M KO was performed on three different porcine costal chondrocyte cell lines (N=3). Also, transfection was performed twice on the different passage cell lines from the same donor.

2b.3 Knockout Validation

The disruption of β2M, gene was evaluated with Sanger sequencing performed on the DNA extract from the selection purified KO cell lines. In addition, β2M gene expression was assessed with RT-qPCR and ELISA. Finally, surface expression of MHC I in the KO cell lines vs. WT controls was assessed and quantified with flow cytometry.

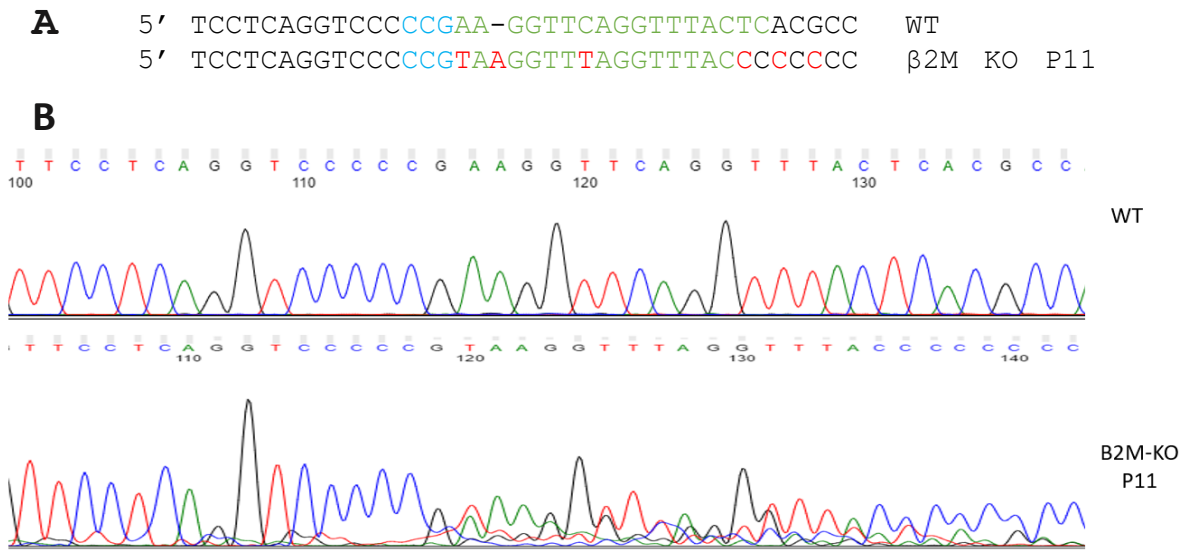
2b.3a DNA/RNA Isolation, PCR, and Sanger Sequencing

Total DNA and RNA was extracted from porcine chondrocytes using Quick DNA/RNA^{TM} Miniprep Isolation Kit (Invitrogen D7001) following the manufacturer's protocol. DNA expression of porcine β2M exon 2 (Forward primer 5' TTGGCCTGAAGGGAAATGGG 3'; Reverse primer 5' CACGCGGCAGCTATACTGAT 3') was interrogated with standard PCR using Qiagen's Taq DNA Polymerase (CAT: 201203). Cycle conditions were denaturation at 95C for 3 min, followed by 35 cycles of 95C for 30s, annealing at 60C for 30s, and 72C for 30s. A final extension at 72C for 10 minutes. The reaction was controlled with GAPDH housekeeping gene. Immediately following PCR, the PCR product was submitted to Azenta/Genewiz for Sanger sequencing

analysis. Retention of the KO was confirmed with Sanger Sequencing in early and advanced passages **(Supplemental Figure 3).**

2b.3b ELISA

β2M protein was detected in wildtype and B2M knockout porcine chondrocytes using a sandwich β2M ELISA kit (MyBioSource MBS1604456) following manufacturer's instructions. Sample preparation



Supplemental Figure 3: Alignment of Sanger sequencing results of primary transfected chondrocytes after several passages. **(A)** β2M Knockout (KO) sequence indicate an insertion and two point-mutations following multiple rounds of puromycin selection and cell passaging. The following sequencing results represent β2M-KO cells at passage 11 with constant puromycin selection. PAM sequence is in blue and sgRNA is in green. The green sgRNA sequence is representative of 20 nucleotides of exon 2 of porcine β2M gene. **(B)** Based on the chromatogram results, it is possible that there is a mixture of many clones within the knockout population. The most likely sequence of these clones is the sequence featured in (A) due to being the highest peaks within the chromatogram. Regardless, the chromatogram represents successful disruption of the β2M gene following the PAM sequence.

consisted of harvesting wildtype and KO cells from monolayers as previously described. Cell suspension of 10^6 cells/ml PBS (pH 7.4) was lysed through five cycles of freeze-thaw. The microtiter plate was pre-coated with porcine β2M antibody. Then standard and sample bound to biotinylated β2M antibodies was added. Next the Streptavidin-HRP enzyme was added for color development. The color intensity was

proportional to the amount of porcine β2M present in the standard and sample. The reaction was stopped by an acidic solution and the absorbance was measured at 450 nm using the Filter Max F3 MultiMode Microplate Reader (Molecular Devices). A standard curve was constructed and β2M concentration (ng/ml) was determined in the wildtype and β2M knockout porcine chondrocyte samples using a 4-parameter regression analysis using the SoftMax Pro 7.1 software. Data was presented as mean µg β2M/µg total protein. Total protein in chondrocyte sample was measured using a BCA protein assay (Prometheus 18440) following manufacturer's protocol.

2b.3c qPCR

For RT-qPCR analysis, total RNA was extracted using Quick DNA/RNA™ Miniprep Isolation Kit (ZYMO D7001) following manufacturer's protocol. 500ng of total RNA from each sample was used for reverse transcription. cDNA was synthesized using SuperScript VILO Master Mix (Invitrogen 11755) following manufacturer's protocol. The reverse transcription thermocycling program consisted of 10 minutes at 25°C, 120 minutes at 42°C, and a termination cycle of 85°C for 5 minutes. QuantiNova™ SYBR Green qPCR master mix (Qiagen 208052) was used to amplify the cDNA samples following manufacturer's protocol using gene specific primers (**Supplemental Table 1**). The RT-qPCR was performed in duplicates on a 96-well plate, in a 20 µl reaction volume. Reaction mixture consisted of 10 µl QuantiNova™ SYBR Green qPCR master mix, 100ng of cDNA, 5uL nuclease free water, and 2 µl of each primer. The RT-qPCR thermocycling regimen consisted of one cycle at 95°C for 2 minutes followed by 39 cycles at 95°C for 5 seconds and 55°C for 10 seconds. The RT-qPCR was performed using the CFX96 Real Time PCR Detection System (BioRad). The relative mRNA expression of genes was calculated by the $2^{-\triangle\triangle CT}$ method using GAPDH as the reference gene.

Supplemental Table 1

Gene	Oligonucleotide Sequence (5'–3')	Working Concentration
GAPDH	F: ACACTCACTCTTCTACCTTTG	10 µM
	R: CAAATTCATTGTCGTACCAG	10 µM
Collagen I	F: GGATACGCGGACTTTGTTGC	10 µM
	R: AGGGCCTGGGATACCATCAT	10 µM
Collagen II	F: GAGAAACCATCAATGGCGGC	10 µM
	R: GCTTTCTTGAGGTTGCCAGC	10 µM
Comp	F: AGATAACGCTGGGTGCAGAC	10 µM
	R: GTCACACTCCATCACCGTGT	10 µM
Arginase	F: CCTGACTGTGTCTTCCGTTCA	10 µM
	R: CAGCCAGTCTTCCCTCTCAG	10 µM
Sox-9	F: AGCAAGACTCTGGGCAAACT	10 µM
	R: GCCGTTCTTCACCGACTTTC	10 µM

2b.3d MHC I expression in β2M-*KO Chondrocytes*

Surface expression of MHC I was assessed and quantified via flow cytometry as described in 2a.3 following three-day stimulation with 0ng and 10ng/ml of IFNγ (Bio-Rad PPP022 5ug).

2b. 3e Off-target analysis

Possible off-target locations of CRISPR/Cas9 were identified and analyzed with CRISPOR and CHOPCHOP. Off-target analysis was compared to results of Sake et al [19], who used the same guide sgRNA.

2c. Assessment of β2M KO cell lines Immunogenicity in co-culture with allogeneic lymphocytes

Porcine allogeneic lymphocytes were isolated from whole blood using Ficoll-Plaque method [21]. Isolated lymphocytes were plated in co-culture with porcine chondrocytes (β2M KO and WT) in lymphocyte culture media (RPMI 1640 supplemented with 10% FBS, 1% Gluta-Max, 1mM Na Pyruvate, 2mM HEPES, 1ul/ml

MEM NEA, and 55uM β-mercaptoethanol, and 100µg/mL human recombinant interlukin-2. Prior to co-culture, porcine chondrocytes (wild type and β2M KO cell lines), were pre-stimulated with 10ng/ml IFNy for three days. Co-culture was done at 1:1 cell ratio for 4 days total. On the third day, 1uM of 5-ethynyl-2-deoxyuridine (Edu) was added to all co-culture groups. On the fourth day, the supernatant containing lymphocytes was collected and lymphocyte proliferation was analyzed with the Click-It EDU Assay Kit (Thermo C10420). Lymphocytes were also labeled with fixable viability dye (Invitrogen Ref 65-0865-14). The flow cytometry data was analyzed on FlowJo software. These experiments were carried out in duplicates and repeated on three β2M KO cell lines (N=3).

2d. MHC I-null Cartilage Tissue Engineering

2d.1 Aggregate Redifferentiation

Following sufficient monolayer expansion (2.a.2), wildtype and β2M-KO chondrocytes were suspended in chondrogenic media (Table 1) and seeded into 90 mm Petri plates coated with 20mg/ml agarose at a density of 1 million cells/mL in a total volume of 15 to 20 mLs. Cells were cultured according to previously published protocol [17] at 37°C in 5% CO2 with orbital rotation at 60 RPM for 24 hours. After 24 hours, plates were maintained under the same conditions but static. The media was replenished every 3-4 days for a total of 10 days. On the 11th day, aggregates were digested to single-cell suspension with 15 mL/plate of 0.05% Trypsin for 45 min at 37°C followed by digestion in 15 mL of 2 mg/mL collagenase solution supplemented with 30 µL/mL (3% v/v) FBS for 90 min. Following an additional wash step, the cell count was obtained, and cell viability was assessed with Trypan blue vital staining.

2d.2 Construct Seeding (self-assembly)

Wildtype and β2M-KO constructs were seeded at 8 million cells in a seeding volume of 300 µL of chondrogenic media into custom-made 7mm x 12mm agarose molds. After 4 hours, constructs were

topped off with an additional 2 mL chondrogenic media supplemented with 10 ng/mL TGFβ-1 (Table 1). The constructs were provided with chondrogenic media that was replenished every other day for the duration of four weeks, at which point construct development was stopped. All constructs were subjected biomechanical and biochemical testing and histology on day 28 of self-assembling.

2d.3 Mechanical Testing

For tensile mechanical testing, dumbbell-shaped samples were cut from wildtype and β2M -KO constructs while maintaining a length to width of approximately 4:1. Each dumbbell shaped sample was photographed. Thickness and width were measured and recorded using imaging software (ImageJ, U. S. National Institutes of Health, Bethesda, Maryland). A uniaxial tensile test was performed on a material testing machine (Instron 5565, Norwood, MA). The samples were elongated at a strain rate of 1%-gauge length per second. Stress/strain curves were generated from the load-displacement data. The load, elongation, and specimen geometry (width and thickness) were loaded into analysis software (Matlab, MathWorks, Natick, MA) and analyzed with a custom program that plots load normalized to cross-sectional area and strain. The output was used to identify the linear portion of the curve to determine tensile stiffness (Young's modulus) and the ultimate tensile strength (UTS) point.

For compressive mechanical testing, flat 3mm in diameter specimens were obtained from wildtype and β2M-KO constructs using a punch-biopsy knife. For the duration of compressive testing, samples were submerged in PBS at room temperature. A uniaxial, unconfined stress-relaxation testing was carried out on Instron 5565 (Norwood, MA). Samples were strained to 10% and 20% sequentially and allowed to relax for 600 and 1200s, respectively. The instantaneous (Ei) and relaxation moduli (Er) were calculated using a custom Matlab program upon fitting the data to a Kelvin solid viscoelastic model at each strain level [[22].

2d.4 Biochemical Testing

The wet and dry weights of representative samples from wildtype and β2M -KO constructs were obtained before and after 24-hour lyophilization, respectively. Lyophilized samples were digested in papain solution (125 µg/mL Papain + 5 mM N-Acetyl-L-Cysteine + 5 mM EDTA (anhydrous) + 100mM Phosphate Buffer) at 1µl of digestion solution per 1µg of sample dry weight at 60□C for 18 hours. The collagen content was assessed by OH-Proline Assay (Sigma Aldrich) following the manufacturer's instructions. The collagen content was then calculated based on a bovine collagen standard curve. The concentration of sulfated glycosaminoglycans in each sample was determined via a GAG Blyscan Assay (Bicolor Life-Science Assays) based on 1, 9-dimethyl methyl blue binding, following manufacturer instructions. The DNA content was assessed via a Pico Green assay (Invitrogen Quanti-iT PicoGreen dsDNA Assay kit) based on pico green fluorescent dye that bind to double-stranded DNA, following the manufacturer instructions. From this data, we were able to infer the number of cells per sample.

2d.5 Histology

Representative samples from wildtype and β2M -KO constructs were fixed in 10% buffered formalin and processed for standard histology and paraffin embedded subsequently [23]. A 5µm sections were obtained from the paraffin blocks and stained with hematoxylin and eosin (H&E), Safranin O/Fast Green, and PicroSirius Red for qualitative assessment of general morphology, cellularity, glycosaminoglycan content, and collagen, respectively.

2e. Statistics

Statistical analyses were carried out GraphPad Prism version 9.5.1 (GraphPad Software, Dotmatics, Boston, Massachusetts, USA). All data presented are expressed as means with standard error. All data were checked for normality and log-transformed when needed. A paired t-test was used to compare

wildtype chondrocytes and β2M-KO chondrocytes in MHC-I expression, β2M expression in qPCR and ELISA, PBMC proliferation and subtype distributions, construct biomechanical properties, and construct biochemical compositions. Results were considered statistically significant at $p < 0.05$.

3. Results

3a. Validation of MHC-I expression on porcine chondrocytes (**Figure 2)**

Wildtype porcine chondrocytes were pre-stimulated with physiological concentrations (0.1-10 ng/mL) of IFNγ for three days and labeled with an anti-MHC class I-FITC conjugated antibody. MHC class I expression was quantified with flow cytometry **(Figure 2A)**. Wild type chondrocytes had very little to no expression of MHC class I when exposed to IFNγ concentrations of 0.1ng/ml of IFNγ. However, the MHC class I expression increased dramatically upon cell stimulation with 1 and 10ng/ml of IFNγ. A significant difference in MHC-I expression by chondrocytes (**Figure 2B)** under physiologically-relevant concentrations of IFNγ invited us to further investigate and compare the immunologic behavior of MHC – I-null chondrocytes vs. wild type controls.

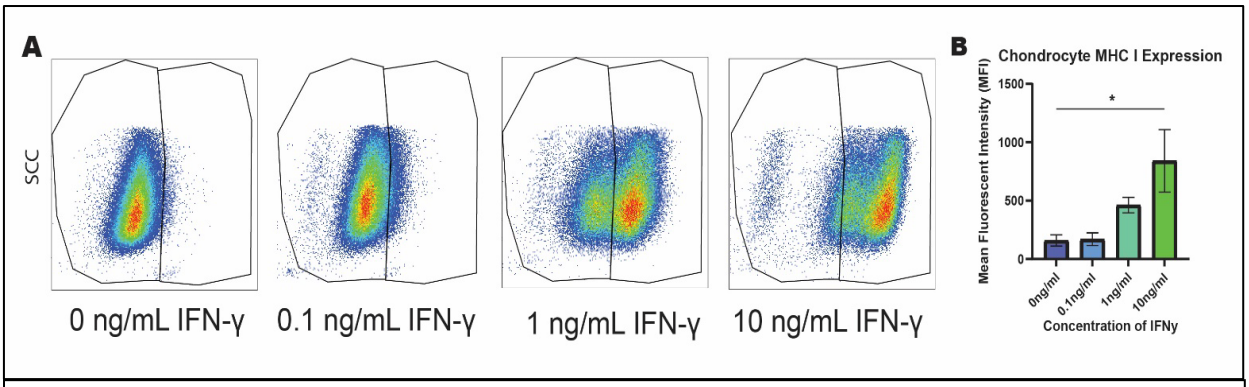


Figure 2: MHC-I expression on wildtype costal chondrocytes stimulated with IFNγ. (A) Flow cytometry dot plots showing the increase in MHC-I (FITC) expression of chondrocytes when stimulated with 0, 0.1, 1, and 10ng/ml of IFNγ. The concentrations of IFNγ reflect physiological conditions of a normal and arthritic joint. (B) Quantification of repeating the experiment in panel A in three different knockout cell lines (N=3).

3b. Generation of β2M-KO chondrocytes

3b.1 β2M *KO plasmid vector construction*

The sgRNA was designed to target the reverse strand of exon 2 of the porcine β2M gene to effectively generate MHC class I-null chondrocytes. The oligos were successfully ligated into BbsI digested pSpCas9 (BB)-2A- Puro (PX459) plasmid. Following ligation, the plasmid was cloned with *E. coli* competent bacteria. The ligation was confirmed with PCR and Sanger sequencing (**Sup. Fig. 1**).

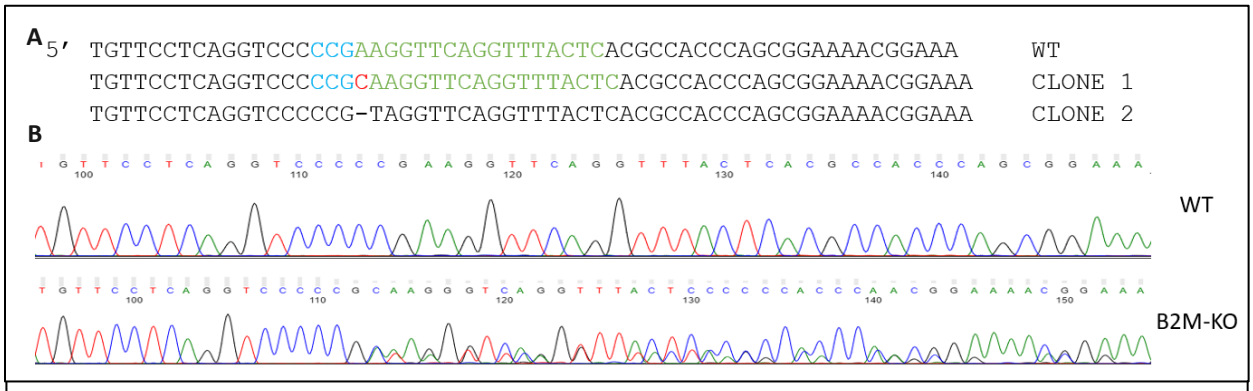


Figure 3: Alignment of Sanger sequencing results of primary transfected chondrocytes. Wildtype (WT) sequences indicate the genomic sequence of porcine B2M. Knockout (KO) sequence indicate the B2M sequence of the primary chondrocytes after transfection and after selection. (A) Clone 1 demonstrates an insertion directly following the PAM site while clone 2 has a substitution of a T base directly after the PAM site. PAM sequence is in blue and sgRNA is in green. Red nucleotides are insertions. The green sgRNA sequence is representative of 20 nucleotides of exon 2 of porcine B2M gene. (B) The chromatogram results of wildtype chondrocytes with normal expression of porcine B2M gene. (C) The chromatogram results of KO chondrocytes with a mixture of multiple clones as specified in (A). Double peaks indicate disruption of B2M gene.

3b.2 Chondrocyte transfection efficiency was optimized using a GFP labeled plasmid **(Sup. Fig. 2)**.

Transfection optimization was performed in a 24 well format. We observed that transfection was most efficient at a 1: 1.5 ratio of GFP plasmid to JetOptimus transfection reagent with 0.5ug of plasmid.

3b.3 Validation of β2M Knockout

3b.3a Sequencing

Chromatogram results indicate a single base insertion in both KO clones **(Figure 3)** resulting in a frame shift. This shift continues downstream for the remainder of the gene sequence. Thus, the results confirm disruption of the gene. In contrast, chromatogram results for wildtype chondrocytes display singular peaks

which indicates that exon 2 of β2M has not been disrupted. Similar sequencing procedure was performed on β2M-KO chondrocytes following many passages with equivalent outcomes (**Supplemental Figure 3).**

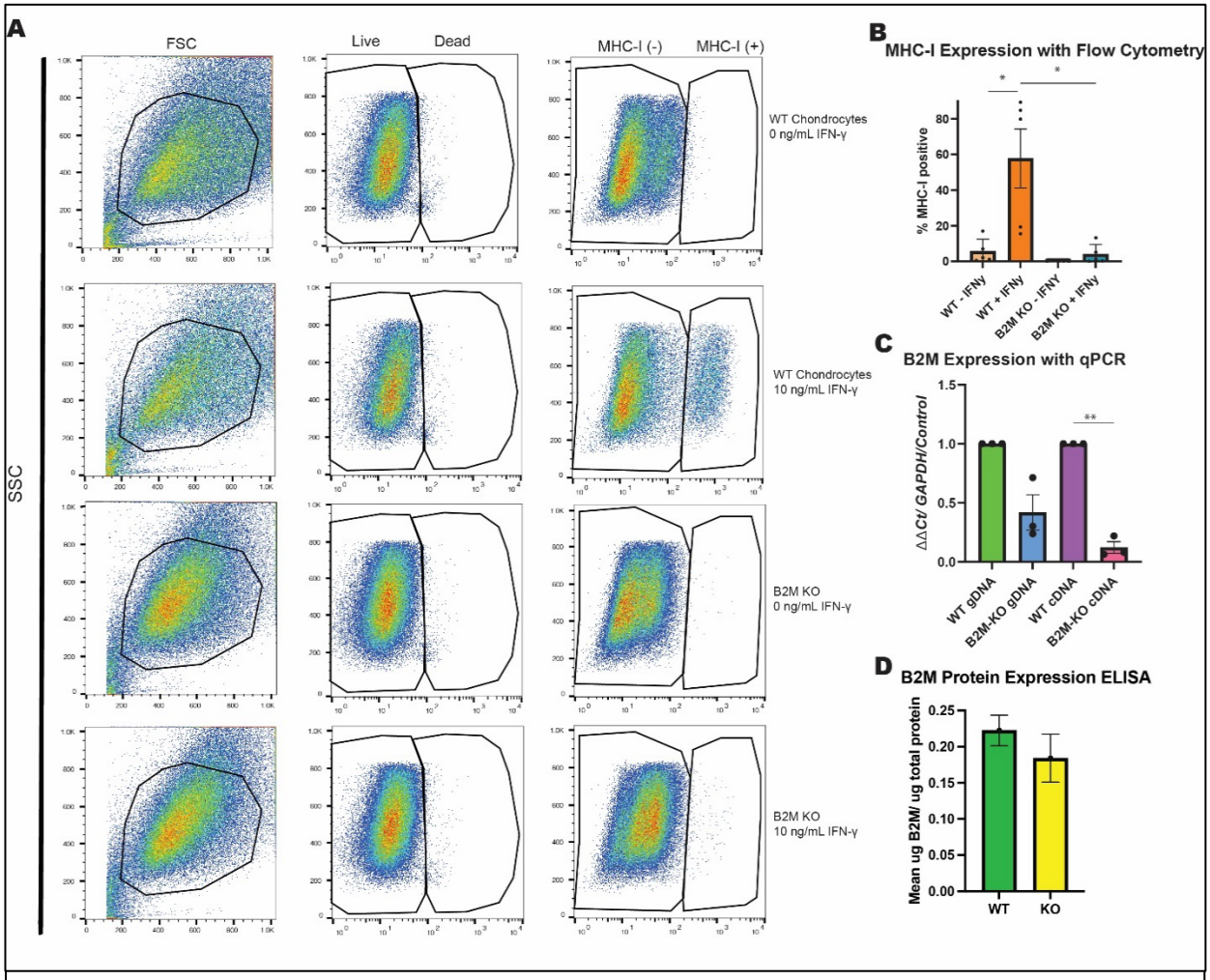


Figure 4: Upregulation of MHC-I in the presence of IFNγ. The groups are categorized as follows: wildtype (WT) chondrocytes, chondrocytes transfected with mock control (PX459), or chondrocytes transfected with PX459 with ligated B2M oligos (B2M KO). Panel (A) shows the gating strategy for the flow analysis. The y axis is side scatter for all plots whereas the x axis is the following channels from left to right: Forward Scatter (FSC) (first column), Viable cells (second column), or MHC-I positive cells (third column). Panel (B) is displaying the average number of MHC-I positive cells from three separate experiments (N=3 donors; n=5 replicates). Panel (C) QPCR Analysis. Pig chondrocytes transfected with empty PX459 backbone plasmid or B2M-KO chondrocytes were analyzed with qPCR for genomic and cDNA expression. All data is calculated by ΔΔCt normalizing to GAPDH and PX459 backbone as the control. B2M-KO chondrocytes showed a decrease in expression of B2M gene at both the genomic and cDNA level (N=3). Panel (D) ELISA. Wildtype (WT) chondrocytes show higher protein expression of B2M in comparison to B2M KO chondrocytes (N=3). Results were considered statistically significant at $p<0.05$ (*).

3b.3b MHC-I Expression of β2M-KO Chondrocytes

Wildtype and β2M-KO chondrocytes were pre-stimulated for 3 days with or without 10ng/ml IFNγ. Cells were stained as previously described in 3a. Wildtype and β2M-KO chondrocytes showed little to no expression of MHC-I with no IFNγ pre-stimulation. However, following stimulation with IFNγ, MHC-I expression increased in wildtype cells but remained low to no expression in β2M-KO chondrocytes (**Figure 4A**). MHC-I expression was quantified on three different knockout cells demonstrating a downregulation in in MHC-1 protein surface expression between WT and KO cell lines ().

3b.3c q-RT-PCR of β2M expression

RNA extracted from wildtype and β2M-KO chondrocytes was used to synthesize cDNA as previously described in 2b.3c. The level of β2M expression was quantified and normalized to GAPDH expression. All calculations were formulated using the delta-delta-CT method. PCR analysis investigated the expression of β2M at the genomic and RNA levels. There were no significant changes in gene length at the genomic level; however, there was a significant decrease in β2M expression in β2M-KO chondrocytes in comparison to WT chondrocytes at the RNA level (**Figure 4C)**. The decrease in β2M expression at the RNA level can be explained by the presence of a premature stop codon immediately following the PAM sequence in exon 2 of porcine β2M.

3b.3d ELISA (Figure 4d)

β2M protein expression trended higher in wildtype chondrocytes compared to β2M-KO chondrocytes but insignificantly **(Figure 4d)**.

3b.3e Off-Target Analysis

We identified 427 total off targets, 13 of which were exonal. The total off-targets disagree with Sake et al. [19] who found only 66 off-targets and no exonal off-targets despite using the same guide sgRNA and off-target analysis software **(Supplemental Table 2)**.

3c. Validation of Knockout Functionality

3c.1– Immunologic Effects of β2M-KO on Allogeneic Peripheral Blood Mononuclear Cell (PBMC) Proliferation (Figure 5a)

In order to determine the functional efficacy of knocking out β2M, we explored the reactivity of allogeneic PBMCs to β2M-KO and WT chondrocytes by measuring PBMC proliferation. Allogeneic PBMCs had significantly higher proliferation when co-cultured with wildtype chondrocytes compared to β2M-KO chondrocytes **(Figure 5)**. In addition, although insignificant, PBMCs had higher proliferation when co-cultured with wildtype chondrocytes compared to PBMCs stimulated alone.

3c.1– Immunologic Effects of β2M-KO on Lymphocyte Granzyme Release (Figure 5b)

Since cytotoxic T cells (CD8 lymphocytes) and NK cell's mechanism of killing target cells is via granzyme mediated perforation, we explored granzyme concentrations in the supernatants from co-culture experiments using ELISA. We detected no significant differences in granzyme secretion in WT and β2M-KO co-culture supernatants **(Figure 5b)**.

3d. Tissue engineering of immuno-universal cartilage

3d.1 – Gross appearance of the constructs (Figure 6a)

Tissue engineered cartilage constructs from both WT and β2M-KO chondrocytes were created in order to validate that the KO had no effect on chondrogenic capacity. The morphology of wildtype and β2M-KO sourced cartilage constructs was smooth and flat (**Figure 6A**) and not grossly different from each other.

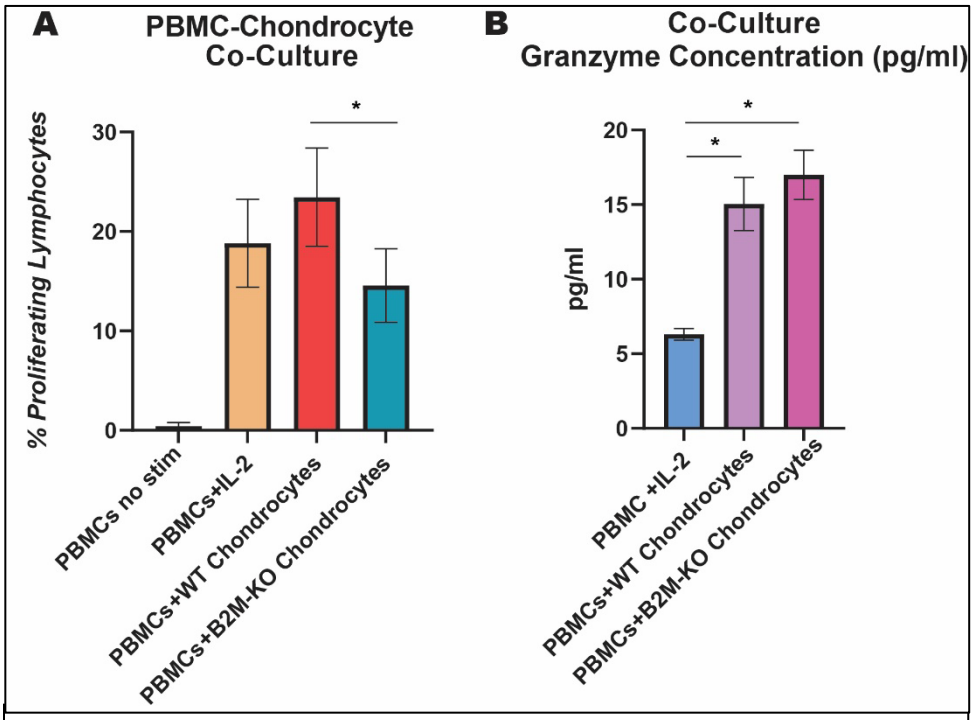


Figure 5: Lymphocyte Reactivity to Wildtype vs β2M-KO Chondrocytes. **(A)** Peripheral Blood Mononuclear Cells (PBMCs) were cultured in four groups: PBMCs alone with no stimulation, PBMCs alone with IL-2 stimulation, PBMCs with IL-2 stimulation and wildtype chondrocytes, and PBMCs with IL-2 stimulation and β2M-KO chondrocytes. PBMC proliferation was measured with Edu-ClickIt proliferation assay. PBMCs had higher proliferation when co-cultured with wildtype chondrocytes than when cultured with β2M-KO chondrocytes or PBMC alone with stimulation. **(B)** The supernatant of PBMC-chondrocyte co-cultures were collected for granzyme analysis. Results show significant differences between control wells and both co-culture groups. However, there were no significant differences between wildtype and β2M-KO co-culture wells. Results were considered statistically significant at $p<0.05$ (*).

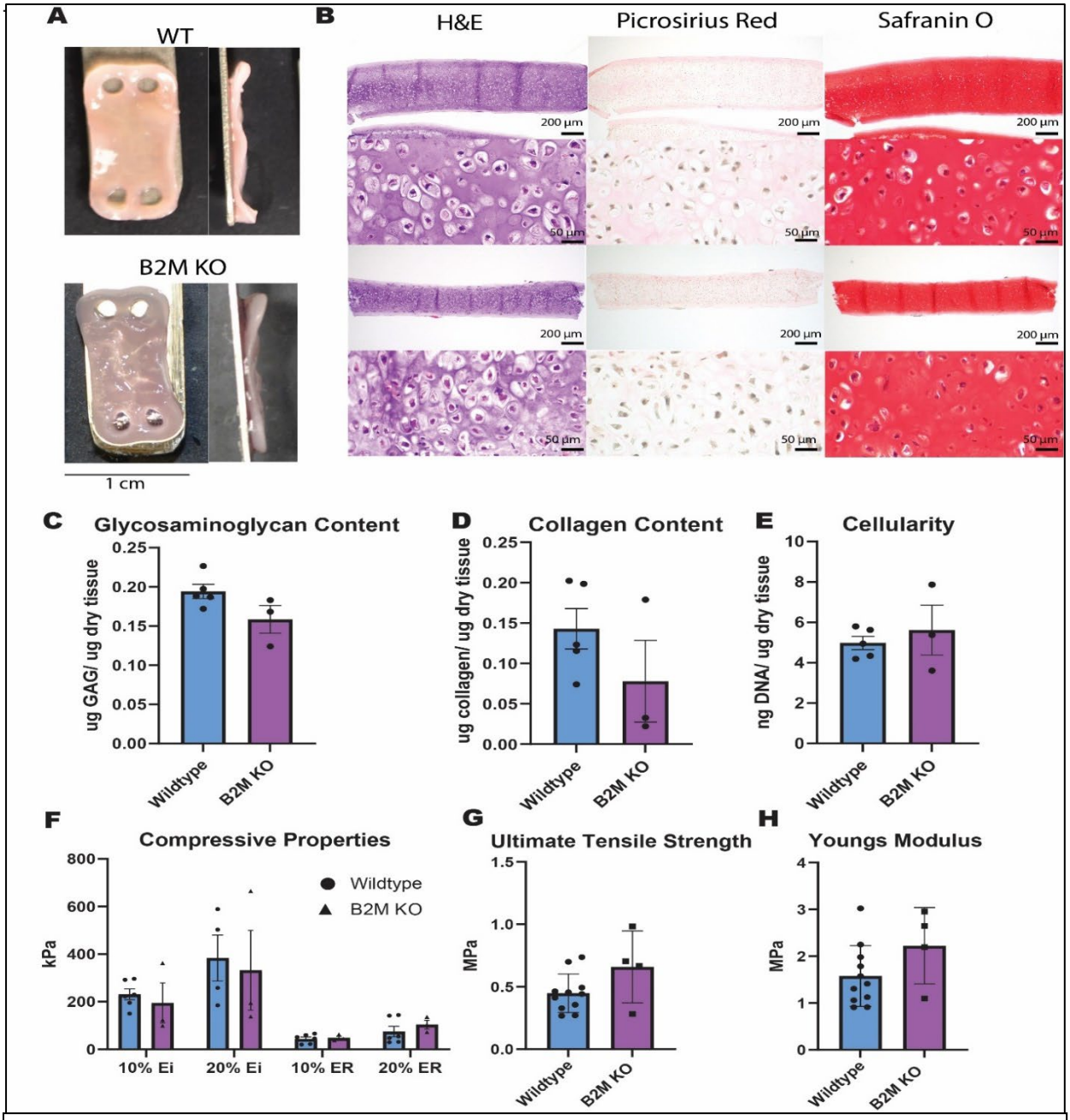


Figure 6: Tissue-engineering of immune universal cartilage constructs. (A) Gross morphology of cartilage constructs derived from wildtype costal chondrocytes (n=6) or β2M-KO chondrocytes (n=3). (B) Histology of cartilage constructs derived from wildtype costal chondrocytes or β2M-KO chondrocytes. H&E staining shows overall cellularity whereas Picrosirius red and Safranin-O show collagen and GAG staining, respectively. (C) Cartilage constructs derived from wildtype costal chondrocytes or β2M-KO chondrocytes show similar GAG concentrations. (D) Cartilage constructs derived from wildtype costal chondrocytes or β2M-KO chondrocytes show slightly less collagen in β2M-KO. (E) Cartilage constructs derived from wildtype costal chondrocytes or β2M-KO chondrocytes show similar cellular density. (F) Cartilage constructs from wildtype costal chondrocytes or β2M-KO chondrocytes show similar compressive properties at 10% and 20% strain for both instantaneous and relaxation moduli. (G) Cartilage constructs from wildtype costal chondrocytes or β2M-KO chondrocytes show similar ultimate tensile strength. (H) Cartilage constructs from wildtype costal chondrocytes or β2M-KO chondrocytes show similar young's modulus. Results were considered statistically significant at $p<0.05$ (*).

width and 16.1035 mm ± 2.73 mm in length. The average dimensions of β2M-KO chondrocyte derived cartilage constructs were 7.937 mm ± 0.3985 mm in width and 16.357 mm ± 0.5831 mm in length. Based on gross morphology of the cartilage constructs, there were no detectable differences.

3d.2 – Histology (Figure 6b)

On histological and morphological evaluation of the constructs generated from the WT costal chondrocytes or β2M-KO chondrocytes no obvious differences were noted. Both constructs were equally cellular and had even distribution of cells though the tissue. All cells appeared viable and exhibited normal chondrocyte morphology, where single cell resides within a single lacuna surrounded by homogeneous basophilic extracellular matrix. The extracellular matrix basophilic staining on H&E indicates abundance of glycosaminoglycans. This observation is supported by strong dark pink-orange staining with Safranin O/Fast green. Collagen is highlighted in pale pink in the ECM between lacunae and in the acellular band circumferentially with Picro Sirius Red stain.

3d.3 – Biochemical data (Figure 6c-e)

Biochemical analyses supported the histological observations. Biochemical analyses revealed no significant differences between WT and β2M-KO in total GAG, collagen, and DNA content. **(Figure 6C)**.

3d.4 – Mechanical data (Figure 6f-g)

We performed compressive and tensile testing on cartilage constructs to determine if the KO affected the mechanical durability of the tissue. TE cartilage constructs derived from wildtype and β2M-KO chondrocytes, showed similar trends in compressive (**Figure 6F)** and tensile properties (**Figure 6G)**. No significant differences were detected for relaxation modulus and instantaneous modulus at 10% and 20% strain, respectively, between wildtype and β2M-KO chondrocytes derived TE cartilage constructs. In

addition, no significant differences were detected for ultimate tensile strength (UTS) and Young's modulus between wildtype and β2M-KO chondrocytes derived TE cartilage constructs. In conclusion, no significant differences in mechanical durability were caused from the KO.

4. Discussion

This study is the first to degenerate MHC-I-null, immuno-universal scaffold-free cartilage constructs. Additionally, this study showed that MHC I expression in chondrocytes is upregulated under inflammatory conditions and that co-culture of such chondrocytes induces allogenic lymphocyte proliferation. MHC-I-null chondrocytes were generated through the disruption of β2M gene using CRISPR-Cas9 technology. The knockout was confirmed with Sanger sequencing, flow cytometry, qPCR, and ELISA. The immunological difference between the KO and WT chondrocytes was then demonstrated in series of co-culture experiments with allogeneic lymphocytes. We detected a significant decrease in lymphocyte proliferation in co-cultures with β2M-KO chondrocytes vs. WT. In addition, we successfully tissue-engineered scaffold-free cartilage constructs from the genetically modified chondrocytes. These constructs displayed similar biochemical composition and mechanical robustness to constructs sourced from wildtype chondrocytes. Collectively, this study demonstrates feasibility of engineering immuno-universal cartilage constructs or cell-suspensions for potential therapeutic applications.

The major hurdle to the clinical translation of allogeneic chondrocytes, is the lack of assurance of immunological safety and efficacy. The main culprit to the immunological safety concerns of transplanting allogeneic cells and tissues is the expression of major histocompatibility complex MHC I molecule. Our data demonstrate that MHC I play a role in the immune recognition of chondrocytes by allogeneic lymphocytes and that this recognition is enhanced by IFNγ stimulation, which is very realistic scenario in arthritis. Our findings agree with findings by Adkisson et al. [24], who showed that chondrocytes have

relatively low expression of MHC-I unless stimulated with IFNγ (**Figure 2)**. However, our results contrast with Adkisson et al. in regard to lymphocyte proliferation, who argued that chondrocytes are immune evasive due to high protein expression of B7 co-stimulatory inhibitors and chondrocyte's inability to stimulate T cell proliferation[24]. The latter discrepancy can be due to the difference in the lymphocyte proliferation techniques used. Additionally, according to Hu et al. [25], there could be several inflammatory subtypes of chondrocytes that may participate in the activation of immune cells and complement-mediated mechanisms in osteoarthritis due to their higher expression of inflammatory chemokines. Further investigation, particularly using in vivo model will help determining the importance of MHC-I molecule in bio-integration of native or engineered cartilage allografts.

This study successfully reproduced the experimentation by Sake et al [19], where MHC-I expression was abolished via genetic disruption of β2M gene. We also confirmed that MHC-I expression is significantly downregulated even in the presence of IFNγ (**Figure 4).** Provided MHC-I is a polygenic and polymorphic trait, achieving its silencing via disruption of a single gene is an elegant, efficient, and time-saving approach. This study's results show that successful disruption of the gene is reproducible in multiple clones (**Figure 3)** and that puromycin selection of the KO cells is feasible and effective, because the knockout was maintained throughout multiple passages (**Supplemental Figure 3**). The latter is significant, because it eliminated the need in flow-assisted cell sorting which can be expensive, requires sophisticated equipment and can be damaging to cells. To ensure the consistency of the KO, we performed at least two rounds of puromycin selection. Interestingly, this study's results indicate that despite the disruption, β2M gene is still transcribed (PCR data) and translated to protein (ELISA data). These results suggest that the KO has a greater effect at the translation level then at the genomic level. Nevertheless, functional MHC-I complex is not achieved (flow cytometry data) **(Figure 4)**. These observations suggest that the assembly

of MHC-I is dependent on its functional counterparts and more studies are needed to determine the fate and the amino-acid sequence of the β2M protein.

The co-culture assays demonstrated a decrease in allogeneic peripheral blood mononuclear cell (PBMC) proliferation when cultured with β2M-KO chondrocytes in comparison to wildtype chondrocytes **(Figure 5)**. In addition, although insignificant, PBMCs had higher proliferation when co-cultured with wildtype chondrocytes compared to PBMCs stimulated alone. These results indicate that wildtype chondrocytes have immunogenic properties and that engineering β2M-KO chondrocytes would be necessary to shield chondrocytes from immunologic detection during cartilage transplantation. This data is further validated by observations made by Wang et al. who found reduced proliferation of peripheral blood mononuclear cells when co-cultured with induced pluripotent stem cells with genetically disrupted β2M gene in a monkey model [26]. We briefly explored the total number of CD8 T cells and total number of proliferating CD8 T cells in one KO cell line. Our results showed a reduction in the total number of CD8 T cells and total number of proliferating CD8 T cells when allogeneic PBMCs were co-cultured with β2M-KO chondrocytes in comparison to wildtype chondrocytes (data not shown). These observations indirectly correlate with data found by Gornalusse et al [27] who found that β2M-KO embryonic stem cells were not lysed by CD8 T cells *in vitro*. These observations agree with the common knowledge of MHC-I-CD8 T cell interaction. Specifically, one of CD8 T cell's functions is to recognize MHC-I complex and foreign or altered peptides presented by it [13]. In case of recognition of non-self CD8 become polarized and activated to lyse the target cells.

Although elimination of MHC expression reduces lymphocyte recognition, the downregulation of MHC can be detected by natural killer (NK) cells through the "missing self-response" [13]. In addition, the presence of minor histocompatibility molecules and tissue-specific antigens may still result in rejection

[13]. Fortunately, various strategies mirroring mechanisms seen in nature have been proposed for cells to evade immune detection [28]. One strategy is the genetic induction of immune-modulatory non-classical MHC molecules. Gornalusse et al [27] demonstrated that β2M null embryonic stem cells and their differentiated cell types were able to evade NK cell detection with the genetic knock-in of HLA-E *in vitro* and *in vivo* [27]. In addition, gene-edited cells also avoided humoral responses [27]. The results of the granzyme ELISA in this study suggest that there are no differences in NK mediated lysis of β2M-KO chondrocytes., Therefor, further genetic manipulation to evade NK cells may not be needed for chondrocytes or cartilage tissue. Albeit, more *in vitro* and *in vivo* investigations of β2M-KO chondrocytes or β2M-KO chondrocyte derived cartilage tissue is needed to determine if further manipulation is needed to evade NK cell detection.

Acknowledging potential off-target effects of CRISPR/Cas9 gene disruption we identified 427 total off targets, 13 of which were exonal. The predicted function of one of the exonal off-targets was cell growth and proliferation **(Supplemental Table 2).** Nevertheless, we were able to expand the KO chondrocytes to the millions of cells sufficient to tissue engineer dozens on cartilage constructs. These constructs had biomechanical and histological properties on par with constructs derived from the wild type cells thus we do not suspect any significant off-target effects, although further studies are needed to confirm o chromosomal aberrations or disruption of other genes.

Supplemental Table 2

General info	
sgRNA	GAGTAAACCTGAACCTTCGG
Total	427

Summary of exonal off targets

Location	Off Target Sequence	Mismatch	locusDesc	Predicted function
Exon 1	ATGGGTAGACCTGATCCTTCCGG	4	NM_001129978.2	Part of the mitochondrial complex of the respiratory chain
Exon 2	CGTGAGTAAACCTGAACCTTCGG	0	NM_213978.1	Part of B2M
Exon 3	GAGTAAACCTGAACCTTCGGGGG	0	NM_213978.1	Part of B2M
Exon 4	GTGAGTAAACCTGAACCTTCGGG	0	NM_213978.1	Part of B2M
Exon 5	GGTGAGGAAACCCGAATCTTAGG	4	XM_003135296.5	DNA binding, enzyme binding, and phosphoprotein binding
Exon 6	GGATTAAACCTGAACCCTCATGG	4	XM_003482013.4	Membrane protein
Exon 7	TGTGAAGGAACCTGAACCTTTGG	4	XM_021075901.1	Striated muscle formation
Exon 8	GTGAGAAAACCCGAACCATATGG	4	XM_021083173.1	Cell growth and proliferation
Exon 9	GGATTAAACCTGAACCCTCATGG	4	XM_021093818.1	Mediates interaction with transcriptional coactivators and ligand bound nuclear receptors (ex: thyroid and retinoid)
Exon 10	GGAGAAAATCAGAACCTTCGTGG	4	XM_021095250.1/XM_021095249.1	Important for neuron/central nervous system development
Exon 11	GTGGGTAATGCTGAACCTTCTGG	3	XR_002338040.1/XR_002338039.1/XR_002338038.1/X	Promotes pre-RNA splicing
Exon 12	TGAGTAAACCTGAACCTTCGGGG	0	XR_002345118.1/XR_002345114.1/XM_021096362.1	Part of B2M
Exon 13	GTGAGGAACCTTGAACCTTACGG	4	XR_002347074.1/XM_021102546.1/XM_001927783.5/	Essential for targeting exocytic vesicles to specific docking sites on the plasma membrane

Tissue engineered cartilage constructs derived from β2M-KO chondrocytes revealed no biomechanical or histological differences from cartilage constructs derived from wildtype chondrocytes (**Figure 6)**. No studies, to our knowledge, have constructed cartilage tissue from genetically modified cells. In the current study, we observed a slight decrease in cartilage compressive properties as well as collagen and glycosaminoglycan content in comparison to wildtype derived cartilage constructs, although insignificant. This data indirectly suggests that chondrogenesis is not affected by genetically modified chondrocytes. This conclusion aligns with Chen et al [29] who observed enhanced chondrocyte proliferation, ECM synthesis and expression of collagen type II in chondrocyte sheets following microRNA targeting of MMP16. In addition, Cui et al [30] showed that cartilage-derived morphogenetic protein 1 transgenic tissue-engineered chondrocyte sheets were successfully constructed, transplanted, and repaired rabbit laryngeal cartilage defects. More cartilage characterization studies are needed to determine if β2M-KO chondrocyte derived cartilage tissue is functionally biomimetic and can integrate and survive long-term in vivo.

In conclusion, the data from this study uncover chondrocyte immunogenic properties and introduce β2M-KO chondrocytes as a potential solution for cell therapy or cartilage tissue engineering. This study's most significant finding is strong evidence against the claim for cartilage immune privilege and a decrease in PBMC proliferation when β2M-KO chondrocytes were co-cultured with allogeneic PBMCs. The limitations of this study were the inability to explore the proliferation and polarization of various lymphocyte subsets due to limited availability of porcine antibodies and insufficient understanding of porcine lymphocytic immunophenotypes. Nevertheless, the results of this study challenge and invite exploration into cartilage immunology with various inflammatory environments. Future in vivo studies need to explore the

relevance and the effect of MHC I matching in bio integration of tissue engineered cartilage constructs and single cells.

5. References

1. *Tong, L., et al., Current understanding of osteoarthritis pathogenesis and relevant new approaches. Bone Research, 2022.* ***10****(1): p. 60.*
2. Montoya, F., et al., *Clinical and experimental approaches to knee cartilage lesion repair and mesenchymal stem cell chondrocyte differentiation.* Biol Res, 2013. **46**(4): p. 441-51.
3. Urlić, I. and A. Ivković, *Cell Sources for Cartilage Repair-Biological and Clinical Perspective.* Cells, 2021. **10**(9).
4. Laurie, S.W., et al., *Donor-site morbidity after harvesting rib and iliac bone.* Plast Reconstr Surg, 1984. **73**(6): p. 933-8.
5. Skouteris, C.A. and G.C. Sotereanos, *Donor site morbidity following harvesting of autogenous rib grafts.* J Oral Maxillofac Surg, 1989. **47**(8): p. 808-12.
6. Oakeshott, R.D., et al., *A clinical and histologic analysis of failed fresh osteochondral allografts.* Clin Orthop Relat Res, 1988(233): p. 283-94.
7. Stevenson, S., et al., *The fate of articular cartilage after transplantation of fresh and cryopreserved tissue-antigen-matched and mismatched osteochondral allografts in dogs.* J Bone Joint Surg Am, 1989. **71**(9): p. 1297-307.
8. Friedlaender, G.E., et al., *Long-term follow-up of patients with osteochondral allografts. A correlation between immunologic responses and clinical outcome.* Orthop Clin North Am, 1999. **30**(4): p. 583-8.
9. Sun, K., C. Tao, and D.A. Wang, *Scaffold-free approaches for the fabrication of engineered articular cartilage tissue.* Biomed Mater, 2022. **17**(2).
10. Smith, B., I.R. Sigal, and D.A. Grande, *Immunology and cartilage regeneration.* Immunol Res, 2015. **63**(1-3): p. 181-6.
11. Garrity, C., et al., *A Fresh Glimpse into Cartilage Immune Privilege.* Cartilage, 2022. **13**(4): p. 119-132.
12. Li, H., et al., *Applications of genome editing technology in the targeted therapy of human diseases: mechanisms, advances and prospects.* Signal Transduction and Targeted Therapy, 2020. **5**(1): p. 1.
13. Murphy, K. and C. Weaver, *Janeway's immunobiology*. 2017. p. 213, 214-216, 231-233, 245-246, 357-358, 364-365, 367-371.
14. Shao, L., et al., *Knockout of beta-2 microglobulin enhances cardiac repair by modulating exosome imprinting and inhibiting stem cell-induced immune rejection.* Cell Mol Life Sci, 2020. **77**(5): p. 937-952.
15. Naeimi Kararoudi, M., et al., *Assessment of Beta-2 Microglobulin Gene Edited Airway Epithelial Stem Cells as a treatment for Sulfur Mustard Inhalation.* Front Genome Ed, 2022. **4**: p. 781531.
16. Ka, Y., et al., *Improved engraftment of human peripheral blood mononuclear cells in NOG MHC double knockout mice generated using CRISPR/Cas9.* Immunol Lett, 2021. **229**: p. 55-61.
17. Vapniarsky, N., et al., *Tissue Engineering of Canine Cartilage from Surgically Debrided Osteochondritis Dissecans Fragments.* Ann Biomed Eng, 2022. **50**(1): p. 56-77.
18. Pham, T.M., et al., *Elevation of Pro-Inflammatory Cytokine Levels Following Intra-Articular Fractures-A Systematic Review.* Cells, 2021. **10**(4).

19. Sake, H.J., et al., *Possible detrimental effects of beta-2-microglobulin knockout in pigs.* Xenotransplantation, 2019: p. e12525.
20. Montague, T.G., et al., *CHOPCHOP: a CRISPR/Cas9 and TALEN web tool for genome editing.* Nucleic Acids Research, 2014. **42**(W1): p. W401-W407.
21. Tan, Y.S. and Y.L. Lei, *Isolation of Tumor-Infiltrating Lymphocytes by Ficoll-Paque Density Gradient Centrifugation.* Methods Mol Biol, 2019. **1960**: p. 93-99.
22. Vapniarsky, N., et al., *Tissue engineering toward temporomandibular joint disc regeneration.* Sci Transl Med, 2018. **10**(446).
23. Carson, L.F., *Histotechnology : a self instructional text*. 2nd ed. 1997, Chicago, IL: American Society of Clinical Pathology.
24. Adkisson, H.D., et al., *Immune evasion by neocartilage-derived chondrocytes: Implications for biologic repair of joint articular cartilage.* Stem Cell Res, 2010. **4**(1): p. 57-68.
25. Hu, X., et al., *Identification of cellular heterogeneity and immunogenicity of chondrocytes via single-cell RNA sequencing technique in human osteoarthritis.* Front Pharmacol, 2022. **13**: p. 1004766.
26. Wang, X., et al., *Diminished expression of major histocompatibility complex facilitates the use of human induced pluripotent stem cells in monkey.* Stem Cell Res Ther, 2020. **11**(1): p. 334.
27. Gornalusse, G.G., et al., *HLA-E-expressing pluripotent stem cells escape allogeneic responses and lysis by NK cells.* Nat Biotechnol, 2017. **35**(8): p. 765-772.
28. Lanza, R., D.W. Russell, and A. Nagy, *Engineering universal cells that evade immune detection.* Nat Rev Immunol, 2019.
29. Chen, X., et al., *Chondrocyte sheet in vivo cartilage regeneration technique using miR-193b-3p to target MMP16.* Aging (Albany NY), 2019. **11**(17): p. 7070-7082.
30. Cui, Y., et al., *Effects of cartilage-derived morphogenetic protein 1 (CDMP1) transgenic mesenchymal stem cell sheets in repairing rabbit cartilage defects.* Genet Mol Res, 2016. **15**(2).

Chapter 3

Exploration of Auricular Chondrocytes as a Cell Source for Cartilage Tissue Engineering for Temporomandibular Joint Disc Using a Porcine Model

Authors:

Nicole Gonzales[1], Carissa Garrity[1], Iris Rivas[1], Natalia Vapniarsky[1*]

[1]Department of Pathology, Microbiology, and Immunology, University of California, Davis, Davis, CA, United States of America

*Corresponding author

Abstract

Temporomandibular joint (TMJ) disorder is characterized by the degeneration, thinning and occasional perforation of the fibrocartilaginous disc within the joint. This disorder leads to arthritis which is irreversible due to the poor regenerative capacity of TMJ disc. Current tissue engineering (TE) therapies offer biomimetic cartilage constructs derived from costal chondrocytes for implantation; however, there are major limitations to utilizing costal chondrocytes as the primary autologous cell source is the invasive tissue collection and progressive ossification of costal cartilage with age. Furthermore, costal cartilage is not elastic type of cartilage while TMJ disc is known to poses elastic fibers in the postero-lateral attachment sites. These limitations invited the exploration of novel cell sources that would eliminate both issues. The objective of this study is to determine if auricular cartilage can be used to generate a TE cartilage constructs with chondrogenic properties akin to the native TMJ disc. We tested the utility of auricular chondrocytes for cartilage TE using scaffold-free self-assembling technology. We successfully generated cartilage constructs from auricular chondrocytes from three donors. We found that constructs

derived from auricular chondrocytes had an instantaneous compressive stiffness between 37kPa- 472kPa. The Young's modulus was 2.0 MPa and the ultimate tensile strength (UTS) was 0.619 MPa. Auricular chondrocyte derived constructs contained 0.144 ug collagen per ug dry weight, 0.185ug GAG per ug dry weight, 0.384ng per ug dry weight, and 81.95 ug elastin per mg dry weight. In conclusion, the results from this study show that auricular chondrocytes can be used a reliable and easily accessible cell source for TE cartilage implants for TMJ disorders.

Key Words: auricular, chondrocytes, tissue-engineering, temporomandibular joint disorder

Introduction:

The temporomandibular joint (TMJ), or jaw joint, is a synovial joint that essential for everyday functions such as talking and chewing. Temporomandibular joint disorder (TMD) is usually characterized by multiple symptoms such as headaches, neck, back, and TMJ pain [31]. This disorder affects 5-12% of the world's population with a high prevalence in younger persons and women[32]. Although some individuals with this disorder do not seek out medical care, a national survey reported that total health care costs per 6-month period for an individual with TMD ranged from $400-625 US dollars [33] with a total economic impact of $4 billion annually [34]. These costs are mainly spent on alleviating the symptoms of the disorder rather than cure. Temporomandibular joint disc (TMJD) derangement has been described as the main precursor to TMD and degeneration of the entire joint. The TMJD is a fibrocartilaginous structure of the TMJ, positioned between the mandibular condyle and the base of the skull [22]. Its main functions are to bear mechanical load, allow for congruity between the parts of the joint, and provide smooth movement between the articulating components of the TMJ [22]. TMJD conditions include disc displacement, disc thinning, and disc perforation [35, 36]. The complex mechanism of these conditions

continues to be elucidated through research, however a successful therapeutic treatment for TMD's has yet to be found.

Current TMD treatments vary from symptomatic therapy for those who are in the early stages of TMD or invasive surgery which is reserved for more advanced cases [37]. Invasive surgeries entail either diskectomy [38] or replacement with a total prosthetic joint [39]. Although diskectomies relieve patients' symptoms, this procedure causes condylar remodeling[40-42]. While total prosthetic joints induce heterotopic bone formation around the implant leading to decreased joint mobility and pain [39, 42]. The lack of efficacious treatment options invites the discovery of a novel therapy for TMJD.

Advancements in tissue engineering technology offer promising tissue replacement options for patients with TMD. Tissue engineering is the combination of cells, scaffolds and biochemical and mechanical stimuli to construct a new tissue[43-45]. However, scaffold tissue engineering presents the risk of scaffold degradation and toxicity, immunogenicity, and scaffold-driven alteration of the cell phenotype [46]. Scaffold-free method eliminates scaffold-related pitfalls and was demonstrated to be successful in cartilage tissue engineering [47]. This methodology allows chondrocytes to self-assemble and recapitulate the properties of native tissue where extracellular matrix is produced by the cells instead of being provided exogenously [47-49]. Previous studies utilized both articular chondrocytes and costal cartilage [50, 51] as a cell source for TMJD tissue engineering. Although costal chondrocytes yield implants with robust extracellular matrix and high mechanical integrity [22] their use for autologous applications is not as attractive. The latter is due to significant second site morbidity that would be needed for the harvest of cells. Furthermore, costal cartilage is not an elastic type of cartilage and thus costal chondrocytes are not programed to generate elastic fibers [52]. Additionally, costal cartilages have age-dependent tendency to undergo ossification [53], rendering them even more limited for use as a cell source especially

in the adults. Cumulatively, these limitations call for the exploration of a novel cell source. Recently, auricular chondrocytes (AuC) (cartilage cells from the ear) have emerged as a potential cell source for tissue engineering [54]. Provided the elastic fibers are an essential structural component of the TMJ disc [55] auricular cartilage elastic properties and less invasive tissue harvesting make auricular cartilage an attractive potential cell source for TMJD tissue engineering.

In order to translate this to human medicine, tissue engineered TMJ implants need to be evaluated for safety and feasibility in large animal models. The farm pig model is often utilized in research settings, especially within the dentistry and maxillofacial sector [56]. Since pigs are physiologically and anatomically similar to humans in their maxillofacial characteristics, this makes them a suitable research subject for this study, especially the Yucatan Minipig [57]. Due to its miniature form, the Yucatan Minipig offers a solution to the farm pigs pitfalls of handling, rapid growth, housing space requirements, surgery, anesthesia, and food costs [57]. Furthermore, elastic fibers are an important constitutive of the TMJ disc and in human disc their highest concentration in in the posterior and lateral attachments [58]. In one report from 1975 similar distribution of elastic fibers was reported in minipigs [59]. Auricular cartilage is defined as elastic type of cartilage due to presence of elastic fibers [60] while costal cartilage is not. Thus, additional advantage of auricular chondrocytes could be their native ability to generate elastic fibers.

The first objective of this study was to examine the population kinetics of AuC's expanded in monolayer. The second objective of this work was to generate cartilage constructs derived from AuC's using the established scaffold-free assembling methodology [22]. Objective three was to characterize and report the biochemical, biomechanical, and histologic properties of AuC-derived cartilage constructs. We hypothesized that dozens of mechanically robust and biologically comparable cartilage constructs can be manufactured from a small amount of primary auricular chondrocytes.

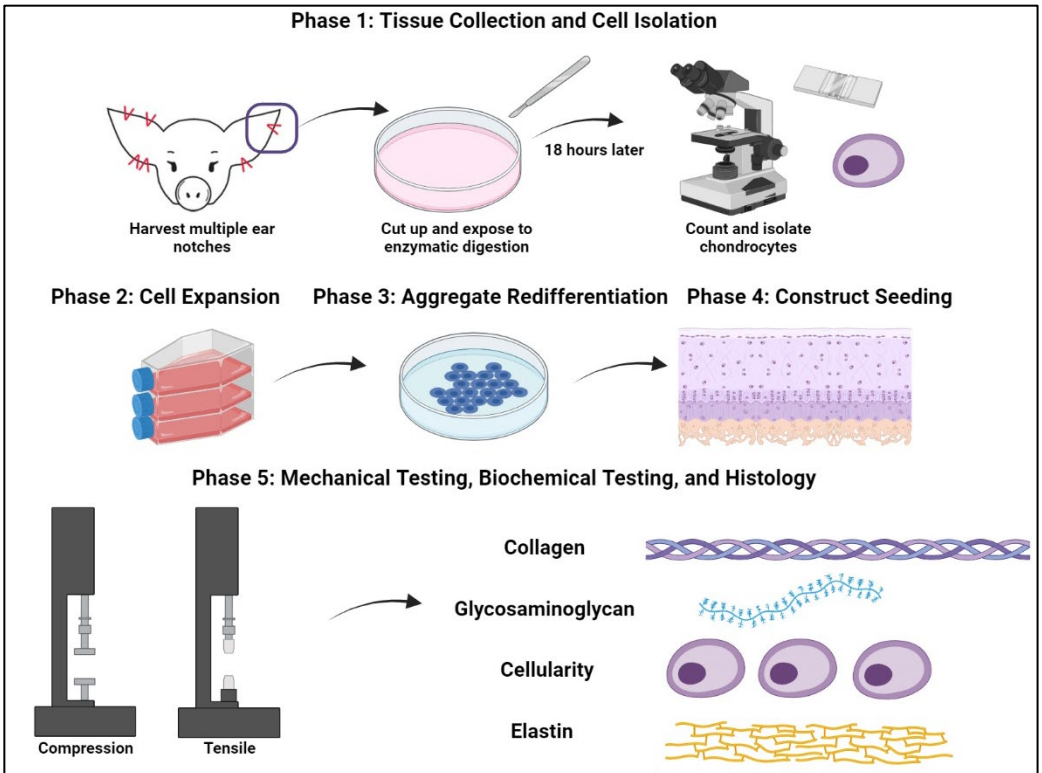


Figure 1: Study Design: Auricular chondrocytes were isolated for porcine ear notches. Tissue was minced and enzymatically digested into single cell suspension. Cells were counted then frozen or plated immediately for expansion. Auricular chondrocytes underwent several weeks of monolayer expansion followed by 10 days of suspended aggregate culture to induce re-differentiation of cells. Following aggregate culture, cells were seeded in high density into custom made agarose wells where cells self-assembled into cartilage tissue. Tissue was grown for additional 28 days following seeding. Upon completion of cartilage tissue-engineering protocol, the tissue was subjected to mechanical, biochemical, and histologic analysis.

Method:

Study Design **(Figure 1)**

Auricular chondrocytes were isolated for porcine ear notches. Tissue was minced and enzymatically digested into single cell suspension. Cells were counted then frozen or plated immediately for expansion. Auricular chondrocytes underwent several weeks of monolayer expansion followed by 10 days of suspended aggregate culture to induce re-differentiation of cells. Following aggregate culture, cells were seeded in high density into custom made agarose wells where cells self-assembled into cartilage tissue.

Tissue was grown for additional 28 days following seeding. Upon completion of cartilage tissue-engineering protocol, the tissue was subjected to mechanical, biochemical, and histologic analysis.

Experiment

Tissue Collection/ Cell Isolation

Triangular ear notch samples (1x0.8x06cm on average) were harvested from three Yucatan Minipigs following standard procedure of pig labeling for identification purposes where ear notches are typically discarded. Sterile instruments were used to collect the tissue and to separate the auricular cartilage from the skin of the pina. The cartilage was cut into 0.5mm pieces and transferred into a 6-well plate to digest in 2-3 ml of 2mg/mL collagenase solution (Worthington Biochemical Corp. 290 active unites/mg DW) supplemented with 3% fetal bovine serum (FBS) (Atlanta Biologicals) for 18 hours at 37°C and 5% CO2 with orbital rotation at 60 RPM. Upon digestion the cells were rinsed and a cell count was obtained via hemocytometer using Trypan blue vital staining. Chondrocytes that were not immediately used were stored in 90% FBS and 10% Dimethyl Sulfoxide (DMSO) (Corning © DMSO, Mediatech Inc.) and cryopreserved in liquid nitrogen.

Chondrocyte Expansion in Monolayer

Auricular chondrocytes were seeded into cell culture flasks with expansion media (Table 1) until cells reached 80% confluency. Cultures were maintained in a humidified atomosphere at 37C and 5% CO2.Chondrocytes were passaged until an adequate number of cells was reached for the aggregate redifferentiation phase. Media was replaced every 3-4 days or at every passage.

For passaging, 0.05% Trypsin (Gibco 0.05% Trypsin-EDTA 1X, Cat#25300-054) was added to the monolayers and left for 10 min at 37°C. Cells were collected, spun down at 400 RPM, and were further digested in 2mg/mL collagenase solution supplemented with 30 μL/mL (3% v/v) FBS for one hour at 37°C

to remove any residual ECM. Once the collagenase digestion was complete, cells were counted and assessed for viability with Trypan blue vital staining.

Population Doubling and Expansion Kinetics

Population doubling times were determined based on a previously described protocol [17]. At each passage, cells were seeded at a constant density of $4*10^4$ cells per cm^2 and allowed to grow to 80-90% confluency. Cells were counted and assessed for viability with Trypan blue vital staining. The duration between each passage was recorded for a total of 25 passages.

Aggregate redifferentiation

Following sufficient expansion in monolayer, auricular chondrocytes were suspended in chondrogenic media (**Table 1**) and seeded into 90mm petri plates coated with 20mg/ml agarose at a density of 1 million cells/mL in a total volume of 20mls. In the first 24hours cells were cultured at 37°C in 5% CO2 with orbital rotation at 60 RPM for 24hours. After 24 hours, plates were left in the same conditions but left static for 10 more days. The media was replenished every 3-4 days during this 10day period. On the 11^{th} day, aggregates were digested into single-cell suspension with 15mL/plate of 0.05% Trypsin for 45 minutes in 37°C. followed by digestion with 2mg/mL collagenase solution supplemented with 30 µL/mL (3% v/v) FBS for 90 minutes. Cells were then spun down at 400RPM and counted. Cell viability was assessed via Trypan blue vital stain.

Scaffold Free Construct Seeding

Cells were seeded at a volume of 8 million cells in a seeding volume of 300 µL of chondrogenic media[1]into custom made 7mm x 12mm agarose molds were made one day prior to digestion of the cells in the aggregate phase. These molds were left overnight with wash media (10566 DMEM + 1% PSF) in 5% CO2

at 37°C. Once cells were quantified via the method above, cells. After 4 hours, constructs were topped off with an additional 2 mLs of chondrogenic media. Seeded constructs were fed fresh chondrogenic media every other day. Cells were unconfined from their agarose scaffold 4-5 days after being seeded and placed in a 6 well plate with 7 mLs of chondrogenic media. Unconfined constructs were left to grow for 4 weeks and fed fresh chondrogenic media every 3-4 days. Constructs were subjected to biomechanical, biochemical, histology analysis on day 28 of self-assembly.

Table 1: Chondrogenic Expansion Media

Component	Manufacturer/catalog #	Expansion media	Chondrogenic media
DMEM	Gibco 10566-016	Full strength	Full strength
Pen/strep amphotericin B	BioWhitaker 17-745E	10 mg/mL	10 mg/mL
MEM non-essential amino acids	Gibco 11140-050	10 mg/mL	10 mg/mL
Insulin/human transferrin/selenium (ITS+) premix	Corning 0354352	10 mg/mL	10 mg/mL
Sodium pyruvate	Thermo P2256-25g	100 µg/mL	100 µg/mL
L-Ascorbate-2-phosphate	Sigma Aldrich A8960-5g	50 µg/mL	50 µg/mL
L-proline	Sigma Aldrich	40 µg/mL	40 µg/mL

	P0380-100g		
Dexamethasone	Sigma Aldrich D4902-25mg	0.0104 mg/mL	0.104 mg/mL
Fetal bovine serum	Atlanta biologicals S11550	100 µL/mL	NA
Human recombinant TGF beta 1	Pepro Tech 100-21 – 10 µg	1 ng/mL	10 ng/mL
Human recombinant FGF	Pepro Tech 100-18B – 100 µg	5 ng/mL	N/A
Human recombinant PDGF	Pepro Tech 100-14B	10 ng/mL	N/A
Human recombinant BMP-2	Pepro tech 120-02-100ug	N/A	30ng/mL

Biochemical Testing:

The wet and dry weights of all constructs were obtained before and after 24-hour lyophilization, respectively.

Then, these lyophilized segments were digested in a papain solution (125 microg/mL Papain + 5 mM *N*-Acetyl-L-Cysteine + 5 mM EDTA (anhydrous) + 100 mM phosphate Buffer) at 1 µL of solution per 1 µg of sample dry weight at 60°C for 18 hours. Collagen content was measured via OH-Proline Assay (Sigma Aldrich) following the manufacturer's instructions. The collagen content was then calculated based on a bovine collagen standard curve. Sample values were compared to both native TMJ values[22, 34] and costal chondrocyte TE construct values[22].

Concentration of sulfated glycosaminoglycans in each sample was determined via a GAG Blyscan Assay (Bicolor Life-Science Assays) based on 1,9-dimethylmethyl blue binding, per the manufacturer's instructions. Sample values were compared to both native TMJ values and costal chondrocyte TE construct values[22].

The DNA content was assessed via a Pico Green assay (Invitrogen Quanti-iT PicoGreen dsDNA Assay kit) based on pico green fluorescent dye that bind to double-stranded DNA, following the manufacturer instructions. From this data, we were able to infer the number of cells per sample.

The concentration of elastin in each tissue sample was determined via a Fastin Elastin Asssay (Biocolor Life-Science Assays) based on synthetic porphyrin binding of water soluble derivative α-elastin per the manufacturer's instruction. Sample values were compared to α-elastin of both native auricular tissue from neonatal and adult minipigs.

Mechanical Testing

Mechanical testing was based on the protocol previously described [61].

For the tensile testing, constructs were cut into a Dumbbell-shaped samples whilst maintaining a length and width of 4:1. Imaging software (ImageJ, U.S. National Institutes of Health, Bethesda, Maryland) was utilized to determine the thickness and width of each dumbbell-shaped sample from a high-resolution photograph. A uniaxial tension test was performed using Instron 5565 (Norwood, MA). Each segment was strained at a rate of 1%-gauge length per second to generate stress/strain curves from load-displacement data. Load, elongation, width, and thickness were analyzed with a software [Matlab, MathWorks, Natick, MA) via a custom coded program that plots load normalized to cross-sectional area and strain. These plots were used to define the segments tensile stiffness (Youngs modulus) and ultimate tensile strength (UTS).

For compressive testing, 3mm in diameter circular sampled were obtained with a punch-biopsy knife. Samples were placed in PBS at room temperature for a uniaxial, unconfined stress-relaxation test via the

Instron 5565 (Norwood, MA). This test strained the samples to 10% and 20% sequentially and allowed a subsequent relaxation for 10-20 minutes respectively. From this test, instantaneous (Ei) and relaxation moduli (Er) were calculated using a custom-made Matlab program [61].

Histology

Tissues-engineered constructs were formalin-fixed and embedded in paraffin following standard procedure [23]. Hematoxylin and eosin (H&E), Safranin-O with Fast Green counterstain (SAFO/FG), and Picosirius Red (PSR) stains were applied on 5 µm sections according to previously published standard protocols [23]. For the comparative purposes elastin staining (Virchow Van Gieson) was applied onto sections of TE constructs sourced form auricular and costal chondrocytes as well as adult and neonatal auricular cartilage and minipig TMJ disc at five anatomic areas (lateral, medial, central, posterior, and anterior [23]. The images were obtained using CellSense/Olympus software and Olympus microscope (OlympusOptical Co., LTD, model: BX40F4) equipped with a color camera (Olympus DP72). All histological preparations were subsequently evaluated by a board-certified histopathologist (NV).

Results:

Cell collection

Triangular ear notch samples measured approximately 0.2x0.6x0.7 cm. On average 0.5x10^6 primary cells were obtained from one triangular ear notch with total area of 0.2cm$^{2.}$ Upon digestion of extracellular matrix with collagenase cell viability was 90-100%.

Macroscopic Morphology and Dimensions of Neocartilage Constructs

Gross morphology of the cartilage constructs was smooth and flat (**Figure 2A**). The average dimensions were 6.25 ± 2.15 mm (width) 12.20 ± 2.28 (length) mm and 0.777 ± 0.135 mm (thickness). After the removal of skin ear notches weight was 7.84 ± 1.844 mg.

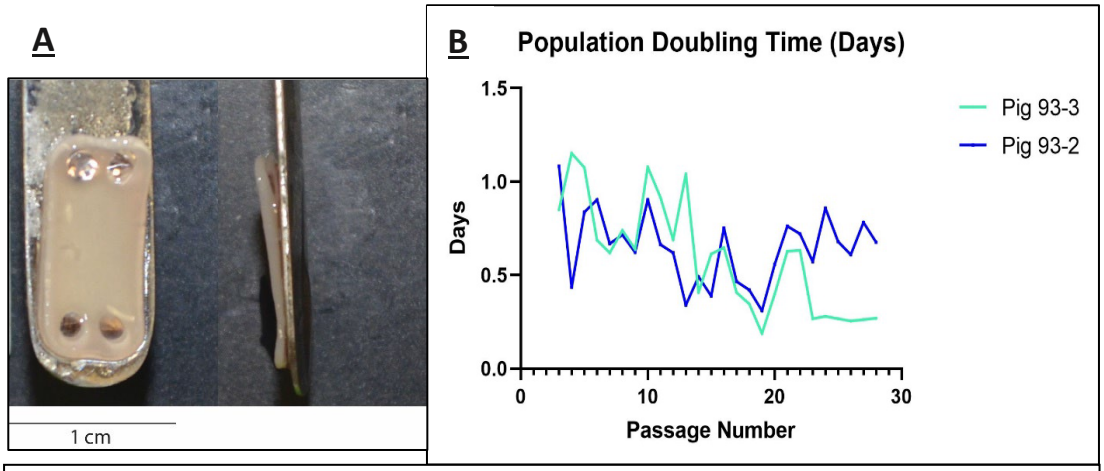


Figure 2: (A) Gross Images of auricular chondrocyte derived TE constructs. **(B)** Population Doubling of Auricular Chondrocytes. Population doubling time of auricular chondrocytes in monolayer up to passage twenty-eight. Two pig donors are reflected (pig 93-2 and 93-3).

Population Doubling

Two pig donors were used for calculating population doubling times. Auricular chondrocytes grew well in monolayer and comparable population doubling times between donors. Auricular chondrocytes-maintained population doubling times consistently over 25 passages (**Figure 2B)**.

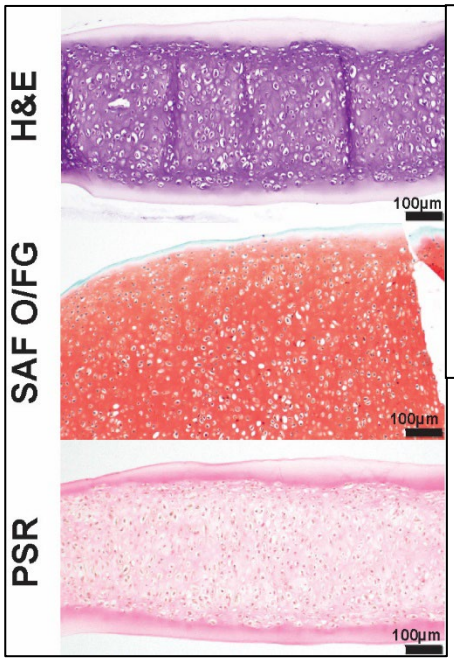


Figure 3: Histology of Auricular Chondrocyte Derived Tissue Engineered (TE) Constructs. Auricular TE constructs were stained with various stains (from top to bottom): hematoxylin and eosin (H&E), Safranin-O/Fast Green, and Picrosirius red. H&E staining shows overall cellularity, shows overall glycosaminoglycan content, and Picrosirius red shows overall collagen content.

Histology

With hematoxylin and eosin staying the construct sections were densely cellular and cells were evenly distributed throughout the section. The histomorphology of the tissue was consistent with cartilage where individual chondrocytes reside in the lacunae and are surrounded by homogeneous basophilic

extracellular matrix (ECM). The intensity of basophilic staining was comparable to native auricular tissue (**Figure 3)** With the application of specials stains more specific features of ECM were highlighted. Specifically, safranin O/fast green counterstain labeling highlighted abundant glycosaminoglycans in the ECM (intense orange staining), while Picrosirius Red underscored the collagen content (pink color) (**Figure 3)**.

The presence of elastic fibers was also interrogated in various native and engineered tissues for comparison with Virchow Van Gieson stain. Elastin fibers were not apparent in the TE construct sections sourced form costal or auricular chondrocytes, but were abundant in the control section of adult porcine pina (**Figure 4**). Neonatal ear had 141.5ug/ml of elastin. Interestingly, very anisotropic elastic fiber distribution was observed in minipig TMJ disc tissue, where elastin fibers we only microscopically apparent in the posterior attachment site of the disc. (**Figure 4**).

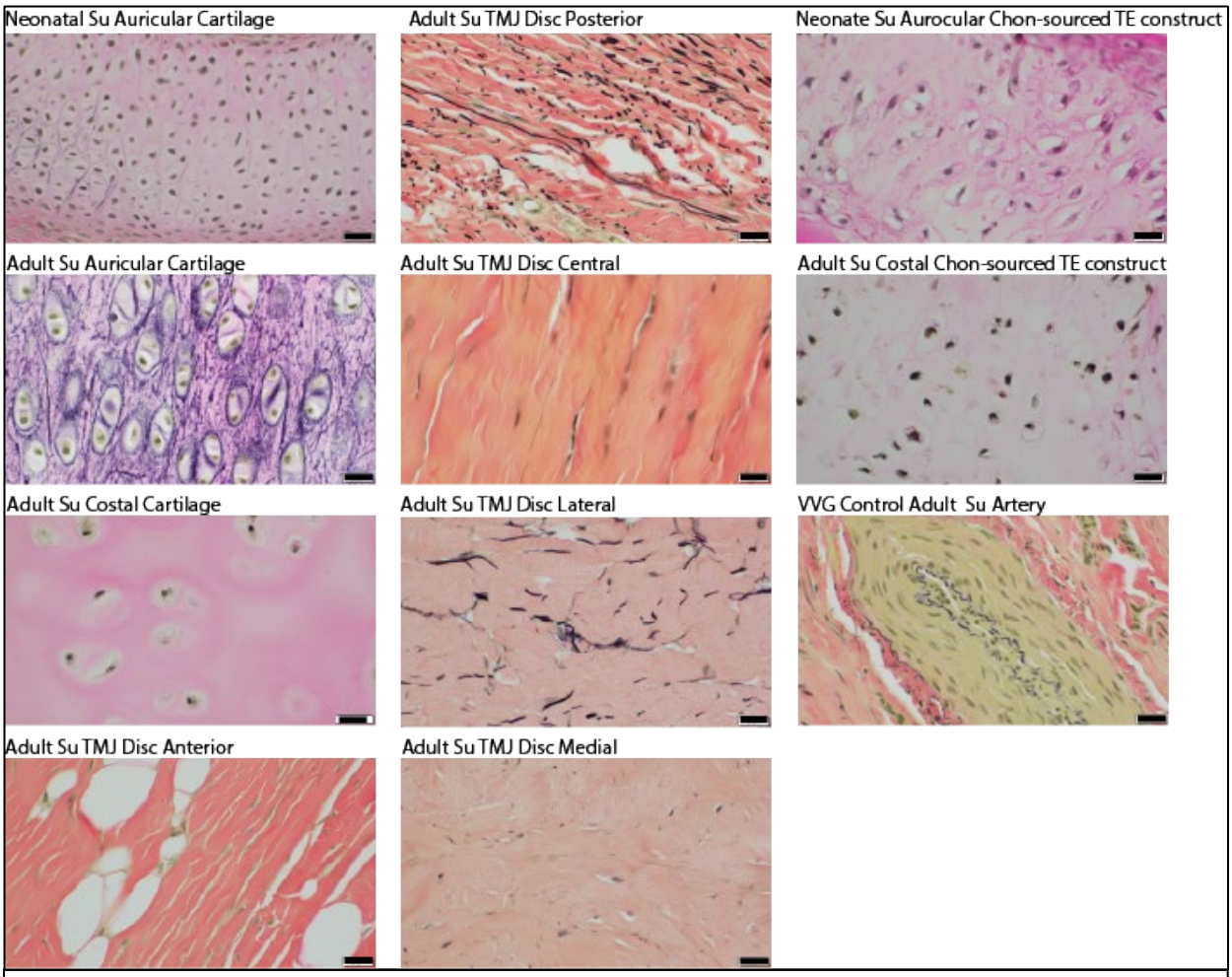


Figure 4: Histology Panel of Swine (Su) Cartilage. Panel of images show Su cartilage from various anatomical locations/sources. Cartilage derived from several locations of the temporomandibular joint (TMJ), auricular cartilage, costal cartilage, and auricular chondrocyte derived tissue-engineered (TE) cartilage constructs. VVG= Verhoeff Van Gieson staining. VVG is a histological technique used to visualize elastic fibers in tissues. The size bar for all images is 20µm.

Biochemistry

Biochemical analyses supported histological observations. Auricular chondrocyte derived TE constructs contained 0.144 ug ± 0.011 collagen per ug dry weight, 0.185ug ± 0.002 GAG per ug dry weight, 0.384ng ± 0.432 per ug dry weight, and 81.95 ug ± 6.54 elastin per mg dry weight. The average water content of all auricular chondrocyte derived TE constructs was 81% ±1.18.

Mechanical Properties

We found that constructs derived from auricular chondrocytes had an Ei at 10% strain of 200.5 kPa ± 43.34, 471.9 kPa ± 92.8 at 20% strain as well 36.99 kPa ± 6.47 Er at 10@ strain and 110.3 kPa ± 16.99 Er at 20% strain. The Young's modulus was 2.0 MPa ± 0.63 and the ultimate tensile strength (UTS) was 0.619 MPa ± 0.177.

Discussion

This study is the first to explore the utility of auricular cartilage-sourced chondrocytes for scaffold free engineering of neocartilage constructs. Using very small tissue sample for isolation of primary cells, auricular chondrocytes were expanded to hundreds of millions using expansion and redifferentiation methods that were previously effectively applied to costal and articular chondrocytes [5,32]. Histology confirmed the chondrogenic morphology and highlighted ECM features that were in agreement with quantitative biochemical tests with exception of elastin. Mechanically, auricular chondrocyte derived constructs were robust and had comparable properties to native porcine TMJ and auricular tissues. Cumulatively, these results demonstrate a feasibility of auricular chondrocytes for scaffold-free cartilage tissue engineering. This methodology can be further explored for clinical applications in TMJ disc and auricular reconstruction and regeneration.

Costal chondrocytes were previously described as an attractive cell source for TMJ disc and other cartilaginous tissues reconstruction and regeneration [50, 62, 63]. Indeed, constructs generated from this cell source were evaluated in minipig TMJ disc thinning model where a successful defect closure was achieved [22]. Interestingly, despite some biochemical and biomechanical discrepancy with the native tissue, the costal cartilage-sourced constructs were able to remodel upon implantation and assume properties more similar with native [22]. Although this study did not compare costal constructs to

auricular their mechanical properties are similar. For instance, in the study conducted by Huwe et al the Instantaneous modulus of the engineered cartilage sourced from costal chondrocytes was ~ 300kPa [64], as compared to 200 and 400 kPa at 10 and 20 percent strain in the present study. Similarly, the Young's modulus and UTS of the constructs from Huwe's measured 1.4 MPa and 0.32 MPa, respectively as compared to Young's modulus of 2 MPa and UTS of 0.6 MPa in the current study [37]. Interestingly, the biochemical properties were different. In the study conducted by Huwe et al [37], the collagen content of the engineered cartilage sourced from costal chondrocytes was ~1.8 collagen/wet weight (%), as compared to 2.6 collagen/wet weight (%) in the present study. Similarly, the glycosaminoglycan (GAG) content of Huwe's constructs was ~7.5 GAG/wet weight (%), as compared to 3.34 GAG/wet weight (%) in the present study [37]. This discrepancy could be attributed to a difference in cell number and ECM production. Auricular derived chondrocytes produce an entirely different type of collagen tissue, usually defined by the production of elastin. Collectively, it is possible that auricular chondrocytes have a shift in biochemical production and cellular metabolism to meet the demands of elasticity.

Auricular cartilage is an elastic type of cartilage which means that auricular chondrocytes are able to synthesize elastin [65]. TMJD is a unique type of fibrocartilage with anisotropic fiber direction and site-specific distribution of elastic fibers [58]. Specifically, it was determined that the bilaminar zone (i.e. posterior disc attachment zone) of the human TMJ disc has the highest elastin fiber concentration [58]. Similar distribution difference in elastic fibers is apparent in the TMJ disc of the minipigs [59] (**Figure 4**). No strong elastin staining was observed on histologic sections of TE auricular chondrocytes-sourced, or costal chondrocyte-sourced TE constructs. However, elastin was detectable in the auricular chondrocytes-sourced constructs with biochemical assay. Precisely, concentration of 81.95ug per mg of dry tissue was detected. In comparison with native neonatal auricular cartilage and adult auricular cartilage this concertation is 1.73 times and 2.36 times less, respectively. Provided that the elastic fibers mature trough

formation of lysyl-oxidase-mediated cross-linking process [66-68], it is possible that once formed, elastin fibers continue to mature via the cross-linking mechanism. The reports on elastin maturation are outnumbered by reports on elastin ageing and degradation with age, inflammation, and environmental damage [67]. Studies on elastin maturation state that elastin formed during neonatal development remains with the individual throughout its life [69] and that genes for elastin and fibrillin pick during neonatal development and then silenced for good [70, 71]. It remains to be determined how structural maturation progresses with age. In case of scaffold-free cartilage tissue engineering, it was postulated that the phase of self-assembling is recapitulating the stage of mesenchymal condensation in embryonic development and that neocartilages engineered with this method continue to mature via collagen fiber cross-linking beyond four weeks of manufacturing process [72]. Collectively, it is possible that auricular chondrocytes-sourced TE constructs need more time to mature and cross-link elastin fibers to be detectable with standard histological methods.

It is crucial to point out that dozens of cartilage constructs were manufactured from a very small stock of primary cells. This manufacturing success is due to the one crucial step in the process of scaffold-free tissue engineering where following monolayer expansion the cells are cultured for additional 10 days in suspension. It is postulated that during the monolayer expansion step chondrocytes undergo de-differentiation, i.e., assume fibroblastic phenotype instead of chondrocytic [73-75]. However, during the suspension culture, where chondrocytes are unable to adhere to the substrate, re-differentiation takes place and chondrocytes resume their chondrocytic properties. This aggregate redifferentiation step allows to conduct extensive in vitro expansion of very small initial stock of primary cells overcoming a huge hurdle of autologous tissue availability [65]. The advantages are clear. Using the smallest tissue biopsy of autologous auricular cartilage, followed by a sufficient expansion to hundreds of millions of cells makes autologous cell sourced tissue engineering an achievable reality. Furthermore, the morbidity of collection

site in the ear is much less than autologous rib collection procedure [76, 77]. Lastly, unlike costal cartilage, auricular cartilages do not have a tendency to ossify with age, presenting a wider timeframe for tissue collection.

In summary, this study is the first to demonstrate the proof of concept and the feasibility of auricular chondrocytes suitability for scaffold-free cartilage tissue engineering. Extending this study to a side-by-side comparison to neocartilages engineered from costal chondrocytes would be essential in further determining the utility and possible advantage of this cell source for regeneration of cartilaginous tissues such as TMJ disc and pinna. The latter can be followed up by a true size pinna or TMJ disc tissue manufacturing.

References

1. Plesh, O., S.H. Adams, and S.A. Gansky, *Temporomandibular joint and muscle disorder-type pain and comorbid pains in a national US sample.* J Orofac Pain, 2011. **25**(3): p. 190-8.
2. Valesan, L.F., et al., *Prevalence of temporomandibular joint disorders: a systematic review and meta-analysis.* Clin Oral Investig, 2021. **25**(2): p. 441-453.
3. National Academies of Sciences, E., et al., *The National Academies Collection: Reports funded by National Institutes of Health*, in *Temporomandibular Disorders: Priorities for Research and Care*, O. Yost, et al., Editors. 2020, National Academies Press (US)Copyright 2020 by the National Academy of Sciences. All rights reserved.: Washington (DC).
4. White, B.A., L.A. Williams, and J.R. Leben, *Health care utilization and cost among health maintenance organization members with temporomandibular disorders.* J Orofac Pain, 2001. **15**(2): p. 158-69.
5. Vapniarsky, N., et al., *Tissue engineering toward temporomandibular joint disc regeneration.* Sci Transl Med, 2018. **10**(446).
6. Farrar, W.B. and W.L. McCarty, Jr., *The TMJ dilemma.* J Ala Dent Assoc, 1979. **63**(1): p. 19-26.
7. Wilkes, C.H., *Internal derangements of the temporomandibular joint. Pathological variations.* Arch Otolaryngol Head Neck Surg, 1989. **115**(4): p. 469-77.
8. Aryaei, A., et al., *Recent Tissue Engineering Advances for the Treatment of Temporomandibular Joint Disorders.* Curr Osteoporos Rep, 2016. **14**(6): p. 269-279.
9. Holmlund, A.B., G. Gynther, and S. Axelsson, *Diskectomy in treatment of internal derangement of the temporomandibular joint. Follow-up at 1, 3, and 5 years.* Oral Surg Oral Med Oral Pathol, 1993. **76**(3): p. 266-71.
10. Mercuri, L.G., *Alloplastic temporomandibular joint replacement: rationale for the use of custom devices.* Int J Oral Maxillofac Surg, 2012. **41**(9): p. 1033-40.
11. Agerberg, G. and M. Lundberg, *Changes in the temporomandibular joint after surgical treatment. A radiologic follow-up study.* Oral Surg Oral Med Oral Pathol, 1971. **32**(6): p. 865-75.

12. Hinton, R.J., *Alterations in rat condylar cartilage following discectomy.* J Dent Res, 1992. **71**(6): p. 1292-7.
13. Eriksson, L. and P.L. Westesson, *Temporomandibular joint diskectomy. No positive effect of temporary silicone implant in a 5-year follow-up.* Oral Surg Oral Med Oral Pathol, 1992. **74**(3): p. 259-72.
14. Legemate, K., et al., *Engineering Human TMJ Discs with Protein-Releasing 3D-Printed Scaffolds.* J Dent Res, 2016. **95**(7): p. 800-7.
15. Brown, B.N., et al., *Inductive, scaffold-based, regenerative medicine approach to reconstruction of the temporomandibular joint disk.* J Oral Maxillofac Surg, 2012. **70**(11): p. 2656-68.
16. Hagandora, C.K., et al., *Poly (glycerol sebacate): a novel scaffold material for temporomandibular joint disc engineering.* Tissue Eng Part A, 2013. **19**(5-6): p. 729-37.
17. Athanasiou, K.A., et al., *Self-organization and the self-assembling process in tissue engineering.* Annu Rev Biomed Eng, 2013. **15**: p. 115-36.
18. Hu, J.C. and K.A. Athanasiou, *A self-assembling process in articular cartilage tissue engineering.* Tissue Eng, 2006. **12**(4): p. 969-79.
19. Huey, D.J., J.C. Hu, and K.A. Athanasiou, *Unlike bone, cartilage regeneration remains elusive.* Science, 2012. **338**(6109): p. 917-21.
20. MacBarb, R.F., et al., *Engineering functional anisotropy in fibrocartilage neotissues.* Biomaterials, 2013. **34**(38): p. 9980-9.
21. Anderson, D.E. and K.A. Athanasiou, *Passaged goat costal chondrocytes provide a feasible cell source for temporomandibular joint tissue engineering.* Ann Biomed Eng, 2008. **36**(12): p. 1992-2001.
22. Huwe, L.W., et al., *Characterization of costal cartilage and its suitability as a cell source for articular cartilage tissue engineering.* J Tissue Eng Regen Med, 2018. **12**(5): p. 1163-1176.
23. He, A., et al., *Cell yield, chondrogenic potential, and regenerated cartilage type of chondrocytes derived from ear, nasoseptal, and costal cartilage.* J Tissue Eng Regen Med, 2018. **12**(4): p. 1123-1132.
24. Qing-Hua, Y., et al., *The significance of the biomechanical properties of costal cartilage in the timing of ear reconstruction surgery.* J Plast Reconstr Aesthet Surg, 2011. **64**(6): p. 742-6.
25. Nabzdyk, C., et al., *Review: auricular chondrocytes - from benchwork to clinical applications.* In Vivo, 2009. **23**(3): p. 369-80.
26. Gross, A., A. Bumann, and B. Hoffmeister, *Elastic fibers in the human temporo-mandibular joint disc.* Int J Oral Maxillofac Surg, 1999. **28**(6): p. 464-8.
27. Mardas, N., et al., *Experimental model for bone regeneration in oral and cranio-maxillo-facial surgery.* J Invest Surg, 2014. **27**(1): p. 32-49.
28. Almond, G.W., *Research applications using pigs.* Vet Clin North Am Food Anim Pract, 1996. **12**(3): p. 707-16.
29. Clément, C., et al., *Quantitative analysis of the elastic fibres in the human temporomandibular articular disc and its attachments.* Int J Oral Maxillofac Surg, 2006. **35**(12): p. 1120-6.
30. Christensen, L.V., *Elastic tissue in the temporomandibular disc of miniature swine.* Journal of oral rehabilitation, 1975. **2**(4): p. 373-377.
31. Griffin, M.F., et al., *Biomechanical Characterisation of the Human Auricular Cartilages; Implications for Tissue Engineering.* Ann Biomed Eng, 2016. **44**(12): p. 3460-3467.
32. Vapniarsky, N., et al., *Tissue Engineering of Canine Cartilage from Surgically Debrided Osteochondritis Dissecans Fragments.* Ann Biomed Eng, 2022. **50**(1): p. 56-77.
33. Allen, K.D. and K.A. Athanasiou, *Viscoelastic characterization of the porcine temporomandibular joint disc under unconfined compression.* J Biomech, 2006. **39**(2): p. 312-22.

34. Carson, L.F., *Histotechnology : a self instructional text*. 2nd ed. 1997, Chicago, IL: American Society of Clinical Pathology.
35. Caccamese, J.F., Jr., R.L. Ruiz, and B.J. Costello, *Costochondral rib grafting.* Atlas Oral Maxillofac Surg Clin North Am, 2005. **13**(2): p. 139-49.
36. Drucker, D.J. and P.L. Brubaker, *Proglucagon gene expression is regulated by a cyclic AMP-dependent pathway in rat intestine.* Proc Natl Acad Sci U S A, 1989. **86**(11): p. 3953-7.
37. Huwe, L.W., et al., *Using Costal Chondrocytes to Engineer Articular Cartilage with Applications of Passive Axial Compression and Bioactive Stimuli.* Tissue Eng Part A, 2018. **24**(5-6): p. 516-526.
38. Bernstein, J.L., et al., *Tissue Engineering Auricular Cartilage Using Late Passage Human Auricular Chondrocytes.* Ann Plast Surg, 2018. **80**(4 Suppl 4): p. S168-s173.
39. Lemaire, R., et al., *Microfibril-associated MAGP-2 stimulates elastic fiber assembly.* J Biol Chem, 2007. **282**(1): p. 800-8.
40. Sherratt, M.J., *Tissue elasticity and the ageing elastic fibre.* Age (Dordr), 2009. **31**(4): p. 305-25.
41. Mithieux, S.M. and A.S. Weiss, *Elastin.* Adv Protein Chem, 2005. **70**: p. 437-61.
42. Shapiro, S.D., et al., *Marked longevity of human lung parenchymal elastic fibers deduced from prevalence of D-aspartate and nuclear weapons-related radiocarbon.* J Clin Invest, 1991. **87**(5): p. 1828-34.
43. Davidson, J.M., K.E. Hill, and J.L. Alford, *Developmental changes in collagen and elastin biosynthesis in the porcine aorta.* Dev Biol, 1986. **118**(1): p. 103-11.
44. Ramirez, F. and L. Pereira, *The fibrillins.* Int J Biochem Cell Biol, 1999. **31**(2): p. 255-9.
45. Hadidi, P., et al., *Temporal development of near-native functional properties and correlations with qMRI in self-assembling fibrocartilage treated with exogenous lysyl oxidase homolog 2.* Acta Biomater, 2017. **64**: p. 29-40.
46. Benya, P.D. and J.D. Shaffer, *Dedifferentiated chondrocytes reexpress the differentiated collagen phenotype when cultured in agarose gels.* Cell, 1982. **30**(1): p. 215-24.
47. Domm, C., et al., *Redifferentiation of dedifferentiated bovine articular chondrocytes in alginate culture under low oxygen tension.* Osteoarthritis Cartilage, 2002. **10**(1): p. 13-22.
48. Benya, P.D., S.R. Padilla, and M.E. Nimni, *Independent regulation of collagen types by chondrocytes during the loss of differentiated function in culture.* Cell, 1978. **15**(4): p. 1313-21.
49. Thomson, H.G., T.Y. Kim, and S.H. Ein, *Residual problems in chest donor sites after microtia reconstruction: a long-term study.* Plast Reconstr Surg, 1995. **95**(6): p. 961-8.
50. Go, J.Y., et al., *Management of chest deformity caused by microtia reconstruction: Comparison of autogenous diced cartilage versus cadaver cartilage graft partial filling techniques.* J Plast Reconstr Aesthet Surg, 2017. **70**(1): p. 104-109.

Chapter 4

Biomechanical Ageing of Cartilage in a Canine Model

Authors:

Carissa Garrity[1], Enmian Chang[1], Iris Rivas[1], Tanya Garcia-Nolen[1], Natalia Vapniarsky[1*]

[1]Department of Pathology, Microbiology, and Immunology, University of California, Davis, Davis, CA, United States of America

*Corresponding author

Abstract

Cartilage degenerative conditions are a public health concern worldwide. Cartilage degeneration can be initiated with trauma but it is also common for cartilage to wear with age. Due to the low regenerative capacity of cartilage, this dilemma invites the exploration and characterization of the mechanisms behind age-related cartilage degeneration. In the following study, multiaxial indentation testing and thickness testing was performed *in situ* to measure the Instantaneous Moduli (Ei) and thicknesses of all articular surfaces in the shoulder and stifle joints across various age groups of dogs (N=20). When considering all surfaces combined, a significantly positive correlation was detected between the Instantaneous moduli (Ei) of articular cartilage and age (p=0.02). Further, there was a significant negative correlation between cartilage thickness and age and articular cartilage collagen content and age (p=0.015). Likewise, there was a significant negative correlation between the cellularity of articular cartilage and age (p=0.019). Interestingly, this study revealed insignificant correlation between GAG and age (p=0.72), and between GAG and Ei of articular cartilage (p=0.14). When considering specific joints individually, similar significant trends of age-related increase in Ei and decrease in thickness were present in the Tibia of the stifle joint. Finally, we observed histological changes consistent with degeneration in articular cartilage but only with geriatric dogs. In conclusion, this study performed multiaxial compression and thickness testing using

Biomomentum Inc. (Montreal, Canada) and produced results that suggest that the aging of articular cartilage is characterized by increase in the instantaneous modulus, decrease in thickness, collagen content, and cellularity but not GAG content.

Key Words: cartilage degeneration, Instantaneous Moduli, thickness, ageing

1. Introduction

Articular cartilage is a shock-absorbing tissue lining the ends of diarthrodial joints that aims to provide a frictionless surface for joint articulation. The high prevalence of cartilage tissue disorders is a public health concern worldwide. Cartilage degeneration is commonly associated with traumatic injury, infections, or age-related wear. In many cases patients are diagnosed with joint disease at the more advance ages of their lives. Thus, it is impossible to determine if prior trauma, overuse due to occupational or physical activity, individual anatomical conformation aspects, and activity levels contributed cumulatively or independently to the current disease manifestation. Comprehensive and wholistic studies on age-related changes of articular cartilages in animals or humans are few and often focused on a limited repertoire of parameters. For instance, many studies in humans and rats have confirmed a decrease in proteoglycan content, cellularity, and thickness with age [78-81]. Other studies have explored physical characteristics such as thickness, or the imaging data [82] in a limited age-range of individuals. No studies, to our knowledge, have been performed on a wide range of individual ages comparing biochemical, biomechanical, and histological parameters of articular cartilages simultaneously on multiple joints.

The low regenerative capacity of cartilage and progressive demand for its regeneration, has invited the exploration of tissue-engineered replacements. However, the limited combined knowledge on the character or rate of changes in cartilage properties with respect to aging makes it difficult to tailor

engineered cartilages to the individual's specific needs. The most common strategies to assess cartilage's properties are biochemical analysis, histology, biomechanical testing, and imaging [83-86]. Biochemical analysis offers an advantageous insight into the cellular and extracellular components most commonly collagens and glycosaminoglycans. For example, studies on porcine and horse cartilage have confirmed a decrease in collagen content [87, 88] and proteoglycan content [87, 89] with age. In addition, some studies have also confirmed an increase in number of senescent chondrocytes in aged cartilage tissue [90, 91]. These findings show important changes in chondrocyte ability to replace and keep up with normal wear and tear [92]. Histological analysis offers important insight into how cellular and extracellular organization contributes to overall cartilage tissue morphology [86]. However, histology and biological assays only offer a "hint" on how mechanical properties of cartilage may be affected. Therefore, evaluating the changes of cartilage wholistically including multiple parameters are crucial in concluding on ageing changes of cartilage tissue and are instrumental in guiding tissue-engineering efforts for cartilage regeneration.

A variety of tests and testing protocols have been explored to investigate the mechanical properties of cartilage. Most common approaches to test cartilage mechanical properties turn to a variety of *ex vivo* protocols [93]. *Ex vivo* protocols can be split into nano or tissue-level testing. Nanoindentation with atomic force microscopy (AFM) has emerged as a metric to understand cartilage biomechanics at a microscopic level [93]. AFM can produce three-dimensional (3-D) topographical images to reflect mechanical properties at a given point. Macroscopic or tissue-based mechanical testing is can be executed via confined or unconfined compression testing [93-95]. Additional mechanical properties assessments of cartilage tissue include tensile and shear testing. Articular cartilage has a robust ability at supporting tensile stresses due to its biochemical composition and organization of collagen fibrils [93, 96]. Shear testing is often used to characterize the cartilage/bone interface and tissue/scaffold interfaces [97, 98]. Uniformly, most of the current mechanical testing methodologies require resection for cartilage form the

subchondral bone, which may not accurately reflect cartilage properties and cartilage-bone interactions as displayed *in vivo.* In fact, a review by Burr et al suggests that tissue-level adaptions of the subchondral bone are thought to occur in osteoarthritis prior to degeneration of the overlying articular cartilage [99] particularly at the bone-cartilage interface [100]. These modifications of bone, cartilage and the interface suggest that, a shift to *in situ* and *in vivo* models may more accurately reflect cartilage's properties.

Several techniques to evaluate *in vivo* cartilage biomechanics have been developed and used clinically. The current *in vivo* methodologies rely on arthroscopy [101], magnetic resonance imaging (MRI) [102], and ultrasound elastography [82]. Although these technologies offer real-time *in vivo* measurements, there are several drawbacks to each method. Some of these analyses are invasive, while others are subjective, and more work remains to be done on correlating the measurement outcomes of these methods with actual biochemical properties of cartilage tissue. [103]. While these methodologies await refinement, *in situ* methodologies continue to be explored with automated indentation testing. An automated in situ indentation and mapping testing became commercially available in 1999 (Biomomentum Inc. Montreal, Canada). The latter technology has been explored for its many advantages such as being non-destructive, allowing repeated measurements, and multiple characterizations at the same location [94, 104, 105]. This development allows to perform non-destructive mapping of mechanical properties of cartilage over the entire articular surface. Subsequently the same cartilage can be explored with biochemical and histological methods. The non-destructive and extensive nature of this testing compensates for the shortcomings of the standard mechanical methods where cartilage is not tested in the context of the subchondral bone.

Dogs are extensively used as a model for human cartilage degeneration and regeneration [81, 106]. Dogs commonly show similar age-dependent degenerative changes in their cartilage to humans [81, 106]. In

fact, cartilage lesions such as fissures, erosion, fibrillation, and eburnation are often found in articulating joints of dogs at necropsy, even in the absence of clinical history of lameness [81, 106]. In contrary to rodent models, dogs completely close their growth plates at skeletal maturity and their relative longevity provides more translational relevance on ageing of cartilage. Considering this, this study of characterizing cartilage's changes with age across two major joints in dogs was conceived. Specifically, automated indentation and thickness mapping on five different articulating surfaces in a wide age range of dogs using the Mach-I Model MA056-v500c test device (Biomomentum Inc., Laval, Canada) was performed. Subsequently, same articular surfaces were interrogated for glycosaminoglycan and collagen content as well as cellularity and histological changes.

2. Methods

2.1 Tissue Collection

Entire shoulder and stifle joints were collected from dogs that died or were euthanized for reasons unrelated to musculoskeletal` disease within less than 24 hours post mortem. The patient's tissue was donated for unpredicted use at the Veterinary Teaching Hospital (VMTH) at the University of California, Davis (UCD). the Patients that received any form of chemotherapy were not included. The entire joints were preserved frozen at -20C wrapped in protease inhibitor-soaked gauze. On the day of testing individual joints were thawed and dissected to expose the articular surfaces. In toto articular surfaces of humeral head, glenoid fossa, femoral condyles, tibial plateau, and trochlea were tested. The samples were collected as intact joints to preserve cartilage integrity, lubrication and moisture. The study contained over 60 surfaces tested between the stifle and shoulder joints. The study used 20 dogs with 4 dogs used per articular surface. Patient information is provided in **Table 1**.

Table 1

Age (Years)	Body Condition Score (BCS)	Breed
2	2	Belgian Malinois
6	6	golden retriever
15	3	English springer
3	3	Cane Corso
2	4	German Shepard
0.134615385	4	chihuahua
2	5	german shepard/pitbull mix
10	6	poodle/dachshund mix
13	5	Shih-Tzu
5	4	Australian sheep dog
5	2	rottweiler
4	2	Pitbull
1.5	4	Pitbull
0.166666667	5	labrador
13	4	labrador
11	6	corgi
5	8	boerboel
4	3	Bernese mountain dog
10	5	corgi/beagle mix

2.2 Mechanical Examination

2.21 Automated Indentation Mapping

The automated indentation and mapping were carried out according to Biomomentum protocol (MA056-SOP10-D v1 Mach-1). For this, a Mach-I Model MA056-v500c test device (Biomomentum Inc., Laval, Canada) and a 70N multi-axial load cell were used. Briefly, osteochondral specimens were mounted on a specimen holder device with cartilage surface facing up fixed by screws circumferentially. The specimen was then submerged into PBS and remained submerged throughout the testing. Two reference points were then identified with a video camera-registration system and a mapping software (Mach-1-MAP). Next, a position grid was superimposed on the live image of the sample and testing points were determined based on the size of the sample. The entire surface was equally covered with sample points. On average 25 points were assigned per articular surface. The instantaneous moduli (IM) of the cartilage were determined using indentation with spherical indenter with 1mm diameter. The calculation of each

sample point was validated and corrected to reflect the surface angle relative to the indenter with an additional four test points surrounding the original point. Any sample point in which the angle of the surface was greater than 60 degrees was excluded. The contact criterion with the sample surface has been set to 0.01 N. The indentation amplitude was set to 0.1 mm by the indentation velocity to 0.1 mm/s, and the relaxation time of 5s.

2.2.2 Automated Thickness Mapping

Thickness testing was performed immediately following indentation testing by replacing the spherical indenter with a 27G x 3/8" needle. The thickness was calculated at each sample point by taking the difference between the vertical position of the needle at the surface (the start of a gradual increase in load) and the position of the needle once it hits subchondral bone (the first inflection point where the load increased significantly) [94]. The testing outcome for thickness for each point were a contact criterion of 1N at a velocity of 0.5mm/s.

2.3 Data Processing and Analysis

The instantaneous modulus (Ei) at each sample point was obtained by fitting the load-displacement curve, using the corresponding sample point thickness and Poisson's ratio (set to 0.5), to Hayes et. al., elastic model for indentation [107] and previously published method [94].

(1) $$Ei = \frac{2P(1-v^2)}{4kw_0^{\frac{3}{2}} * (\mathrm{RX})}$$

Where P= force, v= Poisson's ratio= 0.5, w_0= indenter displacement, k= constant value based on a/h, X= constant value based on a/ha =contact region, h= cartilage thickness R= radius of the indenter. A position grid was superimposed on the image of the sample and the Ei calculation and thickness of the cartilage for each testing point were reflected through a heat map (**Figure 1A, B)** All data was analyzed with the

Semi-Automated Indentation and Thickness Batch Analysis software (Biomomentum Inc., Laval, Canada) based on a previously published method [94] that utilized equations and mathematical analysis from Hayes et al [107].

2.4 Biochemical Analysis

Immediately following mapping, the articular cartilage was harvested from the surface with a scalpel. The wet and dry weights of each quadrant of each surface were obtained before and after 24-hour lyophilization, respectively. Lyophilized samples were digested in papain solution (125 µg/mL Papain + 5 mM N-Acetyl-L-Cysteine + 5 mM EDTA (anhydrous) + 100mM Phosphate Buffer) at 1µl of digestion solution per 1µg of sample dry weight at 60C for 18 hours. The collagen content was assessed by OH-Proline Assay (Sigma Aldrich) following the manufacturer's instructions. The collagen content was then calculated based on a bovine collagen standard curve. The concentration of sulfated glycosaminoglycans (GAG) in each sample was determined via a GAG Blyscan Assay (Bicolor Life-Science Assays) based on 1, 9-dimethyl methyl blue binding, following manufacturer instructions. The DNA content was assessed via a Pico Green assay based on pico green fluorescent dye that bind to double-stranded DNA, following the manufacturer instructions (Invitrogen Quanti-iT PicoGreen dsDNA Assay kit). From this data, we were able to infer the cellularity of the sample.

2.5 Histology

Surfaces not used for mechanical or biochemical testing were sectioned using bandsaw to include cartilage and subchondral bone. The samples were then fixed in 10% buffered formalin and processed for standard histology and paraffin embedding subsequently [23]. A 5µm sections were obtained from the paraffin blocks and stained with hematoxylin and eosin (H&E) for assessment of general morphology.

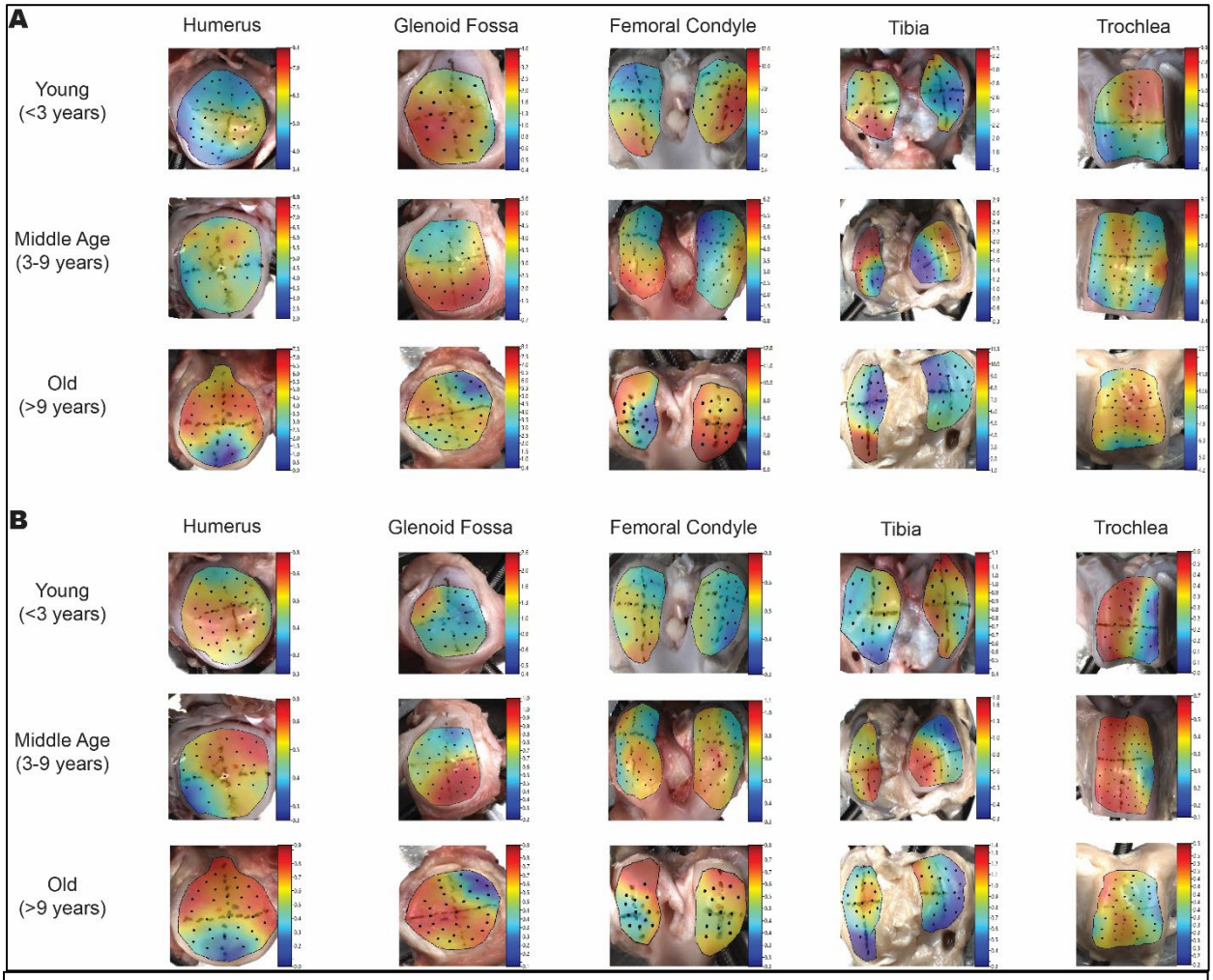


Figure 1: 3D Heat maps displaying articular cartilage's Instantaneous moduli and thicknesses generated with Biomomentum Mach 1. (A) Heat map showing the distribution of Instantaneous moduli (Ei) values at 15% strain (MPa). Each image represents an articular surface across patients of different age groups. (B) Heat map showing the distribution of cartilage thickness (mm). Each image represents an articular surface across patients of different age groups. Scale bar for all images: Red represents higher values while blue are lower values.

2.6 Statistics

A Kruskal-Wallis test was applied to compare stiffness and thickness between body condition scores. A Pearson correlation coefficient and p-value was used to assess the correlations between biochemical properties and mechanical properties, or biochemical properties and age. The effects of the amount of GAG, collagen, and cells on cartilage stiffness and thickness were measured by simple linear regression, where stiffness or thickness was regressed on the biochemical property. Similarly, the effects of age on the three biochemical properties were assessed by regressing age on the amount of GAG, collagen, or the number of cells. A linear mixed effects model was used to account for mechanical measurements across articular surfaces being more similar within the same dog than between dogs. 95% confidence intervals were then calculated to determine the difference in stiffness and thickness across the five articular

surfaces, where the femoral condyle was arbitrarily assigned as the reference group. A p-value < 0.05 was considered significant.

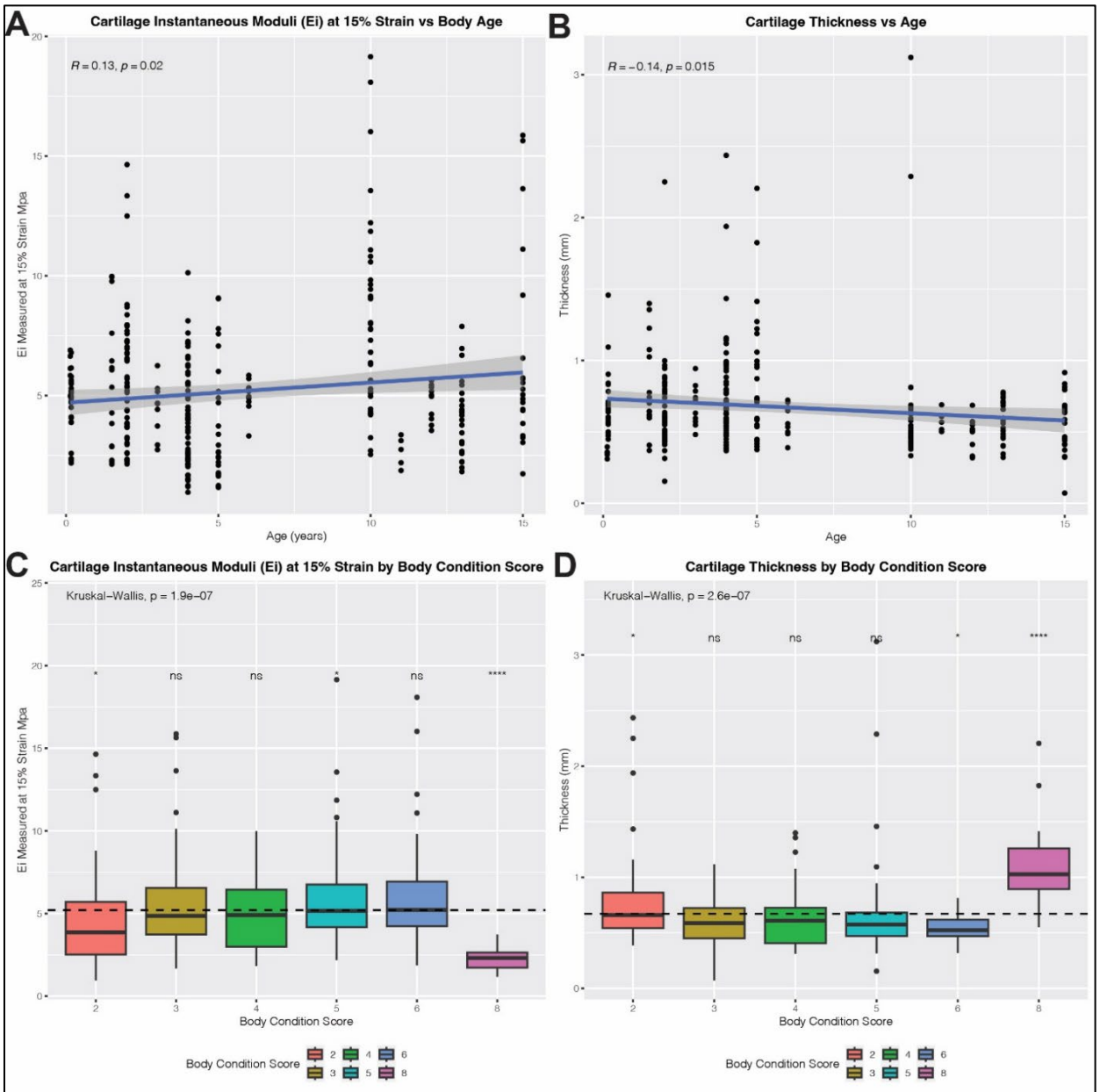


Figure 2: The Effect of Age and Body Condition Score (BCS) on Cartilage Thickness and Ei. **(A)** Cartilage Ei increased significantly with an increase in age. **(B)** Cartilage thickness decreased significantly with age. **(C)** Cartilage Ei differed from the mean stiffness for body condition scores of 2, 5, and 8. There was a general trend of increasing Ei as the body condition scores increased from 2 to 6, with a significant decrease in Ei for canines with a body condition score of 8. **(D)** Cartilage thickness differed significantly from the mean thickness for body condition scores of 2, 6, and 8, and generally decreased as the body condition scores increased from 2 to 6, with a significant increase in Ei for canines with a body condition score of 8. Ei and thickness were observed to be inversely proportional. Results were deemed significant with a p-value < 0.05.

3. Results

3.1 Mechanical Properties

*3.1.1 Effect of Ageing on Cartilage Ei and Thickness (**Figure 2**).*

Across all examined surfaces, the articular cartilage's Ei at 15% strain showed a significant positive correlation with age **(Figure 2A).** In contrast, there was a significant negative correlation of thickness with age **(Figure 2B).**

3.1.2 Effect of Body Condition Score on Cartilage Ei and Thickness

While there is no clear linear trend between Body Condition Score (BCS), cartilage Ei differed from the mean stiffness for body condition scores of 2, 5, and 8. There was a general trend of increasing Ei as the body condition scores increased from 2 to 6, with a significant decrease in Ei for canines with a body condition score of 8. **(Figure 2C).** Cartilage thickness differed significantly from the mean thickness for body condition scores of 2, 6, and 8, and generally decreased as the body condition scores increased from 2 to 6, with a significant increase in Ei for canines with a body condition score of 8. **(Figure 2D)**.

3.1.3 Effect of Ageing and Joint Type on Cartilage Ei and Thickness

The Ei at 15% strain had no correlation with age in the humerus or in the glenoid fossa **(Figure 3A)**. Both surfaces showed no significant correlation between age and Ei at 15% strain. The Ei at 15% strain had a positive correlation with age in the femoral condyle and trochlea, although insignificant. The Ei at 15% strain had a significant positive correlation to age in the tibia **(Figure 3B)**.

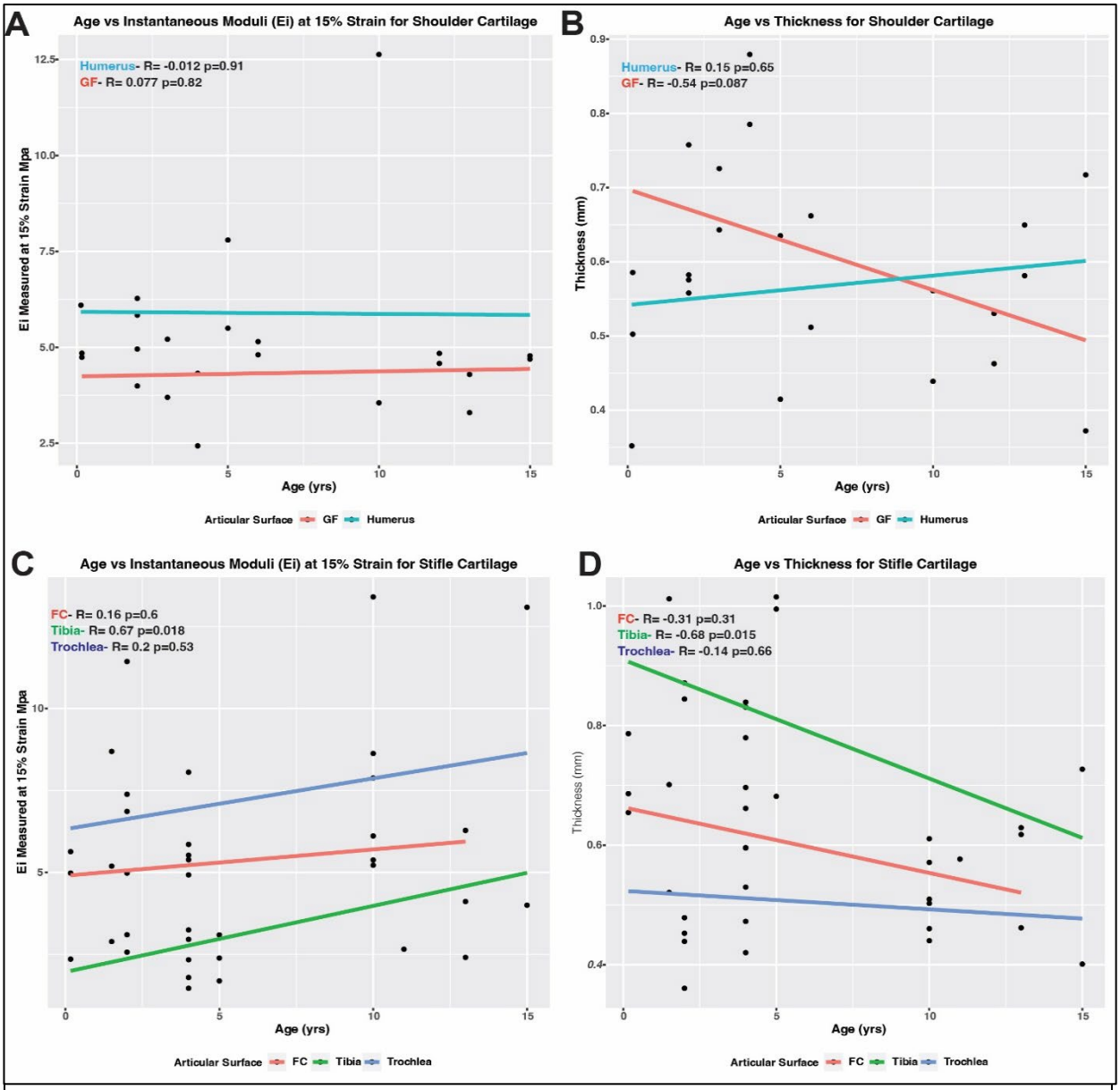


Figure 3: The Effect of Age on Cartilage Thickness and Ei in Each Joint and Surface. **(A)** Cartilage Ei at 15% strain (MPa) vs Age in the Shoulder. Following a linear regression, Ei showed a no correlation to age (Humerus: P=0.97; GF: p=0.82). **(B)** Cartilage thickness (mm) vs Age in the Shoulder. Following a linear regression, thickness showed a no significant correlation to age in the shoulder but the humerus and glenoid fossa showed opposing trends (Humerus: P=0.65; GF: p=0.087). **(C)** Cartilage Ei at 15% strain (MPa) vs Age in the Stifle. Following a linear regression, Ei showed a positive correlation to age. Tibia Ei at 15% strain showed a significant positive correlation to Age (FC: P=0.6; Tibia: p=0.018; Trochlea: p=0.53). **(D)** Cartilage thickness (mm) vs Age in the Stifle. Following a linear regression, thickness showed a negative correlation to age. Tibia thickness showed a significant negative correlation to Age (FC: P=0.31; Tibia: p=0.015; Trochlea: p=0.66). Results were considered statistically significant if P<0.05.

The articular cartilage's thickness had a significant negative correlation with age in the glenoid fossa. In contrast, the thickness trended upward with increased age in the humerus **(Figure 3C)**. The total thickness trended downward with increased age in the femoral condyle and trochlea, although insignificant. The thickness had a significant negative correlation to age in the tibia **(Figure 3D)**.

3.2 Biochemical Properties

3.2.1 GAG and Collagen Correlation with Age

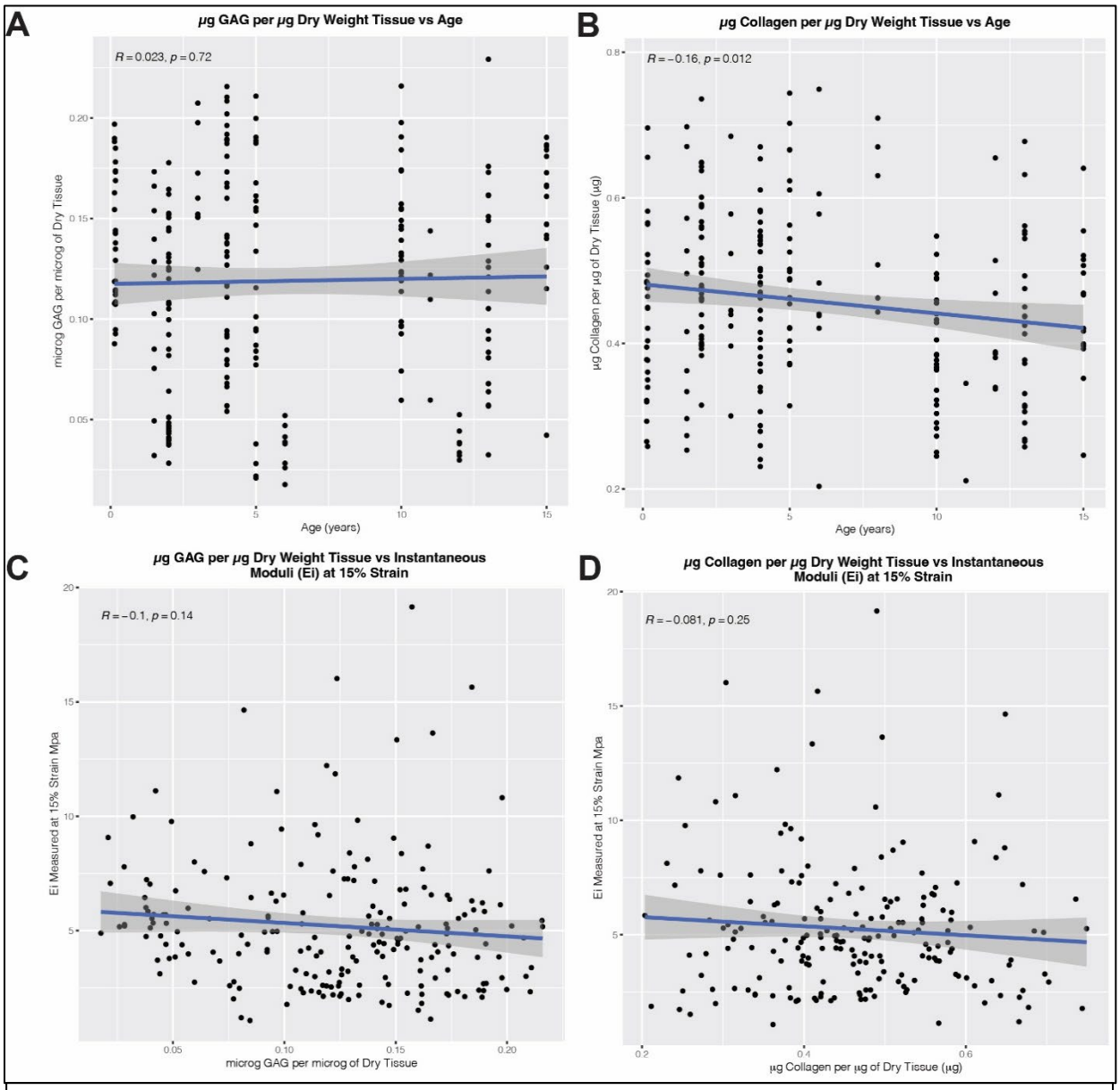


Figure 4: Correlations between GAG and Collagen Composition with Age and Ei. (A) GAG content of cartilage vs Age. Results show no changes in GAG content with Age. (B) Collagen content of cartilage vs Age. Results show a significant decrease in collagen content with Age. (C) GAG content of cartilage vs Ei at 15% strain. Results show a negative correlation between GAG content and Ei at 15% strain. (B) Collagen content of cartilage vs Ei at 15% strain. Results show a negative correlation between collagen content and Ei at 15% strain. Results were considered statistically significant if P<0.05.

This study detected no significant correlation between articular cartilage's GAG content and age **(Figure 4A)**. In contrast, there was a significant negative correlation between total collagen content per dry weight of cartilage tissue and age **(Figure 4B)**.

3.2.2 Effect of Biochemical Composition on Cartilage Ei

This study detected no significant correlation between the total GAG or collagen content of articular cartilage and its Ei when considering all joint surfaces combined. **(Figure 4C, D).** However, the trend of the

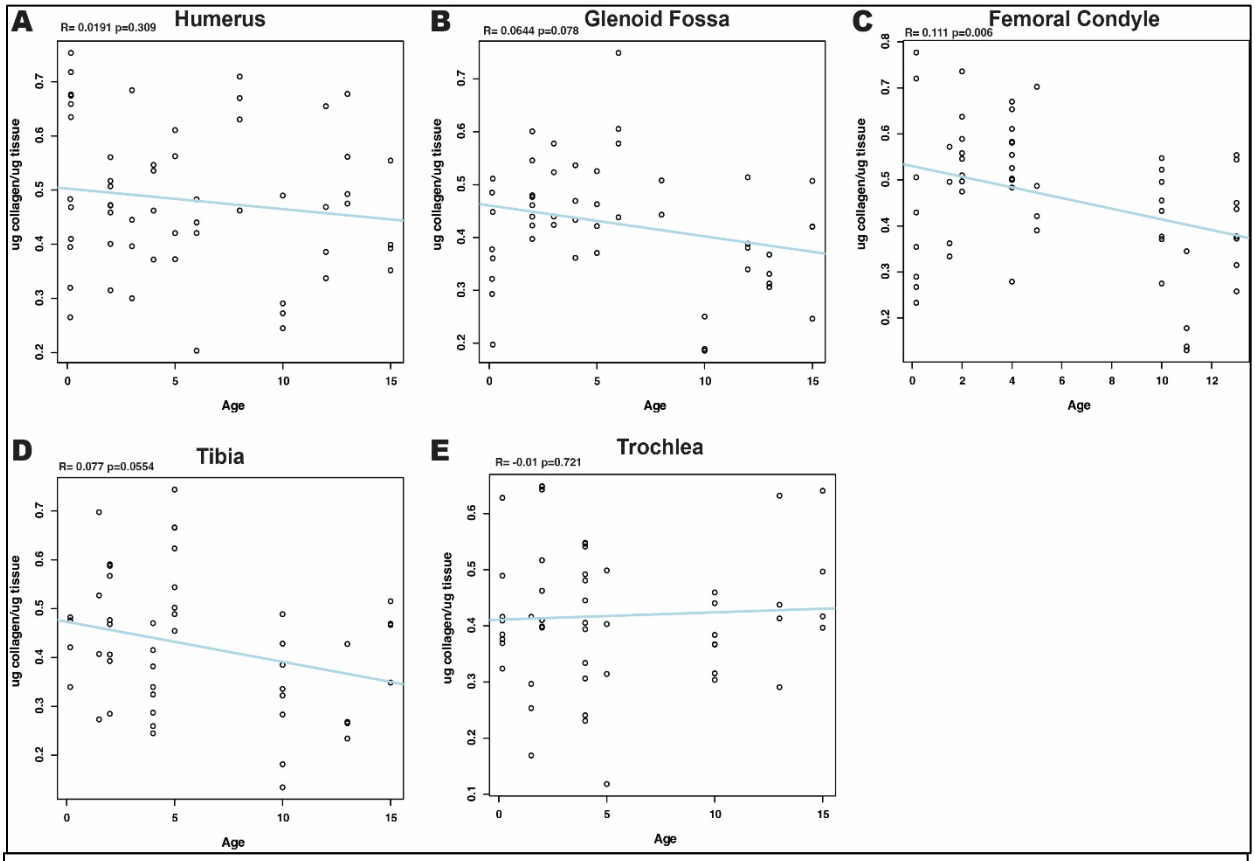


Figure 5: Collagen content vs Age vs Surface. (A) Collagen content vs Age in the Humerus (B) Collagen content vs Age in the Glenoid Fossa. (C) Collagen content vs Age in the Femoral Condyle. (D) Collagen content vs Age in the Tibia. (E) Collagen content vs Age in the Trochlea. Results were considered statistically significant if P<0.05.

correlation for both variables was negative with age.

3.2.3 Effect of Ageing and Joint Type on Biochemical Composition

The total collagen content per dry weight of cartilage tissue showed a negative correlation to age in both the humerus and the glenoid fossa. Collagen content in the humerus **(Figure 5A)** and glenoid fossa**(Figure 5B)** showed a negative correlation to age, although insignificant in both surfaces. The total collagen

content per dry weight of cartilage tissue showed a significant negative correlation to age in the femoral condyle **(Figure 5C)** and tibia **(Figure 5D)**. In contrast, total collagen content per dry weight of cartilage tissue had a positive correlation to age in the trochlea, although insignificant **(Figure 5E)**.

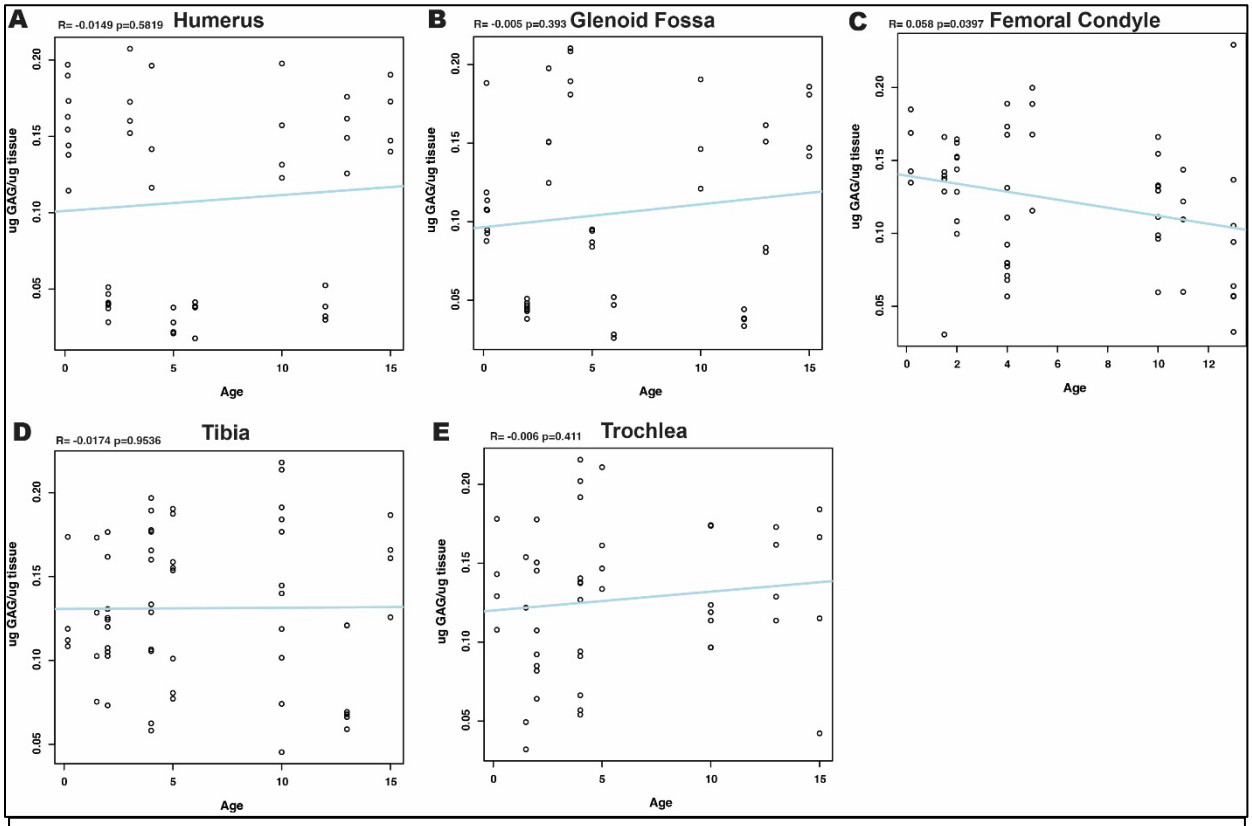


Figure 6: GAG content vs Age vs Surface. (A) GAG content vs Age in the Humerus. (B) GAG content vs Age in the Glenoid Fossa. (C) GAG content vs Age in the Femoral Condyle. (D) GAG content vs Age in the Tibia. (E) GAG content vs Age in the Trochlea. Results were considered statistically significant if $P<0.05$.

The total GAG content per dry weight of cartilage tissue had a positive correlation with age in both the humerus **(Figure 6A)** and glenoid fossa **(Figure 6B)**. The femoral condyle showed a significant negative correlation in GAG with age **(Figure 6C)**. The trochlea **(Figure 6D)** and tibia **(Figure 6E)** in the stifle demonstrated similar trends to the shoulder. The total GAG content per dry weight of cartilage tissue had a positive correlation with age in the trochlea and tibia.

3.2.4 Effect of Ageing and Cellularity

The total ng DNA per mg of dry weight cartilage tissue showed a significant negative correlation of cellularity with age **(Figure 7A).** Histological assessment of cellularity showed similar trends (**Figure 7B).**

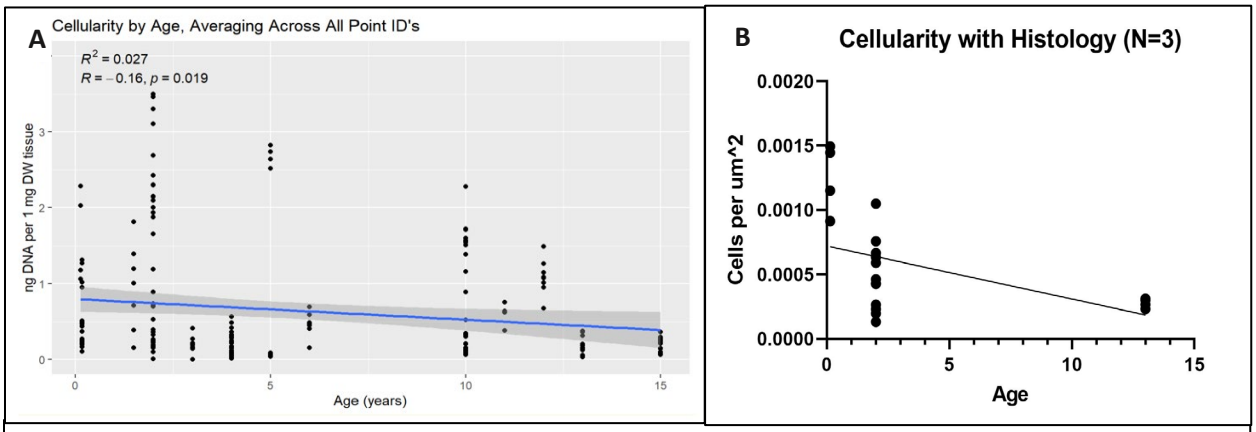


Figure 7: (A) Cellularity correlation with Age in articular cartilage tissue across multiple joint surfaces. Cellularity of cartilage tissue was quantified using Pico Green bicolor assay. **(B)** Histology sections were used to quantify number of cells per unit are using ImageJ (N=3). We observed a significant decrease in cellularity with age (p=0.0311; R=212). Results were considered statistically significant if P<0.05.

3.3 Histology **(Figure 8)**

Histological observations of the representative samples from each age group generally agreed with the biochemistry findings and also revealed evidence of cartilage degeneration with age. Overall cellularity was lower in the older individuals. The subjective assessment of GAG based on the degree of basophilia of the ECM did not reveal obvious trends. However variable degrees of GAG loss were present in the superficial layers in patients of 10+ age group along with superficial cartilage fibrillation and individual chondrocyte death (**Figure 8E and F**). The evidence of fibrillation indicates degenerative process and supports the findings of cartilage thinning.

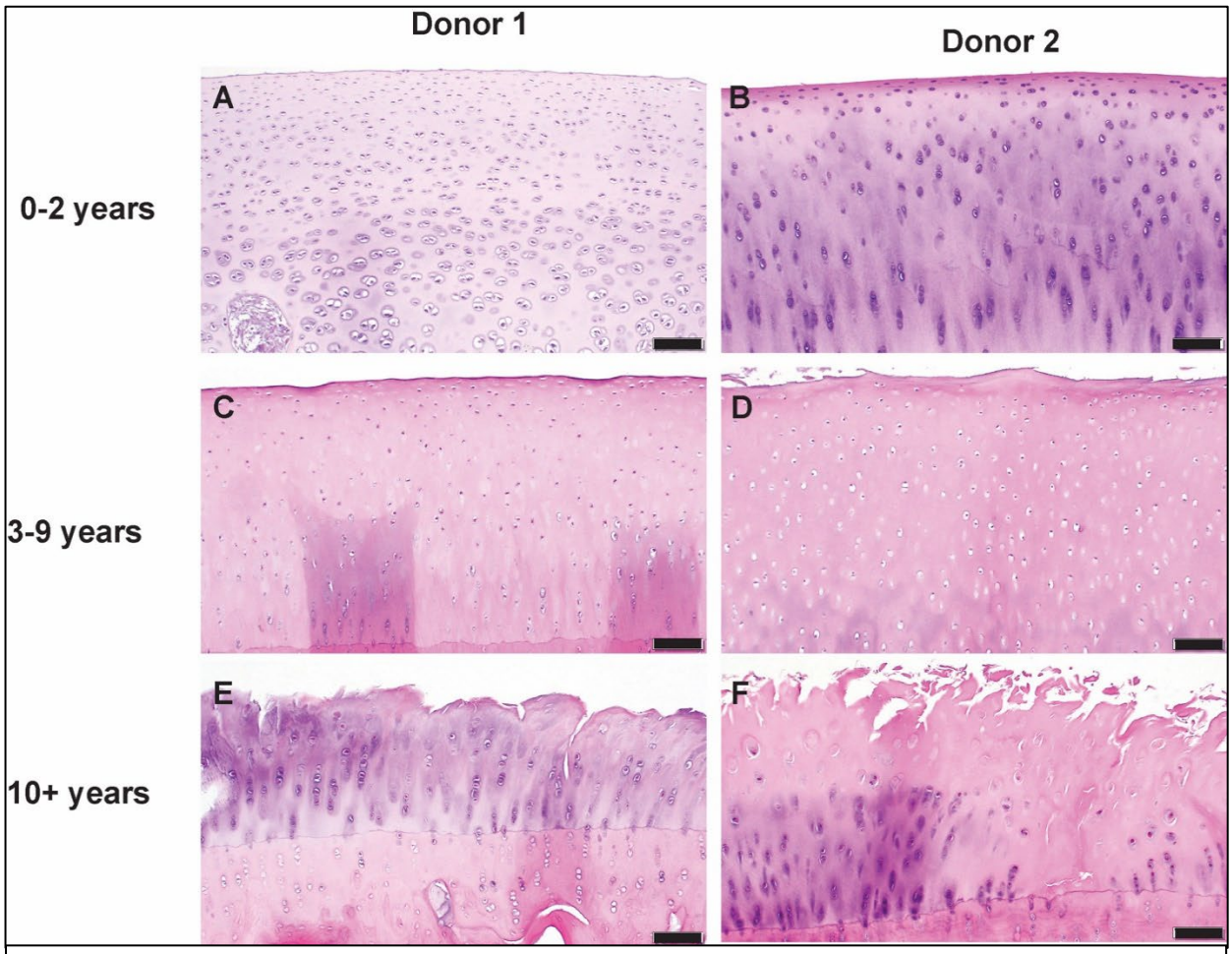


Figure 8: Histology of humeral head across various age groups. H&E= hematoxylin and eosin staining. Bar=100µm. Note thicker articular cartilage in the younger dogs (A-D) and evidence of cartilage thinning and fibrillation in the older group E, F).

4. Discussion:

This study is the first to evaluate the changes in articular cartilage with age using histological, biochemical, and biomechanical parameters across multiple joints in a comprehensive fashion. Multiaxial indentation testing and thickness testing *in situ* allowed generation of three-dimensional maps of biomechanical parameters and thicknesses of the articular surfaces across multiple joints across various age groups of dogs. When considering all surfaces combined, a significantly positive correlation was detected between the Instantaneous moduli (Ei) of articular cartilage and age. A similar association was detected between

Ei and body condition score. Further, there was a significant negative correlation between cartilage thickness and age and articular cartilage collagen content and age. Likewise, there was a significant negative correlation between the cellularity of articular cartilage and age. Interestingly, this study revealed insignificant correlation between GAG and age, and between GAG and Ei of articular cartilage. When considering specific joints individually, similar significant trends of age-related increase in Ei and decrease in thickness were present in the Tibia of the stifle joint. Finally, we observed histological changes consistent with degeneration in articular cartilage but only with geriatric dogs. Collectively, these findings suggest that the aging of articular cartilage is manifested by increase in the instantaneous modulus, decrease in thickness, collagen content, and cellularity but not GAG content. Also, this study shows that there is a great variability in the biochemical and biomechanical properties between specific articular surfaces that may or may not follow the general trends of the ageing changes above.

In the following study we used instantaneous modulus (Ei) as our unit of measurement to represent the biomechanical properties of cartilage. The modulus parameters are derived from a normalization procedure that takes into account the total thickness, cross-sectional area, Poisson ratio, and indenter shape and size (**Equation 1)**. This normalization reflects the internal properties of cartilage in relation to specific environmental conditions. To the best of our knowledge, most studies that investigate the changes in cartilage biomechanics as it relates to age report values as stiffness (N/mm) [108]. Subsequently, most studies investigating canine cartilage biomechanics report values in shear modulus and most studies that investigated Ei of cartilage tissue studied this in species other than dog. As a result, the data from the present study was compared to Ei values found in other species.

In the present study, we found that cartilage Ei had a significant positive correlation with age (**Figure 2).** This is in some alignment with reports from Bielajew et al who found an increase in Ei between neonatal

and juvenile pig cartilage but a decrease in Ei between juvenile and adult porcine cartilage at 10% and 20% strain in the femoral condyle [109]. While the results from Bielajew et al show some similar trends correlating Ei with age, the discrepancies between Bielajew et al. and the current study could be due to a few reasons. 1. The decrease in Ei between juvenile and adult porcine cartilage in Bielajew et al. 's study could be due to the small age range of adult pigs [109]. The pigs considered mature adults were aged 2-3 years whereas the dogs tested in the present study reflected a broader range of geriatric patients. 2. Different methodologies of measuring total thickness and Ei. For example, Bielajew et al measured thickness and Ei using a flat end large diameter indenter whereas the data in the current study used a spherical small diameter indenter. Changing the size and shape of the indenter changes the contact area withstanding the force. This change will reflect in the overall Ei value (**Equation 1).** 3. Interspecies differences in scaling factors to calculate Ei [110]. For example, some studies have reported Poisson ratio of cartilage to fluctuate between 0.07-0.4 within the same species but different surfaces [111, 112]. In addition, the study also showed that the Poisson ratio in humans was significantly less than bovine, dog, monkey, and rabbit. Since Athanasiou et al [111] found that different species show different Poisson ratios between each other and different joints, this made it difficult to compare measurements obtained in various studies to the present. As a result, several factors need to be considered and accounted for to accurately find correlations. More investigation with consistent testing parameters needs to be done to conclude if Ei has a correlation with age across many species.

In this study, we attempted to determine the relationship between cartilage thickness and age in various canine joints. We found that cartilage thickness had a negative correlation with age (**Figure 2).** These results agree with many studies [113] as described in rats[114], rabbits[115], dogs[116], and humans[117, 118]. Additionally, the present study showed that body condition score had no effect on cartilage thickness over age (**Figure 2)**. This corroborated the finding from a study Joseph et al. who showed no

statistically significant associations between weight change and cartilage thickness [119] using MRI imaging. In contrast, a study by Collins et al found that cartilage was thinner and cartilage strain was higher during exercise in patients with a high BMI [120]. These conflicting results could stem from the subjectiveness of BMI and BSC scores. Specifically, BMI is often used as a standard to distinguish between healthy and obese individuals and is calculated based on height and mass of the individual [121]. However, BMI is argued to be a poor indicator of body fat percentage and the distribution of fat mass throughout the body [121, 122]. Likewise, body condition score is a subjective assessment made by clinicians to determine an animal's health [123]. In concert, perhaps quantifying an individual's health in a different way would reflect a stronger correlation to cartilage's properties.

We further attempted to determine if joint type had an impact on the changes in cartilage Ei and thickness with age. However, the results from **Figure 3** show that some joints followed the general trends better than others. type. Specifically, stifle joint showed positive correlations of Ei to age and negative correlations of thickness to age. Specifically, the tibia showed a significant negative correlation between thickness and age but femoral condyle and trochlea showed little if any changes with thickness. These results are supported by Francuski et al [124] who found that thickness of non-calcified tibial cartilage significantly decreased in adult working and non-working dogs in comparison to young dogs. In addition, Francuski et al found that the thickness of non-calcified femoral condyle cartilage showed no changes with age [124]. These results are also in agreement with the current study. Specifically, the shoulder joint showed no correlation to Ei with age and opposing trends of thickness with age, although all insignificant. In contrast with our findings **(Figure 3)**, Chang et al [125] found significant negative correlations between age and morphological parameters, including thickness, of the humeral head in humans. The discrepancy between Chang et al and the current findings could be due to species differences of quadrupeds vs bipeds [126]. The weight distribution of different joints in quadrupeds could also be asymmetrical. For example,

Fish et al found that dogs put more weight on their forelimbs than their hindlimbs [127]. The inconsistent results between the stifle and shoulder joints in the current study could be due to a couple of reasons 1. Anatomical differences for a ball and socket joint vs condylar joint 2. Low statistical power for each individual surface/joint. When all the surfaces were pooled, the results from the current study showed significant correlations; however, when the surfaces were separated out, the statistical power decreased and trends were more difficult to observe. Many studies within the literature explore the knee and hip joints due to the high prevalence of arthritis and high demand for regenerative therapies [128]. Based on the current findings, there is a great variability between joints and surfaces. Future studies are needed in various joints, such as the shoulder, to better understand how age-related degenerative changes in cartilage may differ across joints.

The changes in cartilage Ei with age suggest accompanying changes in biochemical composition with age. In the current study, canine cartilage showed no correlation of GAG with age but shows no correlation to cartilage Ei **(Figure 4).** This data is in agreement with findings from Bielajew et al [109], who found that GAG content in the pig femoral condyle did not change between juvenile and adult pigs. In contrast, others determined that chondrocyte proteoglycan synthesis is negatively correlated with age[129] and the proteoglycans that are produced are more irregular [130, 131]. The restructuring of cartilage extracellular matrix (ECM) with irregular proteoglycans could be affecting the cartilage mechanical properties. In addition, several studies have found that the density of chondroitin sulfate is negatively correlated with age and is replaced with keratan sulfate [131-134]. Keratan sulfate is approximately the same weight as chondroitin sulfate, which may explain why there is no change in GAG composition in the current study **(Figure 4)**. Keratan sulfate is also associated with the pathophysiology of cornea and neural diseases and is thought to disrupt collagen fibril organization [135]. This could explain the decrease in collagen composition as well **(Figure 4)**. According to Akhtar [136]et al , the presence of keratan sulfate could affect

the ability of proteoglycan core proteins to bind to collagen, hence leading to cross-linking. Collagen cross-linking has been associated with aging and increased stiffness of cartilage in pigs [109], horses [137], and humans [138-140]. In fact, Georges et al suggests that crosslinking has a greater impact on stiffness and mechanical properties than the quantity of deposited ECM alone [141, 142]. This directly contrasts with the results in the current study which show that collagen content had little to no effect on cartilage Ei **(Figure 4)**. These results are further illustrated when looking at individual surfaces**.** The GAG (**Figure 5)** and collagen **(Figure 6)** composition of each individual surface showed no significant trends with age. This observation could be due to several reasons. 1. The relatively small sample size of dogs used in this study (N=12) could be hiding significant trends. 2. The pooling of several dog breeds could also be skewing the data results. 3. There could be more factors contributing to cartilage biochemical and biomechanical properties than what was explored in this study. Further data analysis and testing is needed to uncover all the contributing factors.

Histopathological assessment agreed with biochemical data and revealed a negative correlation of thickness and cellularity with age **(Figures 2, Figure 7, and Figure 8).** These results are in alignment with findings from multiple studies that have found a reduction in chondrocytes in healthy aging cartilage and osteoarthritic cartilage[143-145]. In addition, several groups have argued that increased stiffness of the ECM matrix directly influences the behavior and function of cells by reinforcing fibrosis and cellular senescence[90, 146, 147]. Jeon et al found that local clearance of senescent chondrocytes with a senolytic molecule decreased chondrocyte expression of senescent and inflammatory markers while increasing the expression of cartilage tissue ECM proteins [91]. This would reinforce the importance of the results found in the current study. The current study shows an increase in cartilage Ei and a decrease in cell density. Future studies could explore cellular markers specific to cell senescence to confirm.

In conclusion, the data from this study uncovers some important correlations in cartilage aging and brings up new questions. In particular, it would be essential to conduct similar in situ studies on larger sample size of a particular joint types. It would be also interesting to perform a comparative study between canine and human cartilages using the same approach. The main limitation of this study was the small sample size. This limitation may have obscured trends or significant findings. However, the data of this current study presents results that may challenge the current knowledge about cartilage biomechanics. This study is the first, to our knowledge to explore cartilage biomechanics in comprehensive manner *in situ*. Therefore, the challenges it poses to current literature may reflect true values *in vivo.* It is possible that there are more contributing factors to cartilage biomechanics when tested *in situ*. Nevertheless, more investigation is needed to identify specific mechanisms contributing to cartilage aging and how this differs across species. As a result, we can better tailor regenerative therapies or tissue engineered products for the individual.

5. References

1. Tong, L., et al., *Current understanding of osteoarthritis pathogenesis and relevant new approaches.* Bone Research, 2022. **10**(1): p. 60.
2. Montoya, F., et al., *Clinical and experimental approaches to knee cartilage lesion repair and mesenchymal stem cell chondrocyte differentiation.* Biol Res, 2013. **46**(4): p. 441-51.
3. Urlić, I. and A. Ivković, *Cell Sources for Cartilage Repair-Biological and Clinical Perspective.* Cells, 2021. **10**(9).
4. Laurie, S.W., et al., *Donor-site morbidity after harvesting rib and iliac bone.* Plast Reconstr Surg, 1984. **73**(6): p. 933-8.
5. Skouteris, C.A. and G.C. Sotereanos, *Donor site morbidity following harvesting of autogenous rib grafts.* J Oral Maxillofac Surg, 1989. **47**(8): p. 808-12.
6. Oakeshott, R.D., et al., *A clinical and histologic analysis of failed fresh osteochondral allografts.* Clin Orthop Relat Res, 1988(233): p. 283-94.
7. Stevenson, S., et al., *The fate of articular cartilage after transplantation of fresh and cryopreserved tissue-antigen-matched and mismatched osteochondral allografts in dogs.* J Bone Joint Surg Am, 1989. **71**(9): p. 1297-307.
8. Friedlaender, G.E., et al., *Long-term follow-up of patients with osteochondral allografts. A correlation between immunologic responses and clinical outcome.* Orthop Clin North Am, 1999. **30**(4): p. 583-8.
9. Sun, K., C. Tao, and D.A. Wang, *Scaffold-free approaches for the fabrication of engineered articular cartilage tissue.* Biomed Mater, 2022. **17**(2).

10. Smith, B., I.R. Sigal, and D.A. Grande, *Immunology and cartilage regeneration.* Immunol Res, 2015. **63**(1-3): p. 181-6.
11. Garrity, C., et al., *A Fresh Glimpse into Cartilage Immune Privilege.* Cartilage, 2022. **13**(4): p. 119-132.
12. Li, H., et al., *Applications of genome editing technology in the targeted therapy of human diseases: mechanisms, advances and prospects.* Signal Transduction and Targeted Therapy, 2020. **5**(1): p. 1.
13. Murphy, K. and C. Weaver, *Janeway's immunobiology*. 2017. p. 213, 214-216, 231-233, 245-246, 357-358, 364-365, 367-371.
14. Shao, L., et al., *Knockout of beta-2 microglobulin enhances cardiac repair by modulating exosome imprinting and inhibiting stem cell-induced immune rejection.* Cell Mol Life Sci, 2020. **77**(5): p. 937-952.
15. Naeimi Kararoudi, M., et al., *Assessment of Beta-2 Microglobulin Gene Edited Airway Epithelial Stem Cells as a treatment for Sulfur Mustard Inhalation.* Front Genome Ed, 2022. **4**: p. 781531.
16. Ka, Y., et al., *Improved engraftment of human peripheral blood mononuclear cells in NOG MHC double knockout mice generated using CRISPR/Cas9.* Immunol Lett, 2021. **229**: p. 55-61.
17. Vapniarsky, N., et al., *Tissue Engineering of Canine Cartilage from Surgically Debrided Osteochondritis Dissecans Fragments.* Ann Biomed Eng, 2022. **50**(1): p. 56-77.
18. Pham, T.M., et al., *Elevation of Pro-Inflammatory Cytokine Levels Following Intra-Articular Fractures-A Systematic Review.* Cells, 2021. **10**(4).
19. Sake, H.J., et al., *Possible detrimental effects of beta-2-microglobulin knockout in pigs.* Xenotransplantation, 2019: p. e12525.
20. Montague, T.G., et al., *CHOPCHOP: a CRISPR/Cas9 and TALEN web tool for genome editing.* Nucleic Acids Research, 2014. **42**(W1): p. W401-W407.
21. Tan, Y.S. and Y.L. Lei, *Isolation of Tumor-Infiltrating Lymphocytes by Ficoll-Paque Density Gradient Centrifugation.* Methods Mol Biol, 2019. **1960**: p. 93-99.
22. Vapniarsky, N., et al., *Tissue engineering toward temporomandibular joint disc regeneration.* Sci Transl Med, 2018. **10**(446).
23. Carson, L.F., *Histotechnology : a self instructional text*. 2nd ed. 1997, Chicago, IL: American Society of Clinical Pathology.
24. Adkisson, H.D., et al., *Immune evasion by neocartilage-derived chondrocytes: Implications for biologic repair of joint articular cartilage.* Stem Cell Res, 2010. **4**(1): p. 57-68.
25. Hu, X., et al., *Identification of cellular heterogeneity and immunogenicity of chondrocytes via single-cell RNA sequencing technique in human osteoarthritis.* Front Pharmacol, 2022. **13**: p. 1004766.
26. Wang, X., et al., *Diminished expression of major histocompatibility complex facilitates the use of human induced pluripotent stem cells in monkey.* Stem Cell Res Ther, 2020. **11**(1): p. 334.
27. Gornalusse, G.G., et al., *HLA-E-expressing pluripotent stem cells escape allogeneic responses and lysis by NK cells.* Nat Biotechnol, 2017. **35**(8): p. 765-772.
28. Lanza, R., D.W. Russell, and A. Nagy, *Engineering universal cells that evade immune detection.* Nat Rev Immunol, 2019.
29. Chen, X., et al., *Chondrocyte sheet in vivo cartilage regeneration technique using miR-193b-3p to target MMP16.* Aging (Albany NY), 2019. **11**(17): p. 7070-7082.
30. Cui, Y., et al., *Effects of cartilage-derived morphogenetic protein 1 (CDMP1) transgenic mesenchymal stem cell sheets in repairing rabbit cartilage defects.* Genet Mol Res, 2016. **15**(2).
31. Plesh, O., S.H. Adams, and S.A. Gansky, *Temporomandibular joint and muscle disorder-type pain and comorbid pains in a national US sample.* J Orofac Pain, 2011. **25**(3): p. 190-8.

32. Valesan, L.F., et al., *Prevalence of temporomandibular joint disorders: a systematic review and meta-analysis.* Clin Oral Investig, 2021. **25**(2): p. 441-453.
33. National Academies of Sciences, E., et al., *The National Academies Collection: Reports funded by National Institutes of Health*, in *Temporomandibular Disorders: Priorities for Research and Care*, O. Yost, et al., Editors. 2020, National Academies Press (US)

Copyright 2020 by the National Academy of Sciences. All rights reserved.: Washington (DC).

34. White, B.A., L.A. Williams, and J.R. Leben, *Health care utilization and cost among health maintenance organization members with temporomandibular disorders.* J Orofac Pain, 2001. **15**(2): p. 158-69.
35. Farrar, W.B. and W.L. McCarty, Jr., *The TMJ dilemma.* J Ala Dent Assoc, 1979. **63**(1): p. 19-26.
36. Wilkes, C.H., *Internal derangements of the temporomandibular joint. Pathological variations.* Arch Otolaryngol Head Neck Surg, 1989. **115**(4): p. 469-77.
37. Aryaei, A., et al., *Recent Tissue Engineering Advances for the Treatment of Temporomandibular Joint Disorders.* Curr Osteoporos Rep, 2016. **14**(6): p. 269-279.
38. Holmlund, A.B., G. Gynther, and S. Axelsson, *Diskectomy in treatment of internal derangement of the temporomandibular joint. Follow-up at 1, 3, and 5 years.* Oral Surg Oral Med Oral Pathol, 1993. **76**(3): p. 266-71.
39. Mercuri, L.G., *Alloplastic temporomandibular joint replacement: rationale for the use of custom devices.* Int J Oral Maxillofac Surg, 2012. **41**(9): p. 1033-40.
40. Agerberg, G. and M. Lundberg, *Changes in the temporomandibular joint after surgical treatment. A radiologic follow-up study.* Oral Surg Oral Med Oral Pathol, 1971. **32**(6): p. 865-75.
41. Hinton, R.J., *Alterations in rat condylar cartilage following discectomy.* J Dent Res, 1992. **71**(6): p. 1292-7.
42. Eriksson, L. and P.L. Westesson, *Temporomandibular joint diskectomy. No positive effect of temporary silicone implant in a 5-year follow-up.* Oral Surg Oral Med Oral Pathol, 1992. **74**(3): p. 259-72.
43. Legemate, K., et al., *Engineering Human TMJ Discs with Protein-Releasing 3D-Printed Scaffolds.* J Dent Res, 2016. **95**(7): p. 800-7.
44. Brown, B.N., et al., *Inductive, scaffold-based, regenerative medicine approach to reconstruction of the temporomandibular joint disk.* J Oral Maxillofac Surg, 2012. **70**(11): p. 2656-68.
45. Hagandora, C.K., et al., *Poly (glycerol sebacate): a novel scaffold material for temporomandibular joint disc engineering.* Tissue Eng Part A, 2013. **19**(5-6): p. 729-37.
46. Athanasiou, K.A., et al., *Self-organization and the self-assembling process in tissue engineering.* Annu Rev Biomed Eng, 2013. **15**: p. 115-36.
47. Hu, J.C. and K.A. Athanasiou, *A self-assembling process in articular cartilage tissue engineering.* Tissue Eng, 2006. **12**(4): p. 969-79.
48. Huey, D.J., J.C. Hu, and K.A. Athanasiou, *Unlike bone, cartilage regeneration remains elusive.* Science, 2012. **338**(6109): p. 917-21.
49. MacBarb, R.F., et al., *Engineering functional anisotropy in fibrocartilage neotissues.* Biomaterials, 2013. **34**(38): p. 9980-9.
50. Anderson, D.E. and K.A. Athanasiou, *Passaged goat costal chondrocytes provide a feasible cell source for temporomandibular joint tissue engineering.* Ann Biomed Eng, 2008. **36**(12): p. 1992-2001.
51. Huwe, L.W., et al., *Characterization of costal cartilage and its suitability as a cell source for articular cartilage tissue engineering.* J Tissue Eng Regen Med, 2018. **12**(5): p. 1163-1176.

52. He, A., et al., *Cell yield, chondrogenic potential, and regenerated cartilage type of chondrocytes derived from ear, nasoseptal, and costal cartilage.* J Tissue Eng Regen Med, 2018. **12**(4): p. 1123-1132.
53. Qing-Hua, Y., et al., *The significance of the biomechanical properties of costal cartilage in the timing of ear reconstruction surgery.* J Plast Reconstr Aesthet Surg, 2011. **64**(6): p. 742-6.
54. Nabzdyk, C., et al., *Review: auricular chondrocytes - from benchwork to clinical applications.* In Vivo, 2009. **23**(3): p. 369-80.
55. Gross, A., A. Bumann, and B. Hoffmeister, *Elastic fibers in the human temporo-mandibular joint disc.* Int J Oral Maxillofac Surg, 1999. **28**(6): p. 464-8.
56. Mardas, N., et al., *Experimental model for bone regeneration in oral and cranio-maxillo-facial surgery.* J Invest Surg, 2014. **27**(1): p. 32-49.
57. Almond, G.W., *Research applications using pigs.* Vet Clin North Am Food Anim Pract, 1996. **12**(3): p. 707-16.
58. Clément, C., et al., *Quantitative analysis of the elastic fibres in the human temporomandibular articular disc and its attachments.* Int J Oral Maxillofac Surg, 2006. **35**(12): p. 1120-6.
59. Christensen, L.V., *Elastic tissue in the temporomandibular disc of miniature swine.* Journal of oral rehabilitation, 1975. **2**(4): p. 373-377.
60. Griffin, M.F., et al., *Biomechanical Characterisation of the Human Auricular Cartilages; Implications for Tissue Engineering.* Ann Biomed Eng, 2016. **44**(12): p. 3460-3467.
61. Allen, K.D. and K.A. Athanasiou, *Viscoelastic characterization of the porcine temporomandibular joint disc under unconfined compression.* J Biomech, 2006. **39**(2): p. 312-22.
62. Caccamese, J.F., Jr., R.L. Ruiz, and B.J. Costello, *Costochondral rib grafting.* Atlas Oral Maxillofac Surg Clin North Am, 2005. **13**(2): p. 139-49.
63. Drucker, D.J. and P.L. Brubaker, *Proglucagon gene expression is regulated by a cyclic AMP-dependent pathway in rat intestine.* Proc Natl Acad Sci U S A, 1989. **86**(11): p. 3953-7.
64. Huwe, L.W., et al., *Using Costal Chondrocytes to Engineer Articular Cartilage with Applications of Passive Axial Compression and Bioactive Stimuli.* Tissue Eng Part A, 2018. **24**(5-6): p. 516-526.
65. Bernstein, J.L., et al., *Tissue Engineering Auricular Cartilage Using Late Passage Human Auricular Chondrocytes.* Ann Plast Surg, 2018. **80**(4 Suppl 4): p. S168-s173.
66. Lemaire, R., et al., *Microfibril-associated MAGP-2 stimulates elastic fiber assembly.* J Biol Chem, 2007. **282**(1): p. 800-8.
67. Sherratt, M.J., *Tissue elasticity and the ageing elastic fibre.* Age (Dordr), 2009. **31**(4): p. 305-25.
68. Mithieux, S.M. and A.S. Weiss, *Elastin.* Adv Protein Chem, 2005. **70**: p. 437-61.
69. Shapiro, S.D., et al., *Marked longevity of human lung parenchymal elastic fibers deduced from prevalence of D-aspartate and nuclear weapons-related radiocarbon.* J Clin Invest, 1991. **87**(5): p. 1828-34.
70. Davidson, J.M., K.E. Hill, and J.L. Alford, *Developmental changes in collagen and elastin biosynthesis in the porcine aorta.* Dev Biol, 1986. **118**(1): p. 103-11.
71. Ramirez, F. and L. Pereira, *The fibrillins.* Int J Biochem Cell Biol, 1999. **31**(2): p. 255-9.
72. Hadidi, P., et al., *Temporal development of near-native functional properties and correlations with qMRI in self-assembling fibrocartilage treated with exogenous lysyl oxidase homolog 2.* Acta Biomater, 2017. **64**: p. 29-40.
73. Benya, P.D. and J.D. Shaffer, *Dedifferentiated chondrocytes reexpress the differentiated collagen phenotype when cultured in agarose gels.* Cell, 1982. **30**(1): p. 215-24.
74. Domm, C., et al., *Redifferentiation of dedifferentiated bovine articular chondrocytes in alginate culture under low oxygen tension.* Osteoarthritis Cartilage, 2002. **10**(1): p. 13-22.
75. Benya, P.D., S.R. Padilla, and M.E. Nimni, *Independent regulation of collagen types by chondrocytes during the loss of differentiated function in culture.* Cell, 1978. **15**(4): p. 1313-21.

76. Thomson, H.G., T.Y. Kim, and S.H. Ein, *Residual problems in chest donor sites after microtia reconstruction: a long-term study.* Plast Reconstr Surg, 1995. **95**(6): p. 961-8.
77. Go, J.Y., et al., *Management of chest deformity caused by microtia reconstruction: Comparison of autogenous diced cartilage versus cadaver cartilage graft partial filling techniques.* J Plast Reconstr Aesthet Surg, 2017. **70**(1): p. 104-109.
78. Chen, P.J., et al., *Age-related changes in the cartilage of the temporomandibular joint.* Geroscience, 2020. **42**(3): p. 995-1004.
79. Hudelmaier, M., et al., *Age-related changes in the morphology and deformational behavior of knee joint cartilage.* Arthritis Rheum, 2001. **44**(11): p. 2556-61.
80. Ren, P., et al., *Morphological, biochemical and mechanical properties of articular cartilage and subchondral bone in rat tibial plateau are age related.* J Anat, 2018. **232**(3): p. 457-471.
81. Craig, L.E. and A. Reed, *Age-associated cartilage degeneration of the canine humeral head.* Vet Pathol, 2013. **50**(2): p. 264-8.
82. Wang, L., et al., *Theoretical prediction of ultrasound elastography for detection of early osteoarthritis.* ScientificWorldJournal, 2013. **2013**: p. 565717.
83. Ding, C., et al., *Association between age and knee structural change: a cross sectional MRI based study.* Ann Rheum Dis, 2005. **64**(4): p. 549-55.
84. Eschweiler, J., et al., *The Biomechanics of Cartilage-An Overview.* Life (Basel), 2021. **11**(4).
85. Ficklin, T., et al., *Articular cartilage mechanical and biochemical property relations before and after in vitro growth.* J Biomech, 2007. **40**(16): p. 3607-14.
86. Musumeci, G., et al., *Histochemistry as a unique approach for investigating normal and osteoarthritic cartilage.* Eur J Histochem, 2014. **58**(2): p. 2371.
87. Bayliss, M.T. and S.Y. Ali, *Age-related changes in the composition and structure of human articular-cartilage proteoglycans.* Biochem J, 1978. **176**(3): p. 683-93.
88. Asopa, V., T. Vincent, and J. Saklatvala, *The Effects of Age and Cell Isolation on Collagen II Synthesis by Articular Chondrocytes: Evidence for Transcriptional and Posttranscriptional Regulation.* Biomed Res Int, 2020. **2020**: p. 4060135.
89. Oinas, J., et al., *Composition, structure and tensile biomechanical properties of equine articular cartilage during growth and maturation.* Scientific Reports, 2018. **8**(1): p. 11357.
90. Tominaga, K. and H.I. Suzuki, *TGF-β Signaling in Cellular Senescence and Aging-Related Pathology.* Int J Mol Sci, 2019. **20**(20).
91. Jeon, O.H., et al., *Local clearance of senescent cells attenuates the development of post-traumatic osteoarthritis and creates a pro-regenerative environment.* Nat Med, 2017. **23**(6): p. 775-781.
92. Li, Y., et al., *The age-related changes in cartilage and osteoarthritis.* Biomed Res Int, 2013. **2013**: p. 916530.
93. Patel, J.M., et al., *A Systematic Review and Guide to Mechanical Testing for Articular Cartilage Tissue Engineering.* Tissue engineering. Part C, Methods, 2019. **25**(10): p. 593-608.
94. Seidenstuecker, M., et al., *Viscoelasticity and histology of the human cartilage in healthy and degenerated conditions of the knee.* J Orthop Surg Res, 2019. **14**(1): p. 256.
95. Cutcliffe, H.C. and L.E. DeFrate, *Comparison of Cartilage Mechanical Properties Measured During Creep and Recovery.* Sci Rep, 2020. **10**(1): p. 1547.
96. Sophia Fox, A.J., A. Bedi, and S.A. Rodeo, *The basic science of articular cartilage: structure, composition, and function.* Sports Health, 2009. **1**(6): p. 461-8.
97. Schlichting, K.E., et al., *Synthesis of a novel photopolymerized nanocomposite hydrogel for treatment of acute mechanical damage to cartilage.* Acta Biomater, 2011. **7**(8): p. 3094-100.
98. Elder, S., et al., *Effects of antigen removal on a porcine osteochondral xenograft for articular cartilage repair.* J Biomed Mater Res A, 2018. **106**(8): p. 2251-2260.

99. Burr, D.B. and M.A. Gallant, *Bone remodelling in osteoarthritis.* Nat Rev Rheumatol, 2012. **8**(11): p. 665-73.
100. Bobinac, D., et al., *Changes in articular cartilage and subchondral bone histomorphometry in osteoarthritic knee joints in humans.* Bone, 2003. **32**(3): p. 284-90.
101. Lyyra, T., et al., *Indentation instrument for the measurement of cartilage stiffness under arthroscopic control.* Med Eng Phys, 1995. **17**(5): p. 395-9.
102. Chan, D.D., et al., *In vivo articular cartilage deformation: noninvasive quantification of intratissue strain during joint contact in the human knee.* Sci Rep, 2016. **6**: p. 19220.
103. Lakin, B.A., B.D. Snyder, and M.W. Grinstaff, *Assessing Cartilage Biomechanical Properties: Techniques for Evaluating the Functional Performance of Cartilage in Health and Disease.* Annu Rev Biomed Eng, 2017. **19**: p. 27-55.
104. Sim, S., et al., *Non-destructive electromechanical assessment (Arthro-BST) of human articular cartilage correlates with histological scores and biomechanical properties.* Osteoarthritis Cartilage, 2014. **22**(11): p. 1926-35.
105. Sim, S., et al., *Electromechanical probe and automated indentation maps are sensitive techniques in assessing early degenerated human articular cartilage.* J Orthop Res, 2017. **35**(4): p. 858-867.
106. Craig, L.E., K.E. Dittmer, and K.G. Thompson, *Chapter 2 - Bones and Joints*, in *Jubb, Kennedy & Palmer's Pathology of Domestic Animals: Volume 1 (Sixth Edition)*, M.G. Maxie, Editor. 2016, W.B. Saunders. p. 16-163.e1.
107. Hayes, W.C., et al., *A mathematical analysis for indentation tests of articular cartilage.* J Biomech, 1972. **5**(5): p. 541-51.
108. Lyyra, T., et al., *In vivo characterization of indentation stiffness of articular cartilage in the normal human knee.* J Biomed Mater Res, 1999. **48**(4): p. 482-7.
109. Bielajew, B.J., et al., *Proteomic, mechanical, and biochemical characterization of cartilage development.* Acta Biomater, 2022. **143**: p. 52-62.
110. Thambyah, A., A. Nather, and J. Goh, *Mechanical properties of articular cartilage covered by the meniscus.* Osteoarthritis and Cartilage, 2006. **14**(6): p. 580-588.
111. Athanasiou, K.A., et al., *Interspecies comparisons of in situ intrinsic mechanical properties of distal femoral cartilage.* J Orthop Res, 1991. **9**(3): p. 330-40.
112. Jurvelin, J.S., et al., *Topographical variation of the elastic properties of articular cartilage in the canine knee.* Journal of Biomechanics, 2000. **33**(6): p. 669-675.
113. Nocera, I., et al., *Ultrasonography of the Metacarpal/Tarsal-Phalangeal Joints in Healthy Racehorses: Normal Appearance, Breed-Related and Age-Related Features.* Animals, 2022. **12**(19): p. 2657.
114. Schiefke, I., et al., *Morphological and histochemical ageing changes in patellar articular cartilage of the rat.* Annals of Anatomy - Anatomischer Anzeiger, 1998. **180**(6): p. 495-500.
115. Castano Oreja, M.T., et al., *Variation in articular cartilage in rabbits between weeks six and eight.* Anat Rec, 1995. **241**(1): p. 34-8.
116. Brunnberg, M.M., et al., *Cartilage thickness of the trochlea of the talus, with emphasis on sites predisposed to osteochondrosis dissecans, in clinically normal juvenile and adult dogs.* Am J Vet Res, 2011. **72**(10): p. 1318-24.
117. Millington, S.A., et al., *Quantification of ankle articular cartilage topography and thickness using a high resolution stereophotography system.* Osteoarthritis Cartilage, 2007. **15**(2): p. 205-11.
118. Karvonen, R.L., et al., *Factors affecting articular cartilage thickness in osteoarthritis and aging.* J Rheumatol, 1994. **21**(7): p. 1310-8.

119. Joseph, G.B., et al., *Associations between weight change, knee subcutaneous fat and cartilage thickness in overweight and obese individuals: 4-Year data from the osteoarthritis initiative.* Osteoarthritis Cartilage, 2023. **31**(11): p. 1515-1523.
120. Collins, A.T., et al., *The Influence of Obesity and Meniscal Coverage on In Vivo Tibial Cartilage Thickness and Strain.* Orthop J Sports Med, 2020. **8**(12): p. 2325967120964468.
121. Gutin, I., *In BMI We Trust: Reframing the Body Mass Index as a Measure of Health.* Soc Theory Health, 2018. **16**(3): p. 256-271.
122. Nuttall, F.Q., *Body Mass Index: Obesity, BMI, and Health: A Critical Review.* Nutr Today, 2015. **50**(3): p. 117-128.
123. Burkholder, W.J., *Use of body condition scores in clinical assessment of the provision of optimal nutrition.* J Am Vet Med Assoc, 2000. **217**(5): p. 650-4.
124. Francuski, J.V., et al., *Age-related changes in the articular cartilage of the stifle joint in non-working and working German Shepherd dogs.* J Comp Pathol, 2014. **151**(4): p. 363-74.
125. Chang, Z., et al., *Age-Related changes in the morphological features of medial column of the proximal humerus in the Chinese population.* Front Surg, 2023. **10**: p. 1138620.
126. Foster, A.D., *The impact of bipedal mechanical loading history on longitudinal long bone growth.* PLoS One, 2019. **14**(2): p. e0211692.
127. Fish, F.E., et al., *A 60:40 split: Differential mass support in dogs.* Anat Rec (Hoboken), 2021. **304**(1): p. 78-89.
128. Chillemi, C. and V. Franceschini, *Shoulder osteoarthritis.* Arthritis, 2013. **2013**: p. 370231.
129. DeGroot, J., et al., *Age-related decrease in proteoglycan synthesis of human articular chondrocytes: the role of nonenzymatic glycation.* Arthritis Rheum, 1999. **42**(5): p. 1003-9.
130. Bolton, M.C., J. Dudhia, and M.T. Bayliss, *Age-related changes in the synthesis of link protein and aggrecan in human articular cartilage: implications for aggregate stability.* Biochem J, 1999. **337 (Pt 1)**(Pt 1): p. 77-82.
131. Buckwalter, J.A., P.J. Roughley, and L.C. Rosenberg, *Age-related changes in cartilage proteoglycans: quantitative electron microscopic studies.* Microsc Res Tech, 1994. **28**(5): p. 398-408.
132. Sodhi, H. and A. Panitch, *Glycosaminoglycans in Tissue Engineering: A Review.* Biomolecules, 2020. **11**(1).
133. Elliott, R.J. and D.L. Gardner, *Changes with age in the glycosaminoglycans of human articular cartilage.* Ann Rheum Dis, 1979. **38**(4): p. 371-7.
134. Martel-Pelletier, J., et al., *Discrepancies in composition and biological effects of different formulations of chondroitin sulfate.* Molecules, 2015. **20**(3): p. 4277-89.
135. Quantock, A.J., R.D. Young, and T.O. Akama, *Structural and biochemical aspects of keratan sulphate in the cornea.* Cellular and Molecular Life Sciences, 2010. **67**(6): p. 891-906.
136. Akhtar, S., et al., *Keratoconus corneal architecture after riboflavin/ultraviolet A cross-linking: ultrastructural studies.* Mol Vis, 2013. **19**: p. 1526-37.
137. Brama, P.A., et al., *Development of biochemical heterogeneity of articular cartilage: influences of age and exercise.* Equine Vet J, 2002. **34**(3): p. 265-9.
138. Saito, M. and K. Marumo, *Collagen cross-links as a determinant of bone quality: a possible explanation for bone fragility in aging, osteoporosis, and diabetes mellitus.* Osteoporos Int, 2010. **21**(2): p. 195-214.
139. Bank, R.A., et al., *Ageing and zonal variation in post-translational modification of collagen in normal human articular cartilage. The age-related increase in non-enzymatic glycation affects biomechanical properties of cartilage.* Biochem J, 1998. **330 (Pt 1)**(Pt 1): p. 345-51.
140. Lai-Fook, S.J. and R.E. Hyatt, *Effects of age on elastic moduli of human lungs.* J Appl Physiol (1985), 2000. **89**(1): p. 163-8.

141. Georges, P.C., et al., *Increased stiffness of the rat liver precedes matrix deposition: implications for fibrosis.* Am J Physiol Gastrointest Liver Physiol, 2007. **293**(6): p. G1147-54.
142. Blokland, K.E.C., et al., *Regulation of cellular senescence by extracellular matrix during chronic fibrotic diseases.* Clin Sci (Lond), 2020. **134**(20): p. 2681-2706.
143. Kühn, K., et al., *Cell death in cartilage.* Osteoarthritis Cartilage, 2004. **12**(1): p. 1-16.
144. Horton, W.E., Jr., L. Feng, and C. Adams, *Chondrocyte apoptosis in development, aging and disease.* Matrix Biol, 1998. **17**(2): p. 107-15.
145. Aigner, T., H.A. Kim, and H.I. Roach, *Apoptosis in osteoarthritis.* Rheum Dis Clin North Am, 2004. **30**(3): p. 639-53, xi.
146. Zhang, Y., P.B. Alexander, and X.F. Wang, *TGF-β Family Signaling in the Control of Cell Proliferation and Survival.* Cold Spring Harb Perspect Biol, 2017. **9**(4).
147. Hassona, Y., et al., *Progression of genotype-specific oral cancer leads to senescence of cancer-associated fibroblasts and is mediated by oxidative stress and TGF-β.* Carcinogenesis, 2013. **34**(6): p. 1286-95.

Chapter 5

Tilapia Fish Skin Treatment of Third-Degree Skin Burns in Murine Model

Carissa Garrity, Christina Garcia-Rovetta, Iris Rivas, Ubaldo Delatorre, Alice Wong, Dietmar Kultz, Jamie Peyton, Boaz Arzi, and Natalia Vapniarsky

Published in *Journal of Functional Biomaterials* October 2023

https://doi.org/10.3390/jfb14100512

Abstract:

This study explored the feasibility of using fish skin bandages as a therapeutic option for third-degree skin burns. Following the California wildfires, clinical observations of animals with third-degree skin burns demonstrated increased comfort levels and reduced pain when treated with tilapia fish skin. Despite the promises of this therapy, there are few studies explaining the healing mechanisms behind the application of tilapia fish skin. In this study, mice with third-degree burns were treated with either a hydrocolloid adhesive bandage (control) (n = 16) or fish skin (n = 16) 7 days post-burn. Mice were subjected to histologic, hematologic, molecular, and gross evaluation at days 7, 16, and 28 post-burn. The fish skin offered no benefit to overall wound closure compared to hydrocolloids. Additionally, we detected no difference between fish skin and control treatments in regard to hypermetabolism or hematologic values. However, the fish skin groups exhibited 2 times more vascularization and 2 times higher expression of antimicrobial defensin peptide in comparison to controls. Proteomic analysis of the fish skin revealed the presence of antimicrobial peptides. Collectively, these data suggest that fish skin can serve as an innovative and cost-effective therapeutic alternative for burn victims to facilitate vascularization and reduce bacterial infection.

Keywords: wound regeneration; burn therapy; fish skin; hematology; histology

1. Introduction

Severe skin burns are painful and may be life-threatening injuries, posing a substantial public health concern. Worldwide, an estimated 180,000 deaths occur annually due to burns, with the majority occurring in low- and middle-income countries [1]. Non-fatal burn injuries are among the leading causes of morbidity [1]. Treatment of burns typically requires prolonged hospitalization and may result in disfigurement and disability, often with resulting stigma and rejection. In the United States alone, it is estimated that approximately 359,000 people sought medical care for burns in 2020 [2]. Global warming-associated wildfires and the associated burn victims are increasing worldwide at an alarming rate [3]. These statistics associated with burns invite the development of novel, affordable therapies for burn patients.

Burns can be categorized depending on the degree of damage inflicted. First-degree burns are defined as superficial burns consisting of damage only to the epidermis. These burns usually heal within seven days of injury. Second-degree burns involve the epidermis and dermis and can be further categorized into superficial partial thickness (epidermis and papillary dermis) or deep partial thickness (epidermis and reticular dermis). Superficial partial thickness burns typically heal within 10 days and require debridement of damaged skin and daily wound care. Deep partial-thickness burns have a more variable healing time, usually between 10 and 28 days, and require surgical excision and resurfacing in addition to daily wound care. A burn that affects the entire dermis is categorized as third degree, will require surgical excision and resurfacing, and typically heals within three weeks or more. Once a burn reaches tissues deep in the dermis, such as muscle, fat, and bone, it is categorized as a fourth-degree burn and often requires amputation and more extensive reconstruction [4].

Burns injuries are not just limited to skin and can result in systemic complications. Burns exceeding 30% of total body surface area can trigger a systemic inflammatory response, thus resulting in hypovolemic burn shock, a hypercoagulable state, and a risk of sepsis [5]. Furthermore, the extreme metabolic challenge associated with severe burns results in hypermetabolism syndrome. The exact pathophysiology is still elusive, but it has been recognized as a marked increase in catecholamines and cortisol and changes in acute phase protein pathways, leading to increased metabolic rates, systemic increases in catabolism, and multi-organ dysfunction [6]. Hew et al. demonstrated that post-burn hypermetabolism is induced in mice with both large (10% TBSA) and small (2.8% TBSA) burns using parameters such as basal energy expenditure, changes in catabolism, and changes in hormones and inflammatory mediators [7]. These alterations in metabolism and inflammation may impede the healing process of wounds and introduce new complications that necessitate medical attention.

Substantial progress in burn care has significantly improved the survival of burn victims [4]. However, more improvements can be achieved in the area of skin replacement. For example, autologous skin grafting may be currently considered the gold standard for burn treatment, but this option is not suitable for patients with extensive burns and has the disadvantage of inducing morbidity at the collection site [8]. Biological and synthetic skin substitutes offer various advantages; however, at this juncture, there is no ideal skin substitute on the market that provides effective, affordable, and scar-free wound healing [9]. Currently, available treatment options may leave patients at risk of complications such as pain, scarring, and infection, underscoring the need for medical advancements in skin replacement modalities.

Tilapia skin has been explored as a promising burn treatment since it was first used in a clinical trial on humans in Brazil in 2017 [10]. According to Hu et al., 99.14% of peptides extracted from tilapia skin by hydrolysis were less than 5 kDa, with 58% hydrophilic residues. These peptides were effective in reducing the scratch defects of keratinocytes as effectively as an epidermal growth factor. Also, the wound-healing rate in the rabbit in vivo model treated with marine peptides was enhanced compared to burn ointment

and untreated control groups [11]. The abundance and relatively uncomplicated farming of Nile tilapia, combined with its low cost, makes tilapia skin an attractive solution for burn therapy. The affordability of tilapia skin is especially relevant for low-income societies where burn injuries are more prevalent. Furthermore, recent wildfire events in California led to a large number of burn victims among wild and domesticated animals. With a lack of affordable skin-replacement options, tilapia skin was used to treat extensive third-degree burn wounds in these animals. Although no controlled studies were performed, the clinical observations pointed out a marked reduction in pain and an increase in comfort levels of tilapia skin-treated animals. These clinical observations inspired this study, aiming to explore the efficacy of tilapia fish skin bandages for full-thickness burns in mice compared to hydrocolloid bandage-treated controls. Here, we report a comparison of wound sizes, complete blood counts, body weights, histology, various molecular markers, and serum glucose levels between experimental groups. Additionally, we report proteomic analyses of nonstructural peptides of fish and murine skin.

2. Materials and Methods

2.1. Animals

For this experiment, 32 C57BL/6 mice with ages ranging from 12 to 15 weeks were divided into two groups where males and females were equally represented. This study was conducted with the approval of the Institutional Animal Care and Use Committee.

2.2. Study Design

In all mice, scald burn was created on the dorsum at day zero. Body weights were recorded, and blood was collected into heparin and serum tubes. On day seven post-burn induction, the necrotic skin was surgically debrided, and the exposed wound was covered by either fish skin, hydrocolloid bandage (HCB), or adhesive bandage (control) (Duo-DERM Cat # 187660) (**Figure 1).** Half of the mice in fish-skin-treated and HCB controls were humanely euthanized on day 16, while the remainder of the mice were euthanized on day 28 post-burn induction. n. Prior to euthanasia, blood was collected as before. Upon euthanasia, the fish skin and HCB bandages were removed, the wounds photographed, and the body weights of the animals recorded.

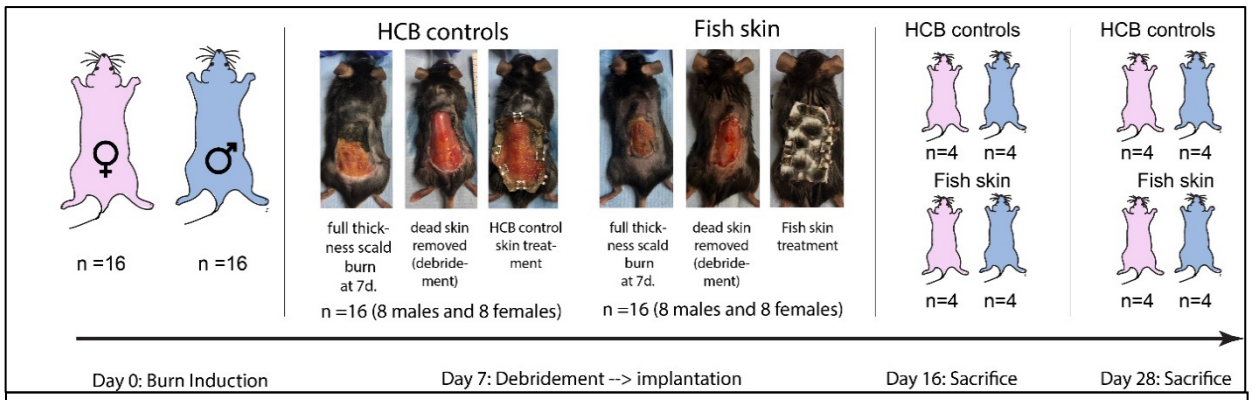


Figure 1. Study design and timeline of the study. A scald burn was induced on the dorsum. On day 7, the burned tissue was surgically debrided, and the wound was dressed in either a hydrocolloid bandage (HCB) or rehydrated fish skin. Both bandages were secured to the intact skin with metal clips. On day 16 and day 28, animals were humanely euthanized for tissue collection. The blood was drawn from the infraorbital sinus under anesthesia at days 0, 7, 16.

2.3. Burn Induction

The mice were anesthetized using isoflurane (0.5–2%) and oxygen (2 L/min) in an induction chamber. During the induction, buprenorphine (0.05 mg/kg SC), Ceftiofur (20 mg/kg SC), and warm saline (5 mL SC) were administered subcutaneously. The mice were then transferred to a table, and maintenance isoflurane anesthesia was delivered via a nose cone. Once no pain reflex was registered on the paw pinch, tetracaine eye drops were applied to each eye, and a heparin-treated hematocrit capillary tube was inserted into the retro-orbital sinus to withdraw blood. Four drops of blood were collected into serum and

EDTA tubes, respectively. The blood was kept on ice until processing within a few hours. A complete blood count (CBC) was performed at UC Davis Comparative Pathology Laboratory, certified for murine blood analysis. Both eyes were then lubricated with ointment to prevent corneal drying during the anesthesia. The dorsum was shaved with beard clippers to expose approximately 2 cm × 3 cm area of skin. Veet hair removal cream was applied to the shaved area for 60 s to remove the hair completely. Once the cream was removed, each mouse was laid onto the plastic bed with the 20 × 30 mm opening (corresponding to 3–5% of total body surface area) overlapping the shaved area of skin. The scald burns were induced according to a previously published protocol with minor modifications [12]. Specifically, the water temperature was raised to 56°C, and the exposure time was increased to 30 s to ensure induction of third-degree burns. Mice were in individual cages after the burn induction. Fluids and buprenorphine were administered prior to burn induction and then twice daily for the three days following burn induction. The mice were monitored daily for 10 days post-burn.

Although the burn-induction conditions were identical for all mice, smaller females with body weights of <25 g did not tolerate the burn procedure well and had to be euthanized before they reached the termination time points. For this reason, the study was repeated on additional mice with the best possible attempt to have a balanced sex representation across groups. The eventual numbers of mice across groups are presented in the results in Section 3.7.

2.4. Burn Debridement and Treatment

On the seventh day post-burn, the mice were weighed, anesthetized, and had blood collected via the same procedure outlined above. Once blood was collected, the wounded area of each mouse was surgically debrided, and fish skin or HCB (control) was applied to completely cover the wound (Supplementary Materials Video S1). Each dressing was secured to the surrounding skin with metal clips.

2.5. Sacrifice and Sample Collection

On the day of sacrifice, mice were anesthetized, and blood was drawn as previously described, but no fluids or other medications were administered. Upon sacrifice, the clips were removed before weighing. Anesthetized animals were placed into a CO2 chamber until no rib movement was observed. Post mortem, the skin samples from the burn-healthy skin interface were harvested and preserved frozen or fixed in formalin for further RNA isolation, proteomic analysis, and histology.

2.6. Fish Skin Preparation

The fish skin bandages were produced at UC Davis using a patented protocol https://patents.google.com/patent/US11612675B1 (accessed on 20 August 2023) [13]. This protocol is approved and publicly available. Briefly, whole tilapia fish were cleaned from scales and celomic contents. The skin was removed from the very fresh tilapia fish (<2 h post-mortem) by traction from the rostral-dorsal aspect of the fish body towards the tail using the pincher tool (**Supplementary Materials Figure S1**).



Figure S1. Schematic of tilapia skin preparation. The skin was cut along the solid lines and then pulled in the direction of the arrow from the dorso-cranial corner (*). The procedure was repeated on opposite side.

The removed skin was placed in the ice bath for 10 min to prevent deterioration while processing other fish. The myofascial tissue was then thoroughly scraped away with a blunt knife or a hard scraper. After that, the skins were rinsed in a new container with sterile 0.9% saline and then transferred to the container containing 2% Chlorhexidine gluconate (VetOne 30159, VetOne,

Boise, ID, USA) at 1 mL solution per each 1 cm2 of skin. The skins were soaked in this solution with gentle agitation for 30 min before a repeated rinse with saline. The process of Chlorhexidine gluconate soak and rinse was repeated one more time before the skins were transferred into 50% glycerol solution in saline for 1 h soak at room temperature with gentle agitation. Subsequently, the skins were soaked in 75% and 99% glycerol (Thermo 17904, Thermo Fisher Scientific, Waltham, MA, USA) for 1 h at room temperature and then 24 h at 4 _C, respectively. After that, the skins were preserved in 100% glycerol with 1% pen strep for up to three months.

Before application to the wounds, the skins were rehydrated in three subsequent soaks of sterile 0.9% saline for 20 min each. Once rehydrated, the skins were used in their entirety.

2.7. Wound Size

Photographs were taken on the day of debridement and the day of sacrifice once the bandages had been removed. Photographs were analyzed with Image J software (Java 1.8.0_172 (64-bit), National Institutes of Health, Bethesda, MD, USA), where the total area of the burn was measured at the time of debridement and upon sacrifice to yield the closure index (Closure index = ([wound size at Day 7] − [wound size at day 16/28]/[wound size on day 7]). Thus, a closure index value of one is indicative of complete closure, while a value of zero indicates a complete absence of wound closure. The closure indexes were compared between control and fish skin bandage-treated groups at two time points (day 16 and day 28).

2.8. Blood Analyses

Heparinized blood was submitted for complete blood count, while serum was analyzed for glucose.

2.9. PCR Testing

Total RNA was extracted from mouse skin using TRIzol (Invitrogen,Waltham, MA, USA) following the manufacturer's protocol, and cDNA was generated using the QuantiTect Reverse Transcription Kit (Qiagen, Venlo, The Netherlands). RNA expression of genes listed in **Table 1** was determined by real-time quantitative RT-PCR (Qiagen, Venlo, The Netherlands) using Qiagen's QuantiNova SYBR Green PCR buffer. Each reaction was carried out in duplicates. Cycle conditions were denaturation at 95 _C for 2 min, followed by 40 cycles of denaturation at 95 _C for 5 s and annealing/extension at 60 _C for 10 s. The final melting curve step was performed according to Bio-Rad's CFX 96 (Bio-Rad Laboratories, Hercules, CA, USA). The level of expression of the target gene was normalized to GAPDH. All calculations were formulated using the delta-delta-CT method. Primer sets were designed from known murine gene sequences or generated from previously published data (**Table 1**).

Table 1. QRT-PCR primer sets.

Target Gene	Forward Primer 5′→3′	Reverse Primer 5′→3′	Reference
Cathelicidin antimicrobial peptide (CRAMP)	CCTAGACACCAATCTCTACC	GTCTCCTTCACTCGGAACC	[14]
β-defensin 1	CCAGATGGAGCCAGGTGTTG	AGCTGGAGCGGAGACAGAATCC	[15]
Substance P = Protachykinin-1 (Tac1)	CCAGATCTCTCACAAAAGGC	TTTCGTAGTTCTGCATCGCGC	[16]
Bradykinin receptor B1 (BDKRB1)	TGGAGTTGAACGTTTTGGGTTT	GTGAGGATCAGCCCCATTGT	[17]
Bradykinin receptor B2 (BDKRB2)	CTGGGTGTTTTGGAGAGGTGT	ACGAGCATCAGGAAGCAGAT	[18]
Calcitonin gene-related protein (CGRP)	GGACTTGGAGACAAACCACCA	GAGAGCAACCAGAGAGGAACTACA	[19]
Neuropeptide Y	AGGCTTGAAGACCCTTCCAT	ACAGGCAGACTGGTTTCAGG	[20]
Vascular endothelial growth factor (VEGF)	GCAGAAGTCCCATGAAGTGAT	GTCTCAATTGGACGGCAGTAG	[21]
Fibroblast growth factor (FGF2)	GTCACGGAAATACTCCAGTTGGT	CCCGTTTTGGATCCGAGTTT	[21]
GAPDH	CATCACTGCCACCCAGAAGACTG	ATGCCAGTGAGCTTCCCGTTCAG	[21]
Interleukin 6 (IL-6)	CAAAGCCAGAGTCCTTCAGA	GATGGTCTTGGTCCTTAGCC	[22]
Inducible nitric oxide synthase (iNOS)	CAG CTG GGC TGT ACA AAC CTT	CAT TGG AAG TGA AGC GGT TCG	
Neuronal nitric oxide synthase (nNOS)	ACTGACACCCTGCACCTGAAGA	GGAAGTCAGAAGATGTCCGCAC	

2.10. Proteomics

Skin samples were analyzed after tryptic in-solution digestion. Briefly, proteomics samples were collected, processed, and analyzed with LCMS using nanoAcquity (Waters, Milford, MA, USA) and Impact II (Bruker Daltonics, Billerica, MA, USA), as previously published [23–25]. Sequences of identified peptides were searched against mice and tilapia with PEAKS X Plus (BSI, Inc., Waterloo, ON, Canada) against Uniprot proteomes (UP000005207, UP000000589) to identify proteins present in samples. Identified proteins

were then blasted against NCBI (https://blast.ncbi.nlm.nih.gov/Blast.cgi, accessed on 8 July 2020) using their six-digit accession number.

The complete set of proteomic and all other raw data is provided in a (Supplementary Materials Table S1) and Public Data Repository (https://data.mendeley.com/datasets/hssv66g4kb/4, accessed on 14 September 2023). We screened and compared the peptides between murine and fish skin, created a new list of peptides that were present in the fish skin but not murine skin, and excluded structural peptides in both species. After the elimination of structural or Identical peptides from both species, the list was reduced to uncharacterized nonstructural peptides. Their sequences were then blasted against the mammalian protein database. Only proteins with > 90% identity to uncharacterized peptides in fish skin are reported here with STRING Consortium Version 11.5 (STRING, Zurich, Switzerland).

2.11. Histology

Initial histological evaluation was performed on hematoxylin and eosin-stained sections, where the extent of granulation tissue, presence and severity of inflammation, type of inflammatory cells, presence of bacterial contamination, and degree of re-epithelialization were assessed. Subsequently, snapshot images of the granulation tissue at the lesion interface at 20X and 200X magnification were acquired. The vascularization in the granulation tissue was then quantified via manual count with ImageJ on 200X magnification images. The quantification of vessels was normalized to the area of the section. Additional 5 µm sections were generated from the same paraffin blocks for immunohistochemical evaluation. Immunoreactivity for Factor VIII was applied in order to more precisely highlight and quantify the degree of neovascularization. Similarly, using 20X magnification images of the burn section snapshots, the thicknesses of the skin were measured at the burned–healthy skin interface location with ImageJ.

2.12. Immunohistochemistry (IHC)

All samples were sectioned at 5 µm. Briefly, FFPE sections were deparaffinized in xylene and hydrated in 100% ethanol before blocking endogenous peroxidase activity by incubating sections in 0.3% hydrogen peroxide in methanol for 30 min. Sections were then hydrated in decreasing concentrations of ethanol (95% and 70%, respectively). Enzymatic antigen retrieval was performed with Proteinase K (200 ug/mL) for 10 min at room temperature (RT) (Millipore IHC Select, Millipore, Louisville, KY, USA). Next, sections were blocked at (RT) with 10% horse serum in phosphate-buffered saline and Tween-20 (PBST) for 30 min. Sections were incubated with Polyclonal Rabbit Anti-Human vonWillebrand Factor [1:2000] (Dako, A0082, Santa Clara, CA, USA) diluted in PBST for one hour at RT. One-step antigen detection was performed with Rabbit-on-Canine HRP-polymer (Biocare Medical, RC542, Concord, CA, USA) incubation for 30 min at RT. Vector NovaRed® Peroxidase (HRP) Substrate Kit (Vector Laboratories, SK, 4800, Newark, CA, USA) was used to detect the antigen in murine skin samples. The specimens were then counterstained with Mayer's Hematoxylin Solution (Sigma-Aldrich, MHS16, Youngstown, OH, USA) and washed in tap water to blue the stain. Specimens were dehydrated with a quick dip in 100% ethanol and xylene and coverslipped using a mounting medium (Vector labs Cat # H-5000-60, Detroit, MI, USA). Histological images were analyzed and captured on Olympus BX46 (EVIDENT, Bethlehem, PA, USA) equipped with a color camera Olympus DP 27. All images were captured at 20X magnification. The vasculature counts were performed on captured images with ImageJ.

2.13. Statistical Analysis

Statistics were created using GraphPad Prism version 9.5.1 (GraphPad Software, Dotmatics, Boston, MA, USA). All data presented are expressed as means with standard error. All data were checked for normality and transformed accordingly. Two-way ANOVA tests were used to compare control and fish-skin-treated mice at all time points in our PCR data and complete blood count evaluation. A paired t-test was used to compare fish-skin-treated groups to controls in CBC data, wound closure index, wound area, serum

glucose, and body weight. All data were analyzed further to explore differences between male and female mice post-burn. Paired t-tests were used to compare male and female mice for each time point and parameter. Results were considered statistically significant at $p < 0.05$.

3. Results

3.1. Wound Size Evaluation and Quantification of Mice Treated with Fish Skin

The wound size was measured on day 7 and on day 16 or day 28 (Figure 2A). The average percent of the total body surface area burned on day 7 was between 3 and 5%. Significant differences were detected in the wound closure indexes (Figure 2B). As mentioned earlier, a wound closure index of one indicates a full wound closure, while an index of zero indicates no wound closure. Fish skin treatment showed no benefit in wound closure over the controls at the 16-day time point. Specifically, the closure index was significantly higher in control mice than in the fish-skin-treated mice at 16 days. However, at the 28-day time-point, there was no significant difference in wound closure indexes between the groups. In both control mice and fish-skin-treated mice, there was a significant increase in the wound closure index at the 28-day time point relative to the 16-day time point.

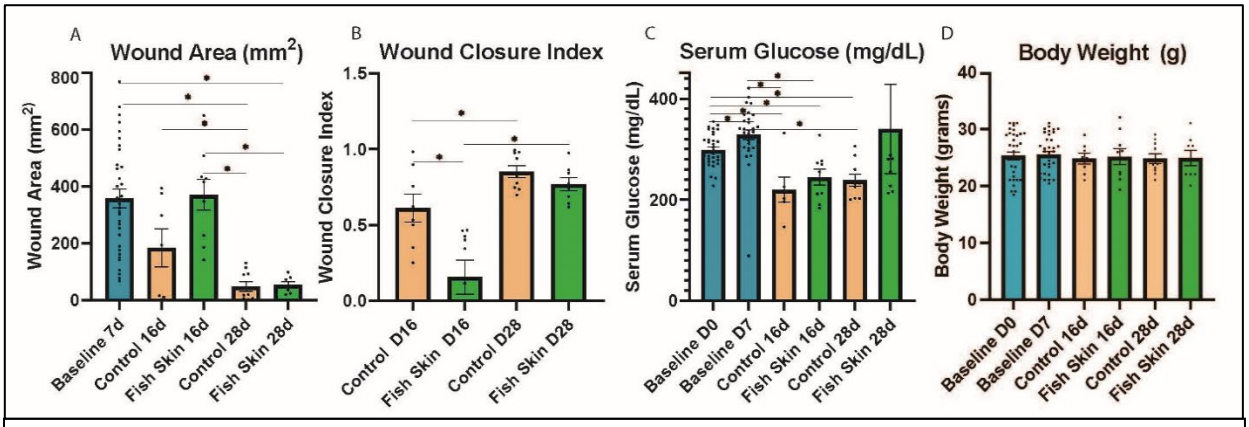


Figure 2. Wound healing and metabolism. (**A**) Wound area on day 7, day 16, and day 28. (**B**) The wound closure index was calculated with the following formula: (Closure index = ([wound size at Day 7] / [wound size at day 16/28]/[wound size at day 7]. (**C**) Body weight at days 0, 7, 16, and 28. (**D**) Serum glucose at days 0, 7, 16, and 28. Normal serum levels are indicated by the gray box. Asterisks annotation: p _ 0.05 (*). Baseline groups represent the average parameters of all mice, regardless of treatment. All mice were treated the same until day 7.

3.2. Serum Glucose

We detected no significant differences in glucose levels between treatment groups at any time point in this study. On day 16, both HCB and fish-skin-treated mice showed a significant decrease in glucose relative to days 0 and 7 baseline values (Figure 2C). On day 28, control mice continued to have significantly lower than day 0 and day 7 glucose levels; in contrast, fish-skin-treated mice returned to the original value range.

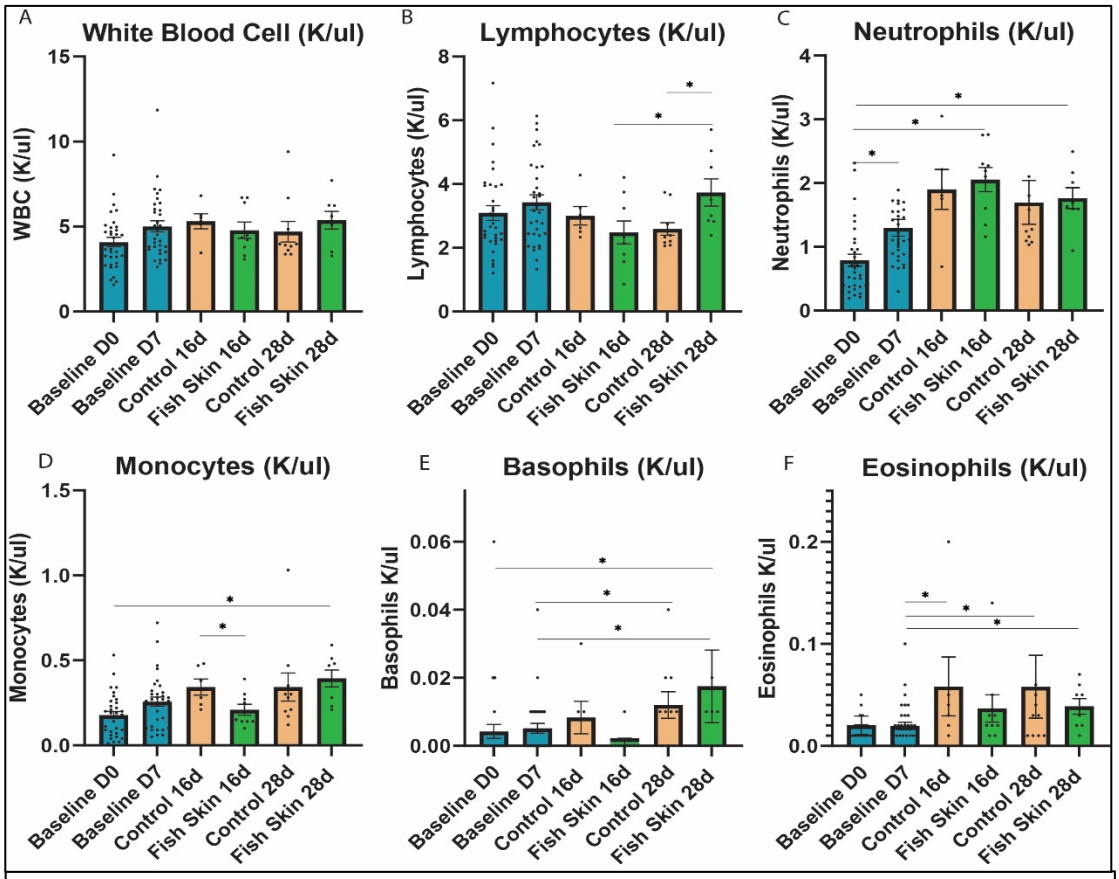


Figure 3. Complete leukocyte blood count analysis. (**A**) White blood cell count on days 0, 7, 16, and 28. (**B**) Lymphocyte counts on days 0, 7, 16, and 28. (**C**) Neutrophil counts on days 0, 7, 16, and 28. (**D**) Monocyte counts on days 0, 7, 16, and 28. (**E**) Basophil counts on days 0, 7, 16, and 28. (**F**) Eosinophil counts on days 0, 7, 16, and 28. Asterisks annotation: $p \leq 0.05$ (*). Baseline groups represent the average parameters of all mice, regardless of treatment. All mice were treated the same until day 7.

3.3. Evaluation of Body Weight Changes

All mice, HCB and fish-skin-treated, showed no significant changes in body weight at any time point (Figure 2D). None of the test individuals dropped their body weight below the baseline range.

3.4. Complete Blood Count Evaluation

3.4.1. White Blood Cells

All mice, controls and fish-skin-treated, showed no significant changes in total white blood cell (WBC) count at any time point (Figure 3A). Control mice showed a minimal increase in WBC count on day 16 and then a slightly lower WBC count on day 28. In contrast, fish-skin-treated mice showed virtually no change in counts on days 16 and 28.

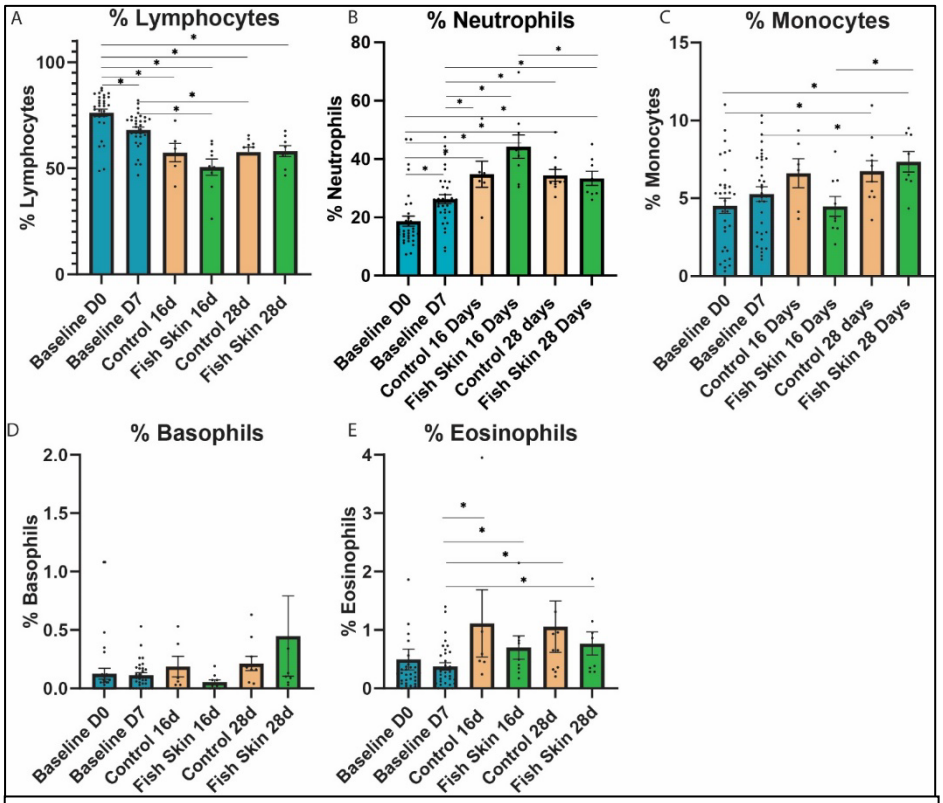


Figure S2. Percent Leukocyte Blood Analysis. (**A**) Percent lymphocytes at days 0 ,7, 16, and 28. (**B**) Percent neutrophils at days 0, 7, 16, and 28. (**C**) Percent monocytes at days 0, 7, 16, and 28. (**D**) Percent basophils at days 0, 7, 16, and 28. (**E**) Percent eosinophils at days 0, 7, 16, and 28. $P \leq 0.05$ (*). Baseline groups represent the average parameters of all mice, regardless of treatment. All mice were treated the same until day 7.

3.4.2. Lymphocytes

Absolute lymphocyte counts were significantly lower in the controls than in fish-skin treated mice at the 28 d time point (Figure 3B). Although insignificant, an opposite trend was observed between the groups at the 16 d time point. Fish-skin-treated mice had

significantly higher counts on day 28 relative to day 16. Data on lymphocyte percentages, provided in the Supplementary Materials (Figure S2A), generally follow the trend discussed above.

3.4.3. Neutrophils

Both groups showed similar trends in absolute neutrophil counts (Figure 3C) as well as neutrophil percentages (Figure S2B), and we detected no significant differences in neutrophil counts or percentages between control and fish-skin-treated groups at any time points. Mice treated with fish skin had significantly higher neutrophil counts on day 16 and day 28 relative to day 0. At 28 days, fish-skin-treated mice showed an insignificant reduction in neutrophil absolute counts relative to day 16. Neutrophil counts of HCB treated mice, although insignificant, showed an increase at day 16 and day 28 relative to baseline values. However, neutrophil counts of HCB-treated mice decreased at day 28 relative to day 16.

3.4.4. Monocytes

Both groups showed similar trends of monocyte populations throughout the study. Absolute count (Figure 3D) and percentage (Figure S2C) of monocytes trended higher in HCB than fish skin groups except at day 28. However, the only significant difference between the control and fish skin groups was that monocyte counts were higher in controls at day 16. Control mice showed no significant difference in monocyte counts between 16 d and 28 d time points. In contrast, fish-skin-treated mice showed a significant increase in the number of monocytes on day 28 relative to day 0. Both groups showed a progressive increase in monocyte counts among the time points relative to the day 0 baseline.

3.4.5. Basophils

All mice, HCB and fish-skin-treated, showed no significant differences in basophil percentages (Figure S2D) at any time point. However, basophil counts (Figure 3E) showed significant changes relative to baseline

values in both groups. Fish-skin-treated mice showed a significant increase in basophil count on day 28 relative to day 7 and day 0. In contrast, HCB-treated mice only showed a significant change on day 28 relative to day 7.

3.4.6. Eosinophils

Both groups showed similar trends in absolute eosinophil counts (Figure 3F) as well as eosinophil percentages (Figure S2E), and we detected no significant differences in eosinophil counts or percentages between control and fish-skin-treated groups at any time point. Eosinophil percentage and absolute counts trended higher in controls relative to fish skin. Mice treated with fish skin showed a significant increase in the percentage of eosinophils on day 16 and day 28 relative to day 7 (Figure S2E). Similarly, mice treated with fish skin showed a significant increase in eosinophil counts on day 28 relative to day 7. HCB groups also showed a significant increase in the percentage and number of eosinophils on day 16 and day 28 relative to day 7. Overall, no significant effect of fish skin treatments was found in eosinophil populations relative to controls.

3.4.7. Red Blood Cell (RBC) Counts

Both fish skin and control mice showed similar trends and no significant differences in RBC counts at any time point (Figure 4A). In both groups, RBC counts were below the baseline at 16 d time points. At 28 d, the values returned to the 7d baseline range in both groups. The RBC counts decreased significantly in the fish-skin-treated group between days 7 and 16, but not in controls.

3.4.8. Platelets

The platelet counts followed the opposite trend of RBC counts and demonstrated an expected increase between day zero and days 7, 16, and 28 (Figure 4B). Fish-skin-treated mice showed a significant increase

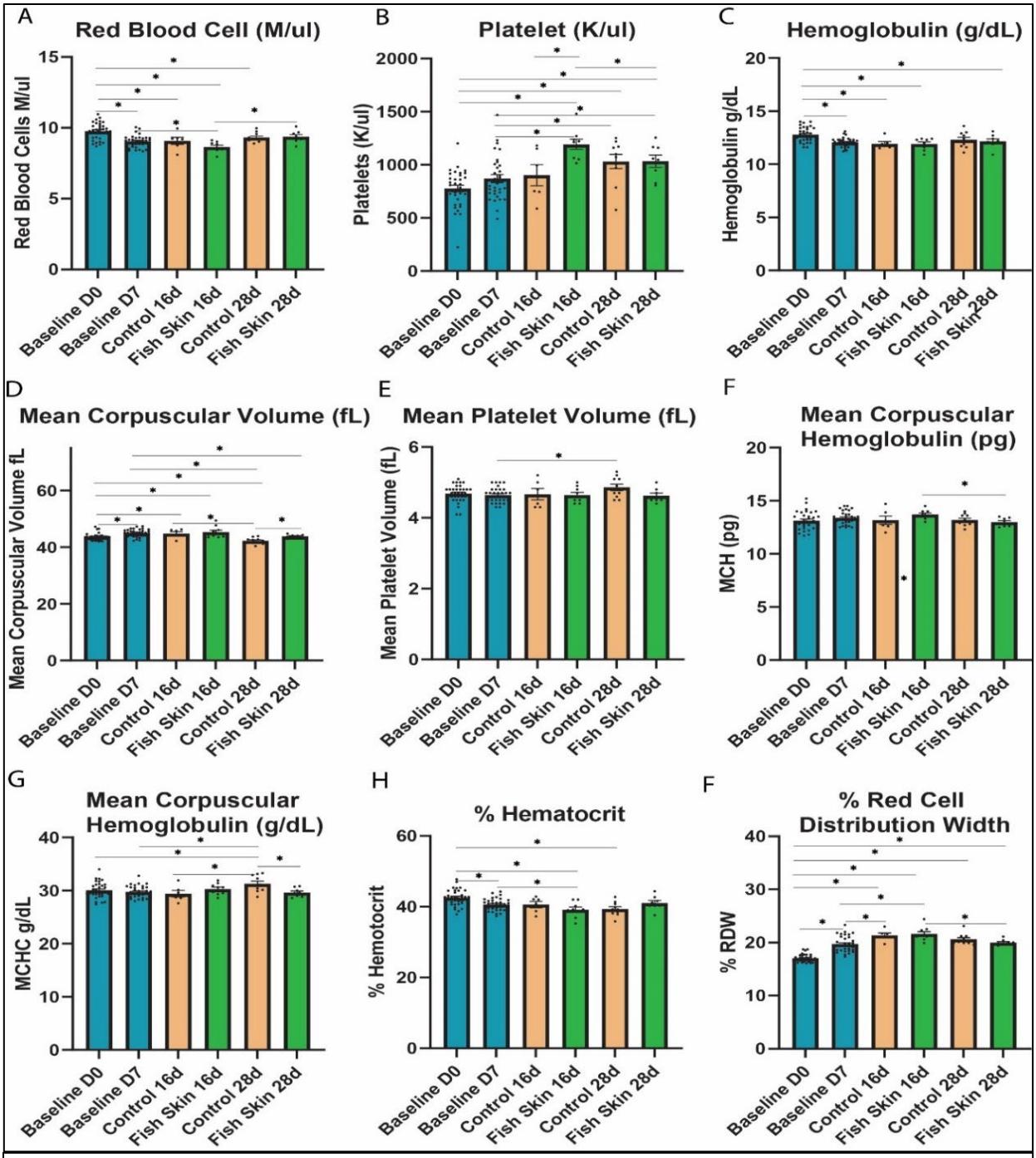


Figure 4. Complete blood parameter analysis. (**A**) Red blood cell count on days 0, 7, 16, and 28. (**B**) Platelet cell count at days 0, 7, 16, and 28. (**C**) Hemoglobulin concentration on days 0, 7, 16, and 28. (**D**) Mean corpuscular volume on days 0, 7, 16, and 28. (**E**) Mean platelet volume on days 0, 7, 16, and 28. (**F**) Mean corpuscular concentration on days 0, 7, 16, and 28. (**G**) Mean corpuscular hemoglobulin on days 0, 7, 16, and 28. (**H**) Percent hematocrit on days 0, 7, 16, and 28. (**I**) Percent red blood cell distribution width on days 0, 7, 16, and 28. Asterisks annotation: $p \leq 0.05$ (*). Baseline groups took the average of all mice, regardless of treatment. All mice were treated the same until day 7.

in platelet counts at day 16 and day 28 relative to both baseline time points. In contrast, HCB-treated mice

only showed a significant increase in platelet counts on day 28 relative to both baseline time points. Platelet counts showed a significant difference between HCB and fish-skin-treated mice on day 16. However, this trend dissipated at day 28 when the platelet counts were almost identical between the study groups.

3.4.9. Hemoglobulin

Both groups had a decrease in hemoglobulin levels on day 16 relative to baseline values (Figure 4C). Hemoglobulin levels increased minimally on day 28 relative to day 16 in both groups, but there were no significant differences between the groups at any time point of the study.

3.4.10. Mean Corpuscular Volume (MCV)

HCB and fish-skin-treated mice showed opposite trends with regard to the mean corpuscular volume (MCV) of red blood cells (Figure 4D). MCV values in both groups were almost identical to 7 d baseline values. However, on day 28, both groups had a decrease relative to day 16 and 7 time points. Fish-skin-treated mice showed significantly lower and closer to the baseline MCV value relative to the control at day 28.

3.4.11. Mean Platelet Volume (MPV)

MPV had a significantly higher value in controls on day 16 relative to day 7. Otherwise, no significant difference was recorded between treatment groups at any time point in the study (Figure 4E).

3.4.12. Mean Corpuscular Hemoglobulin (MCH)

HCB groups maintained a normal and consistent level of mean corpuscular hemoglobulin (MCH) throughout the study (Figure 4F). MCH values of fish-skin-treated mice remained identical to baseline

groups on day 16 but then significantly decreased on day 28 relative to day 16. In contrast, MCH values of HCB-treated mice, although insignificant, remained lower than baseline values. Overall, there were no significant differences between the control and fish skin groups at any time point.

3.4.13. Mean Corpuscular Hemoglobulin Concentration (MCHC)

Fish-skin-treated mice maintained a consistent level of MCHC similar to baseline values throughout the study (Figure 4G). MCHC values of HCB groups decreased slightly initially but then showed a significant increase on day 28 relative to day 7 and relative to day 16. Additionally, the MCHC of HCB groups on day 28 was significantly higher than fish skin groups on day 28.

3.4.14. Percent of Hematocrit

Both fish skin and control groups showed similar trends of hematocrit throughout the study. On day 16, hematocrit values of fish skin trended lower than controls (Figure 4H). This trend was reversed at day 28 when hematocrit values of fish skin groups increased and surpassed the values of control groups. Fish skin groups showed significant decreases on day 16 relative to day 7 and day 0. Similarly, hematocrit values of HCB groups decreased significantly on day 28 relative to day 0. Control groups maintained a fairly consistent level for the remainder of the study. There were no significant differences between fish skin and control groups.

3.4.15. Percent Red Blood Cell Distribution Width (RDW)

Both fish skin and control groups showed similar trends of increasing RDW at all time points. There were no significant changes between the control and fish skin groups (Figure 4I). However, fish skin groups suggested higher rates of change between different time points in comparison to control groups. For example, both groups had a significant increase in RDW values on day 16 relative to day 7 and day 0.

3.5. Histology

Histology confirmed the presence of full-thickness skin burns in all mice (Figure 5). Sections collected on day 7 (during the debridement procedure) contained denatured epidermis, dermis, hypodermis, hair follicles, and panniculus carnosus. The coagulative necrosis affecting these structures was characterized by a loss of cellular detail, sprinkling of nuclear fragments, and uniform eosinophilia. These layers formed a thick crust layered with abundant fibrin, degenerate neutrophils, cellular debris, fragmented hair shafts, and extravasated RBCs.

Sections collected on day 16 had markedly thickened and hypercellular hypodermis, especially prominent at the lesion interface with the normal skin. The hypercellularity was contributed by abundant fibroblasts

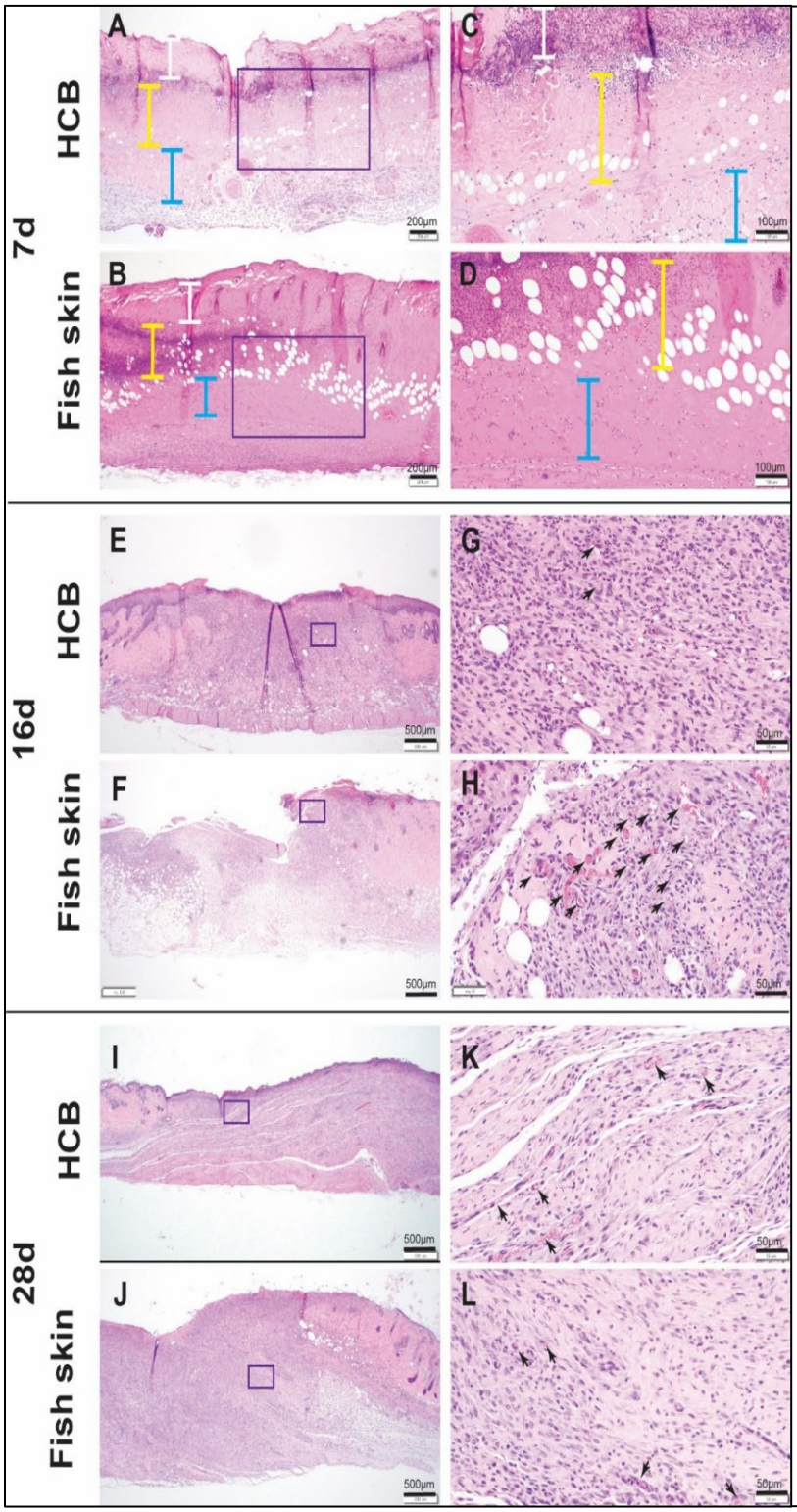


Figure 5. Histology. (**A**–**D**): Low- (**A**,**B**) and high- (**C**,**D**) magnification images of murine skin seven days post-burn induction. High-magnification snapshots represent areas highlighted by purple rectangles. Note full-thickness coagulative necrosis of epidermis and dermis (white vertical line), hypodermis (yellow vertical line), and panniculus carnosus (blue vertical line). The coagulative necrosis is characterized by diffuse eosinophilia and loss of cellular and nucellar detail. Subtending the necrotic dermis, there is a band of degenerate leucocytes (predominantly neutrophils). (**E**–**H**): Low- (**E**,**F**) and high- (**G**,**H**) magnification of murine skin 16 days post-burn induction. High-magnification snapshots represent areas highlighted by purple rectangles. Newly formed capillaries (angiogenesis) are indicated by black arrows. Note more pronounced angiogenesis in the granulation tissue areas of the fish-skin-treated mice. (**I**–**L**): Low- (**I**,**J**) and high- (**K**,**L**) magnification images of murine skin 28 days post-burn induction. High-magnification snapshots represent areas highlighted by purple rectangles. Note angiogenesis is almost equivalent in the granulation tissue in controls and fish-skin-treated mice (black arrows).

and inflammatory cells (histiocytes, neutrophils, lymphocytes, and occasional mast cells) supported by a loose, at times, myxomatous matrix. Multiple small-caliber blood vessels and capillaries were abundant in these locations (angiogenesis). When quantified by the manual count using ImageJ, mice treated with fish skin had more pronounced angiogenesis than controls, albeit the difference was not found to be statistically significant. Interestingly, and consistent with the clinical observation of skin contraction around the burn, the panniculus carnosus layer extended farther than the epidermis towards the lesion center. Some re-epithelialization was observed at the lesion interface with the healthy skin, where a thickened epidermal layer of the intact skin was contiguous with a thin (1–2 cell thick) layer of neo-epidermis covering the granulation tissue formed instead of hypodermis and dermis. The skin thickness at the interface of the burn wound with healthy skin was not significantly different between the treatment groups at the 16 d time point, but the fish-skin-treated group trended slightly higher than the control. No new hair follicle formation was observed in the regenerating skin regions in any of the treatment groups.

Skin sections from the 28 d time point had a similar appearance to that described for 16d with the exception of a much smaller wound size and, in some cases, almost complete reepithelialization of the granulation tissues bed. No new hair follicle formation was observed in the regenerating skin regions in

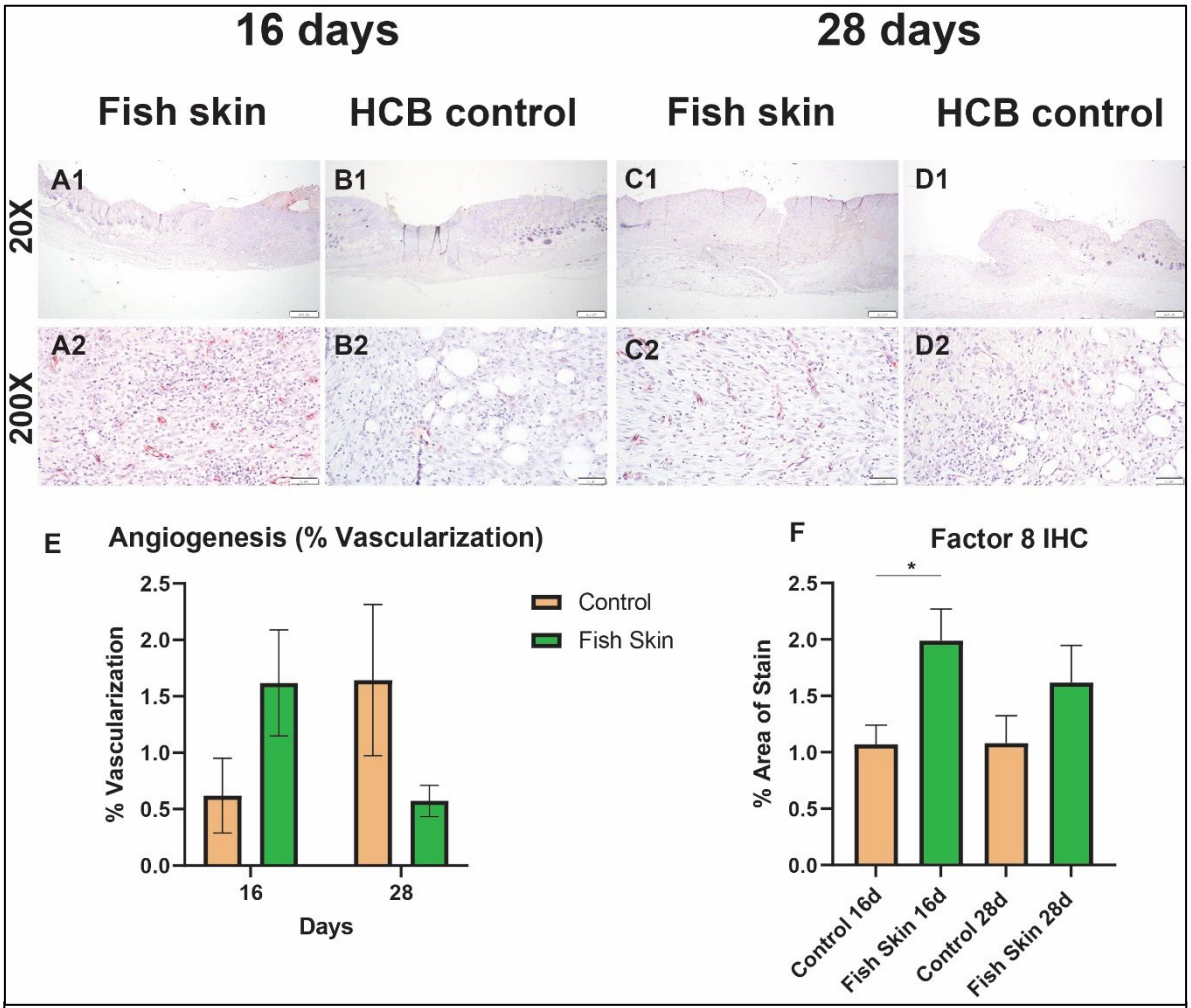


Figure 6. Quantification of angiogenesis. (**A1**,**C1**) and (**A2**,**C2**) micro-captures represent low and high magnification images of Factor 8-immunolabeled histological section of skin from the burn healthy skin interface in fish skin-treated mice. (**B1**,**D1**) and (**B2**,**D2**) micro-captures represent low and high magnification images of immunolabeled histological section of skin from the burn-healthy skin interface.in mice treated with HCB. (**E**) Blood vessel formation was quantified with ImageJ on H&E-stained histology sections. (**F**) Blood vessel formation was quantified with ImageJ on Factor 8- immunolabeled sections. All counts were normalized to the area of the section. Asterisks annotation: $p \leq 0.05$ (*).

any of the treatment groups. Some regenerative changes were observed in the carnosus muscle. These included the rowing of myocyte nuclei and the formation of the thin, slightly basophilic in color myofibers. Quantification of angiogenesis on HE sections detected a higher but statistically insignificant trend in fish-

skin-treated individuals. This trend was reversed on day 28. The skin thickness at the interface with healthy skin was significantly higher in fish-skin-treated mice at this time point (Figure S3).

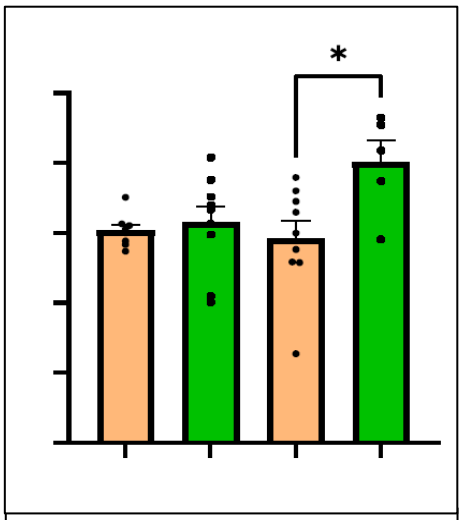


Figure S3. The thickness of the skin at the burn-healthy skin interface measure on the

3.6. Immunohistochemistry

Immunolabeling for factor 8 revealed a significant increase in the number of vessels in the fish-skin-treated mice at the 16 d time point. A similar trend, albeit statistically insignificant, was detected on day 28 (Figure 6).

3.7. Survival Outcomes

The burn induction had a detrimental effect on some of the smaller mice (females with a body weight of 20 to 23 g), and as a result, some losses were encountered. Specifically, these mice exhibited hunched body posture and tremors, refused to eat and drink, and had increased skin turgor, indicative of dehydration. Due to these reasons, the decision for humane euthanasia was made. Due to these losses, we repeated the study on additional animals to keep a sufficient representation of males and females across groups. Table 2 represents the final counts and distribution of males and females among treatment groups. Nonetheless, no statistically significant differences were observed between males and females for any outcome parameters examined.

3.8. PCR Results

PCR analysis investigated the expression of several genes encoding for pain perception, antimicrobial peptides, wound healing-associated proteins, and angiogenesis. Substance P (SubP) is a neuropeptide responsible for pain perception and the recruitment of early responders of inflammation [26]. The expression of this gene was reversed between the fish skin and control groups (Figure 7A). Specifically, on

day 16, SubP expression trended higher in the fish skin group than in controls, while on day 28, this trend was reversed. Overall, the fish skin group had a trend of decreased SubP expression with respect to study time points, while the opposite was detected in controls. However, neither of the differences was found to be statistically significant. Similar trends were observed for bradykinin receptors B1 and B2 (Figure 7B,C). Bradykinin Receptors B1 and B2 (BKRB1 and BKRB2) are G-protein coupled receptors that bind bradykinin. Bradykinin peptides are responsible for eliciting many responses, such as vasodilation, edema, pain fiber stimulation, and inflammation [27–29]. BKRB1 expression trended higher in control groups at both time points. The expression of BKRB2 had the opposite trend among treatment groups. Specifically, on day 16, BKRB2 expression trended higher in fish skin than in control groups, while on day 28, this trend was reversed. Neither of the differences was found to be statistically significant. Calcitonin gene-related protein (CGRP) is another neuropeptide responsible for pain transmission and vasodilation [30,31]. CGRP expression trended similarly to BKRB2 (Figure 7D). The expression of neuropeptide Y (NPY), another stress response neuropeptide, trended higher in the fish skin group than controls at all time points (Figure 7E). However, similarly to BKRB1 and BKRB2, fish-skin-treated mice exhibited decreased expression of these genes over the study's time points, while controls tended to remain unchanged.

Gene expression of defensin (Figure 7F) and cathelicidin antimicrobial peptide (CAMP) (Figure 7G) was performed to assess if fish skin treatment offers any benefit in protection against bacterial infections [32]. The fish skin group had 2.5 times more defensin expression than controls on day 16. Defensin expression increased slightly in control groups on day 28 but was still lower than in fish-skin-treated mice. However, CAMP expression did not follow similar trends. CAMP expression was minimally higher in the fish skin group than in controls on day 16, and this trend was reversed on day 28. No significant differences were observed between fish skin and control groups in either defensin or CAMP expression.

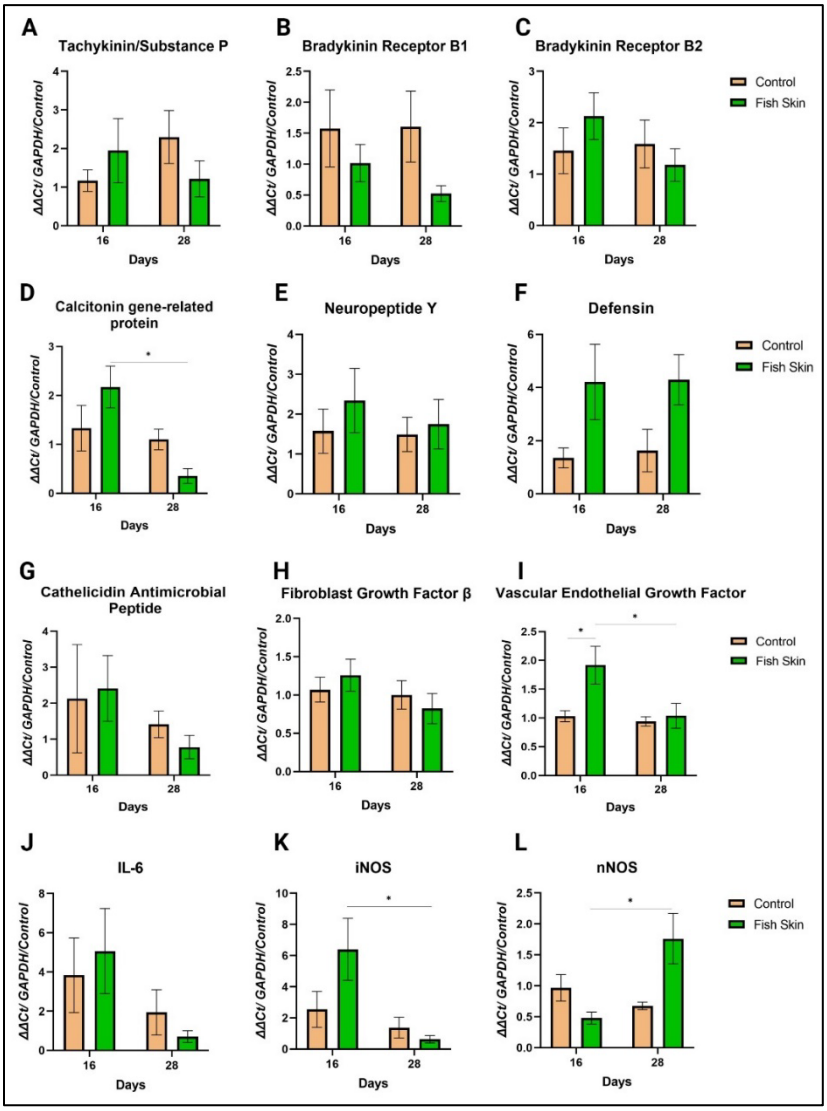


Figure 7. Gene expression analysis with QRT-PCR. The DDCt values for each gene are calculated by averaging duplicate runs and normalizing the expression of the gene to GAPDH and control mice. (**A**) Gene Expression of Tachykinin/Substance P at day 16 and day 28 of control and fish skin groups normalized to controls and GAPDH expression. (**B**) Gene Expression of Bradykinin receptor B1 at day 16 and day 28 of control and fish skin groups normalized to controls and GAPDH expression. (**C**) Gene Expression of Bradykinin receptor B2 at day 16 and day 28 of control and fish skin groups normalized to controls and GAPDH expression. (**D**) Gene Expression of Calcitonin gene-related protein at day 16 and day 28 of control and fish skin groups normalized to controls and GAPDH expression. (**E**) Gene Expression of Neuropeptide Y at day 16 and day 28 of control and fish skin groups normalized to controls and GAPDH expression. (**F**) Gene Expression of Defensin at day 16 and day 28 of control and fish skin groups normalized to controls and GAPDH expression. (**G**) Gene Expression of Cathelicidin Antimicrobial Peptide at day 16 and day 28 of control and fish skin groups normalized to controls and GAPDH expression. (**H**) Gene Expression of Fibroblast Growth Factor 2 at day 16 and day 28 of control and fish skin groups normalized to controls and GAPDH expression. (**I**) Gene Expression of Vascular Endothelial Growth Factor at day 16 and day 28 of control and fish skin groups normalized to controls and GAPDH expression. (**J**) Gene Expression of Interlukin-6 at day 16 and day 28 of control and fish skin groups normalized to controls and GAPDH expression. (**K**) Gene Expression of inducible nitric oxide synthase at day 16 and day 28 of control and fish skin groups normalized to controls and GAPDH expression. (**L**) Gene Expression of neuronal nitric oxide synthase

The expression of fibroblast growth factor 2 (FGF2) (Figure 7H) was investigated for its important role in wound healing. Fibroblast growth factor _ (FGF2) is a signaling protein responsible for initiating tissue repair, cell growth, and sometimes vascularization [33,34]. At day 16, FGF2 expression in the fish skin group trended higher than in controls, while this trend was reversed at day 28. The expression of FGF2 decreased in the fish skin group over study time points, whereas the control group stayed principally unchanged. No significant differences between fish skin and control groups were detected at any time points.

The expression of vascular endothelial growth factor (VEGF) gene was carried out for its central role in angiogenesis. Fish-skin-treated mice had nearly two times more VEGF expression than control mice on day 16 (Figure 7I). On day 28, fish-skin-treated mice showed a significant decrease in VEGF relative to day 16 that leveled out to values similar, yet still higher, than HCB groups.

The expression of interleukin-6 (IL-6), neuronal (n), and inducible isoform (i) nitric oxide synthases (NOS) was investigated for their important role in inflammation, vascularization, stress, and insulin resistance. On day 16, IL-6 expression in fish-skin-treated mice trended higher than in controls, while this trend was reversed on day 28 (Figure 7J). The expression of IL-6 decreased in both groups over the study's time points. Similar trends were observed with the expression of iNOS (Figure 7K). These trends were reversed for the expression of nNOS (Figure 7L). Collectively, no significant differences between fish skin and control groups were detected at any time points.

3.9. Proteomics

After removing cell-structure-related (actins, keratins, etc.) proteins and extracellular matrix-related proteins (collagens) from the list of total peptides identified in fish and murine skin samples, we found 22 uncharacterized peptides in the fish skin that were not detected in the murine skin. Among these proteins, 11 had up to 90% sequence similarity with mammalian anti-inflammatory or pain relief peptides, 7 with wound/tissue repair peptides, and 7 with antimicrobial peptides (Figure 8). Some proteins had overlapping functions in each of the groups listed.

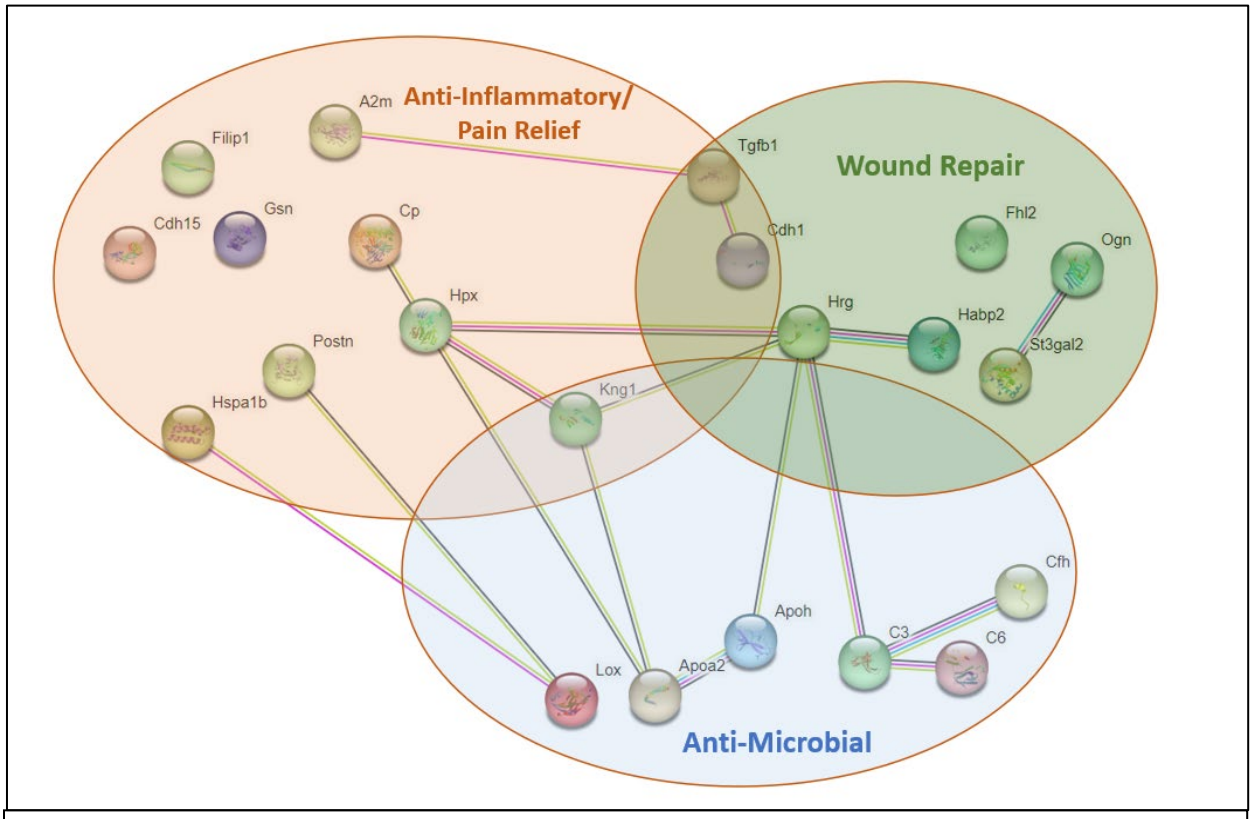


Figure 8. Proteomic analysis. Proteomic analysis revealed 22 nonstructural proteins unique to fish skin. A2M = alpha-2-macroglobulin; FILP1 = Filamin A Interacting Protein 1; CDH15 = Cadherin 15; GSN = gelsolin; CP = Ceruloplasmin; HPX = Hemopexin; POSTN = periostin; HSPA1B = Heat shock protein 1B; KNG1 = Kiniogen 1; CDH1 = Cadherin 1; TGFB = Transforming growth factor beta; HRG = Histidine-rich glycoprotein; FHL2 = four and a half LIM; HBP2 = hyaluronan-binding protein; OGN = osteoglycin; ST3GAL2 = CMP-N-acetylneuraminate-beta-galactosaamine-alpha- 2,3-sialyltransferase; APOH = Apolipoprotein; C6 = Complement 6; APOA2 = Apolipoprotein-A; CFH = Complement factor-H; C3 = Complement 3; LOX-protein-lysine 6- oxidase.

4. Discussion

This study is the first to evaluate the effects of fish skin burn treatment using histological, hematological, and molecular methods in a comprehensive and controlled fashion in a murine model. We also performed

a proteomic comparison between mammalian and fish skin and identified unique proteins with anti-inflammatory, wound-repair, and antimicrobial properties in fish skin. Burn treatment with fish skin offered no benefit compared to hydrocolloid treatment in wound closure. We detected no difference between fish skin and HCB treatment regarding hematological values or systemic glucose concentration. However, we found that fish-skin-treated mice had increased angiogenesis at the earlier time point than the HCB-treated controls. We also detected a trend of higher antimicrobial peptide expression in fish-skin-treated mice compared to controls. Collectively, these findings provide insight into the main drivers behind fish skin therapy for burns and provide directions for further investigation.

Wound closure is an important indicator of therapeutic efficacy. Accelerating wound healing is ideal for a faster return to function. Contrary to our hypothesis and the published report by Ibrahim et al. [35], who showed a decrease in the percentage of overall wound size over 3 weeks in donkey metacarpal wounds treated with fish skin vs. untreated controls, our study detected no benefit of fish skin therapy on wound closure (Figure 2). This disagreement can be due to the difference in experimental design and animal species. Specifically, donkeys belonging to the family of Equidae heal their wound in a fashion similar to humans, i.e., by re-epithelializing the granulation tissue bed forming at the wound site [36]. In contrast to Equidae and humans, mice heal their wounds by contracting the dermis-associated panniculus carnosus muscle [37–39]. In our experiments, we observed that shortly after application, the fish skin bandages became hard shell-like structures, while HCB bandages remained soft and pliable throughout the course of the study. As a result, HCB-treated burn wounds contracted more efficiently, and their size reduction was more rapid than fish-skin-treated wounds. In other words, fish-skin treatment acted similarly to Dunn's wound-splinting model [38], while HCB treatment did not, rendering it not the most appropriate control treatment for this study. It is possible that repeating this study using a large animal model such as

a pig [40] or using a splinting approach would be more appropriate to evaluate the wound-closure effects of fish skin burn wound treatment.

We attempted to determine if mice in our study had evidence of hypermetabolic syndrome. However, the steady body weight and lack of hyperglycemia suggest that hypermetabolic syndrome did not occur in this study (Figure 2). Hypermetabolic syndrome usually occurs in cases with more extensive burns comprising TBSA of 60% or more [41]. In the current study, the % TBSA affected by burn ranged between 3 and 5% and was probably insufficient to cause hypermetabolic syndrome. The fluctuations in glucose values thus likely reflect a stress response rather than hypermetabolism syndrome. Also, an increase in IL-6 was reported to be associated with hypermetabolism syndrome in pediatric patients [42,43]. Specifically, a marked increase relative to pre-burn values was reported around day 7, with a subsequent decrease of approximately 1.5 to 2-fold at days 16 and 28, respectively [42], with a bio-plex ELISA assay. In our study, a similar decrease in IL-6 expression was detected, but it remains to be determined if RNA expression also correlated with the protein levels. In concert, more studies and probably a more extensive burn area would be needed to determine the effects of fish skin therapy on hypermetabolic syndrome.

Leukograms from the mice showed no evidence of infection or excessive consumption (Figure 3). In comparison with reports from human studies [44,45], neutrophil counts had similar fluctuations in our study, most likely reflecting the expected response to extensive tissue damage. Further studies evaluating the neutrophils' specific phenotypes and secretome patterns [46] are essential to identify the potential benefits of fish skin therapy for burns. Monocytes, like neutrophils, are also considered one of the first responders to arrive at the site of burn injury during the early inflammatory phase. Interestingly, we detected significantly fewer systemic monocytes in fish-skin-treated mice than in controls on day 16. On day 28, the monocyte counts were similar between the treatment groups, and counts trended higher than

on day 16 or at the baseline, but not substantially (Figure 3). Histopathological evaluation of H&E sections of the burn sites revealed no difference in macrophage or neutrophil infiltration between groups, but this assessment is subjective and requires more detailed investigation. It is important to investigate if fish skin treatment has an effect on macrophage polarization to types one and two [47]. M1 macrophages usually secrete high levels of iNOS and IL-6 [48,49]. Our PCR data demonstrated that iNOS and IL-6 expression was higher in fish-skin-treated skin samples than in HCB controls on day 16. On day 28, these trends were reversed, and IL-6 and iNOS expression were higher in HCB than in the fish-skin-treated group. These data indirectly suggest that fish skin treatment may be more inductive for the M1 macrophage phenotype at the earlier time points than the HCB control. These results align with studies by Guo et al., who found that burn injury increased the expression of iNOS but not nNOS [50]. Immunohistochemical studies are needed to assert this assumption.

We identified significantly higher lymphocyte counts in the fish-skin-treated mice than in HCB controls at the 28d time point (Figure 3). This observation is intriguing and deserves a deeper investigation. Specifically, provided the fish skin is a xenogeneic tissue, it may induce an immune response in the recipient mice. A further look into specific lymphocyte phenotypes at the wound site and local and systemic cytokine profiles would be required to answer this question.

Fluctuations in red blood cell values in this study are numerous, but all primarily reflect an expected response to minimal blood loss [51], with no significant differences identified between the treatment groups. According to Duncan et al., reticulocytes (i.e., newly formed RBC) have a larger MCV and lower hemoglobin concentration. Hence, baseline MCV combined with a lower-than-baseline MCHC represents regenerative erythropoiesis [51]. Our study revealed a significant decrease in RBC counts on day 16, followed by an increase on day 28 in both groups. The latter changes most likely represent marginal blood

loss. This assumption is supported by the fluctuation in hemoglobin concentration, where a slight decrease on day 7 was followed by an increase in values on day 16 and a further increase on day 28 in both groups.

Thrombocyte (platelet) counts agree with the RBC counts and suggest that blood loss may have been greater in the fish-skin-treated mice as a significant increase in platelet counts was recorded on day 16 relative to day zero and day 7 baselines. The counts normalized and were identical between the controls and fish-skin-treated mice on day 28 (Figure 4). It is possible that the adhesive nature of the HCB bandage facilitated better hemostasis and prevented blood loss, while fish skin offered no advantage in hemostasis. Nevertheless, blood loss was not significant, and no mice exhibited signs of anemia at any time point in the study.

Blood vessel formation is crucial to transport nutrients, immune cells, and oxygen to facilitate wound healing. According to the most recent understanding of the burn model zones [52], the tissue fromthe outer two zones of the burnwound be salvageable if vasculature is revived quickly [53]. In the present study, histology sections revealed more vessel formation in the fish-skin-treated group at day 16 than in controls (Figures 5 and 6). The earlier vessel formation in fish-skin-treated mice aligns with reports by Ibrahim et al. [35], who showed a similar trend of vascularization on day 14 of metacarpal wounds in donkeys treated with fish skin compared to metacarpal wounds dressed with sterile, non-adherent dressing pads. The qPCR analysis agreed with the histological observations. It showed significantly greater (two-fold) expression of VEGF on day 16 in fish-skin-treated groups compared to controls, reflecting the beneficial effect of fish skin on angiogenesis. Lastly, the thicknesses of the skin at the interface of the burn with healthy skin were significantly thicker in fishskin-treated mice at the 28 d time point, suggestive of a thicker layer of granulation tissue in these animals.

The unpublished data from clinical treatments of veterinary patients with tilapia fish skin during recent fires in California suggested that fish skin therapy for burns had an immediate pain-mediating effect. For example, bears with burned paws could walk after fish skin application but not when wounds were treated conservatively with bandaging. We therefore attempted to explore if fish skin treatment of burns on mice would have some effects on pain mediators or their receptors. Close observation of experimental animals and unchanged body weight throughout the study did not support a difference in pain sensation between experimental groups. Our PCR exploration of pain-associated gene expression of substance P, bradykinin receptor 2, neuropeptide Y, and calcitonin gene related protein did not reveal significant differences between treatment groups, and thus neither confirm nor corroborate clinical observations of pain relief (Figure 7). Further, more mechanistic investigations on the fish skin's effect on pain sensation using specific agonists and antagonists to determine if fish skin has any benefit in pain mitigation would be needed to elucidate this aspect.

Fish-skin-treated mice had nearly two times more expression of defensin (Figure 7) in comparison to controls at all time points, albeit not statistically significant. Clinical studies performed on human patients with burns found that defensin expression is reduced in burn wounds [54]. The increased expression of defensin in fish-skin-treated mice may suggest that fish skin facilitated the secretion of this peptide. Although no bacterial infection was detected in any of the groups in this study, further studies with controlled bacterial infections may be beneficial to further investigate the relevance of this finding. A similar but less-pronounced trend was detected in the expression of cathelicidin antimicrobial peptide in this study. Albeit not significantly different from controls, cathelicidin antimicrobial peptide expression trended higher in fish-skin-treated mice. Provided the importance of this antimicrobial peptide in controlling bacterial infection in a knockout mouse model [55], further study would be beneficial.

Proteomic analysis of fish skin revealed 22 unidentified nonstructural peptides (Figure 8). Upon blasting these sequences against the database, identity with mammalian antimicrobial, tissue repair, and anti-inflammatory peptides was detected. Specifically, the FHL2 peptide was identified. This peptide is involved in platelet activation, pathogen clearance, cytokine regulation, and cell proliferation [56]. According to Wixler et al., the failure of tissue repair is always accompanied by the suppression of FHL2 [56]. Other nonstructural peptides relevant to this study, such as apolipoprotein, periostin, hemopexin, and gelsolin, were also detected. Although the functions of many of these peptides are still not fully understood, all of them are mentioned in the context of wound healing. For example, apolipoproteins are lipoproteins with many metabolism-related functions. Specifically, Apolipoprotein E was shown to correct delayed wound healing in Apolipoprotein E-deficient mice [57], and Apolipoprotein A could suppress the growth of Escherichia coli and Klebsiella pneumoniae [58]. Periostin was explored in a mouse wound-repair study, where signaling through integrin molecules was shown to promote the proliferation and migration of fibroblasts [59]. Another study detected overexpression of this peptide in the pericytes of burned skin, and its function was related to scar formation and fibrosis [60]. Gelsolin function is related to actin modulation and clearance after tissue injury [61]. Administration of recombinant gelsolin was reported to cause antioxidant activity in a concentration-dependent manner in murine fibroblasts [62]. Also, decreased gelsolin plasma concentration was associated with increasing burn sizes and the severity of sepsis in human patients [63]. Undeniably, more work needs to be performed to identify fish skin peptides with the most crucial biological functions relevant to burns and other types of wound repair.

In conclusion, the data from this study uncover some of the potential key contributors to fish skin's healing properties and the advantages of using fish skin in the treatment of burn wounds. This study's most significant finding is increased angiogenesis with fish skin treatment. The limitation of this study was the

inability to objectively assess the wound closure efficacy due to the innate biological constraints of the model. This limitation may have obscured the additional advantages of this treatment and therefore warrants exploring the wound-closure speed in a different animal model, such as a pig. It was also difficult to maintain equal age-matched male-to-female distribution across the treatment groups due to adverse responses to the burns by the smaller females (<25 g). Nevertheless, females who completed the study were not statistically different from males in any outcome parameters. More studies need to be performed to identify specific components of fish skin and their mechanistic role in wound healing. Also, application to other types of wounds, such as diabetic wounds, bacterial wounds, antibiotic-resistant bacterial skin infections, or pressure sores, would be interesting. Moreover, combining fish skin with stem cell treatment would be an exciting direction to explore.

Supplementary Materials: The following supporting information can be downloaded at: https://www.mdpi.com/article/10.3390/jfb14100512/s1, Figure S1: Schematic of tilapia skin preparation; Figure S2: Percent Leukocyte Blood Analysis; Figure S3: The thickness of the skin at the burn-healthy skin interface measure on the histological sections; Video S1: Debridement procedure.

Author Contributions: Conceptualization, N.V.; Methodology, J.P.; Validation, U.D. and N.V.; Formal analysis, N.V.; Investigation, D.K. and N.V.; Resources, J.P.; Data curation, C.G., C.G.-R., I.R., U.D., A.W., D.K., J.P. and B.A.; Writing—original draft, C.G.; Writing—review & editing, D.K., J.P., B.A. and N.V.; Visualization, I.R.; Supervision, N.V.; Project administration, N.V.; Funding acquisition, N.V. All authors have read and agreed to the published version of the manuscript.

References

1. Burns. Available online: https://www.who.int/news-room/fact-sheets/detail/burns (accessed on 15 June 2021).
2. National Center for Health Statistics. National Hospital Ambulatory Medical Care Survey: 2020 Emergency Department Summary Tables; Center of Disease Control: Atlanta, Georgia, 2020.

3. Xu, R.; Yu, P.; Abramson, M.J.; Johnston, F.H.; Samet, J.M.; Bell, M.L.; Haines, A.; Ebi, K.L.; Li, S.; Guo, Y.Wildfires, Global Climate Change, and Human Health. N. Engl. J. Med. 2020, 383, 2173–2181. CrossRef]
4. Zuo, K.J.; Medina, A.; Tredget, E.E. Important Developments in Burn Care. Plast. Reconstr. Surg. 2017, 139, 120e–138e. [CrossRef][PubMed]
5. Nielson, C.B.; Duethman, N.C.; Howard, J.M.; Moncure, M.; Wood, J.G. Burns: Pathophysiology of Systemic Complications and Current Management. J. Burn. Care Res. 2017, 38, e469–e481. [CrossRef]
6. Williams, F.N.; Herndon, D.N.; Jeschke, M.G. The hypermetabolic response to burn injury and interventions to modify this response. Clin. Plast Surg. 2009, 36, 583–596. [CrossRef] [PubMed]
7. Hew, J.J.; Parungao, R.J.; Shi, H.; Tsai, K.H.; Kim, S.; Ma, D.; Malcolm, J.; Li, Z.; Maitz, P.K.; Wang, Y. Mouse models in burns research: Characterisation of the hypermetabolic response to burn injury. Burns 2020, 46, 663–674. [CrossRef] [PubMed]
8. Ruffolo, R.R., Jr. Spare alpha adrenoceptors in the peripheral circulation: Excitation-contraction coupling. Fed. Proc. 1986, 45, 2341–2346. [PubMed]
9. Halim, A.S.; Khoo, T.L.; Mohd Yussof, S.J. Biologic and synthetic skin substitutes: An overview. Indian J. Plast. Surg. 2010, 43, S23–S28. [CrossRef] [PubMed] J. Funct. Biomater. 2023, 14, 512 21 of 22
10. Lima Júnior, E.M.; De Moraes Filho, M.O.; Costa, B.A.; Rohleder, A.V.P.; Sales Rocha, M.B.; Fechine, F.V.; Forte, A.J.; Alves, A.; Silva Júnior, F.R.; Martins, C.B.; et al. Innovative Burn Treatment Using Tilapia Skin as a Xenograft: A Phase II Randomized Controlled Trial. J. Burn Care Res. 2020, 41, 585–592. [CrossRef]
11. Hu, Z.; Yang, P.; Zhou, C.; Li, S.; Hong, P. Marine Collagen Peptides from the Skin of Nile Tilapia (Oreochromis niloticus): Characterization and Wound Healing Evaluation. Mar. Drugs 2017, 15, 102. [CrossRef]
12. Medina, J.L.; Fourcaudot, A.B.; Sebastian, E.A.; Shankar, R.; Brown, A.W.; Leung, K.P. Standardization of deep partial-thickness scald burns in C57BL/6 mice. Int. J. Burn. Trauma 2018, 8, 26–33.
13. Peyton, J. Fish Skin Biologic Bandage. US11612675B1, 28 March 2023.
14. Kin, N.W.; Chen, Y.; Stefanov, E.K.; Gallo, R.L.; Kearney, J.F. Cathelin-related antimicrobial peptide differentially regulates T- and B-cell function. Eur. J. Immunol. 2011, 41, 3006–3016. [CrossRef] [PubMed]
15. Chong, K.T.; Thangavel, R.R.; Tang, X. Enhanced expression of murine beta-defensins (MBD-1, -2, - 3, and -4) in upper and lower airway mucosa of influenza virus infected mice. Virology 2008, 380, 136–143. [CrossRef]
16. Pinto, F.M.; Pintado, C.O.; Pennefather, J.N.; Patak, E.; Candenas, L. Ovarian steroids regulate tachykinin and tachykinin receptor gene expression in the mouse uterus. Reprod. Biol. Endocrinol. 2009, 7, 77. [CrossRef] [PubMed]
17. Duchene, J.; Lecomte, F.; Ahmed, S.; Cayla, C.; Pesquero, J.; Bader, M.; Perretti, M.; Ahluwalia, A. A novel inflammatory pathway involved in leukocyte recruitment: Role for the kinin B1 receptor and the chemokine CXCL5. J. Immunol. 2007, 179, 4849–4856. [CrossRef]
18. Shariat-Madar, Z.; Mahdi, F.; Warnock, M.; Homeister, J.W.; Srikanth, S.; Krijanovski, Y.; Murphey, L.J.; Jaffa, A.A.; Schmaier, A.H. Bradykinin B2 receptor knockoutmice are protected fromthrombosis by increased nitric oxide and prostacyclin. Blood 2006, 108, 192–199. [CrossRef] [PubMed]
19. Yin, M.; Li, C.; Peng, X.D.; Zhao, G.Q.; Wu, Y.; Zheng, H.R.; Wang, Q.; Xu, Q.; Jiang, N. Expression and role of calcitonin gene-related peptide in mouse Aspergillus fumigatus keratitis. Int. J. Ophthalmol. 2019, 12, 697–704. [CrossRef] [PubMed]

20. Du, M.; Butchi, N.B.;Woods, T.; Morgan, T.W.; Peterson, K.E. Neuropeptide Y has a protective role during murine retrovirusinduced neurological disease. J. Virol. 2010, 84, 11076–11088. [CrossRef]
21. Fang, T.D.; Nacamuli, R.P.; Song, H.M.; Fong, K.D.; Warren, S.M.; Salim, A.; Carano, R.A.; Filvaroff, E.H.; Longaker, M.T. Creation and characterization of a mouse model of mandibular distraction osteogenesis. Bone 2004, 34, 1004–1012. [CrossRef]
22. Benczik, M.; Gaffen, S.L. The interleukin (IL)-2 family cytokines: Survival and proliferation signaling pathways in T lymphocytes. Immunol. Investig. 2004, 33, 109–142. [CrossRef]
23. Kultz, D.; Li, J.; Gardell, A.; Sacchi, R. Quantitative molecular phenotyping of gill remodeling in a cichlid fish responding to salinity stress. Mol. Cell. Proteom. MCP 2013, 12, 3962–3975. [CrossRef]
24. Li, J.; Levitan, B.; Gomez-Jimenez, S.; Kultz, D. Development of a Gill Assay Library for Ecological Proteomics of Threespine Sticklebacks (Gasterosteus aculeatus). Mol. Cell. Proteom. MCP 2018, 17, 2146–2163. [CrossRef] [PubMed]
25. Root, L.; Campo, A.; MacNiven, L.; Con, P.; Cnaani, A.; Kultz, D. A data-independent acquisition (DIA) assay library for quantitation of environmental effects on the kidney proteome of Oreochromis niloticus. Mol. Ecol. Resour. 2021, 21, 2486–2503. [CrossRef]
26. Graefe, S.B.; Mohiuddin, S.S. Biochemistry, Substance P. In StatPearls Copyright © 2022; StatPearls Publishing LLC.: Treasure Island, FL, USA, 2022.
27. Perkins, M.N.; Kelly, D. Induction of bradykinin B1 receptors in vivo in a model of ultra-violet irradiation-induced thermal hyperalgesia in the rat. Br. J. Pharmacol. 1993, 110, 1441–1444. [CrossRef] [PubMed]
28. Koumbadinga, G.A.; Désormeaux, A.; Adam, A.; Marceau, F. Effect of interferon- on inflammatory cytokine-induced bradykinin B1 receptor expression in human vascular cells. Eur. J. Pharmacol. 2010, 647, 117–125. [CrossRef]
29. Hall, J.M. Bradykinin receptors. Gen. Pharmacol. 1997, 28, 1–6. [CrossRef]
30. McCulloch, J.; Uddman, R.; Kingman, T.A.; Edvinsson, L. Calcitonin gene-related peptide: Functional role in cerebrovascular regulation. Proc. Natl. Acad. Sci. USA 1986, 83, 5731–5735. [CrossRef]
31. Brain, S.D.; Williams, T.J.; Tippins, J.R.; Morris, H.R.; MacIntyre, I. Calcitonin gene-related peptide is a potent vasodilator. Nature 1985, 313, 54–56. [CrossRef] [PubMed]
32. Chromek, M.; Slamová, Z.; Bergman, P.; Kovács, L.; Podracká, L.; Ehrén, I.; Hökfelt, T.; Gudmundsson, G.H.; Gallo, R.L.; Agerberth, B.; et al. The antimicrobial peptide cathelicidin protects the urinary tract against invasive bacterial infection. Nat. Med. 2006, 12, 636–641. [CrossRef]
33. Chen, M.; Bao, L.; Zhao, M.; Cao, J.; Zheng, H. Progress in Research on the Role of FGF in the Formation and Treatment of Corneal Neovascularization. Front. Pharmacol. 2020, 11, 111. [CrossRef]
34. Yun, Y.R.;Won, J.E.; Jeon, E.; Lee, S.; Kang,W.; Jo, H.; Jang, J.H.; Shin, U.S.; Kim, H.W. Fibroblast growth factors: Biology, function, and application for tissue regeneration. J. Tissue Eng. 2010, 2010, 218142. [CrossRef]
35. Ibrahim, A.; Soliman, M.; Kotb, S.; Ali, M.M. Evaluation of fish skin as a biological dressing for metacarpal wounds in donkeys. BMC Vet. Res. 2020, 16, 472. [CrossRef] [PubMed]
36. Hartwell, S.W. surgical wounds in human beings: A histologic study of healing with practical applications: I. Epithelial healing. Arch. Surg. 1929, 19, 835–847. [CrossRef]
37. Wang, X.; Ge, J.; Tredget, E.E.; Wu, Y. The mouse excisional wound splinting model, including applications for stem cell transplantation. Nat. Protoc. 2013, 8, 302–309. [CrossRef] [PubMed] J. Funct. Biomater. 2023, 14, 512 22 of 22

38. Dunn, L.; Prosser, H.C.; Tan, J.T.; Vanags, L.Z.; Ng, M.K.; Bursill, C.A. Murine model of wound healing. J. Vis. Exp. 2013, 75, e50265. [CrossRef]
39. Naldaiz-Gastesi, N.; Bahri, O.A.; López de Munain, A.; McCullagh, K.J.A.; Izeta, A. The panniculus carnosus muscle: Anevolutionary enigma at the intersection of distinct research fields. J. Anat. 2018, 233, 275–288. [CrossRef] [PubMed]
40. Seswandhana, R.; Anzhari, S.; Ghozali, A.; Dachlan, I.; Wirohadidjojo, Y.W.; Aryandono, T. A Modified Method To Create A Porcine Deep Dermal Burn Model. Ann. Burn. Fire Disasters 2021, 34, 187–191.
41. Jeschke, M.G.; Mlcak, R.P.; Finnerty, C.C.; Norbury,W.B.; Gauglitz, G.G.; Kulp, G.A.; Herndon, D.N. Burn size determines the inflammatory and hypermetabolic response. Crit. Care 2007, 11, R90. [CrossRef]
42. Jeschke, M.G.; Gauglitz, G.G.; Kulp, G.A.; Finnerty, C.C.; Williams, F.N.; Kraft, R.; Suman, O.E.; Mlcak, R.P.; Herndon, D.N. Long-term persistance of the pathophysiologic response to severe burn injury. PLoS ONE 2011, 6, e21245. [CrossRef]
43. Jeschke, M.G.; Chinkes, D.L.; Finnerty, C.C.; Kulp, G.; Suman, O.E.; Norbury, W.B.; Branski, L.K.; Gauglitz, G.G.; Mlcak, R.P.; Herndon, D.N. Pathophysiologic response to severe burn injury. Ann. Surg. 2008, 248, 387–401. [CrossRef]
44. Laggner, M.; Lingitz, M.T.; Copic, D.; Direder, M.; Klas, K.; Bormann, D.; Gugerell, A.; Moser, B.; Radtke, C.; Hacker, S.; et al. Severity of thermal burn injury is associated with systemic neutrophil activation. Sci. Rep. 2022, 12, 1654. [CrossRef]
45. Mulder, P.P.G.; Vlig, M.; Boekema, B.; Stoop, M.M.; Pijpe, A.; van Zuijlen, P.P.M.; de Jong, E.; van Cranenbroek, B.; Joosten, I.; Koenen, H.; et al. Persistent Systemic Inflammation in Patients With Severe Burn Injury Is Accompanied by Influx of Immature Neutrophils and Shifts in T Cell Subsets and Cytokine Profiles. Front. Immunol. 2020, 11, 621222. [CrossRef] [PubMed]
46. Kawasaki, T.; Nakamura, K.; Jeschke, M.G.; Kogiso, M.; Kobayashi, M.; Herndon, D.N.; Suzuki, F. Impaired ability of burn patient neutrophils to stimulate _-defensin production by keratinocytes. Immunol. Cell. Biol. 2012, 90, 796–801. [CrossRef]
47. Italiani, P.; Boraschi, D. From Monocytes to M1/M2 Macrophages: Phenotypical vs. Functional Differentiation. Front. Immunol. 2014, 5, 514. [CrossRef] [PubMed]
48. Panaro, M.A.; Brandonisio, O.; Acquafredda, A.; Sisto, M.; Mitolo, V. Evidences for iNOS expression and nitric oxide production in the human macrophages. Curr. Drug Targets Immune Endocr. Metabol. Disord. 2003, 3, 210–221. [CrossRef] [PubMed]
49. Bogdan, C. Regulation of lymphocytes by nitric oxide. Methods Mol. Biol. 2011, 677, 375–393. [CrossRef]
50. Guo, Y.; You, Y.; Lv, D.; Yan, J.; Shang, F.F.;Wang, X.; Zhang, C.; Fan, Q.; Luo, S. Inducible nitric oxide synthase contributes to insulin resistance and cardiac dysfunction after burn injury in mice. Life Sci. 2019, 239, 116912. [CrossRef]
51. Latimer, K.S. Duncan and Prasse's Veterinary Laboratory Medicine: Clinical Pathology; Wiley: Hoboken, NJ, USA, 2011.
52. Hettiaratchy, S.; Dziewulski, P. ABC of burns: Pathophysiology and types of burns. BMJ 2004, 328, 1427–1429. [CrossRef] [PubMed]
53. Tan, J.Q.; Zhang, H.H.; Lei, Z.J.; Ren, P.; Deng, C.; Li, X.Y.; Chen, S.Z. The roles of autophagy and apoptosis in burn wound progression in rats. Burns 2013, 39, 1551–1556. [CrossRef]
54. Poindexter, B.J.; Bhat, S.; Buja, L.M.; Bick, R.J.; Milner, S.M. Localization of antimicrobial peptides in normal and burned skin. Burns 2006, 32, 402–407. [CrossRef]
55. Kolar, S.S.; Baidouri, H.; Hanlon, S.; McDermott, A.M. Protective role of murine _-defensins 3 and 4 and cathelin-related antimicrobial peptide in Fusarium solani keratitis. Infect. Immun. 2013, 81, 2669–2677. [CrossRef]

56. Wixler, V. The role of FHL2 in wound healing and inflammation. Faseb. J. 2019, 33, 7799–7809. [CrossRef] [PubMed]
57. Gordts, S.C.; Muthuramu, I.; Amin, R.; Jacobs, F.; De Geest, B. The Impact of Lipoproteins on Wound Healing: Topical HDL Therapy Corrects Delayed Wound Healing in Apolipoprotein E Deficient Mice. Pharmaceuticals 2014, 7, 419–432. [CrossRef][PubMed]
58. Beck, W.H.; Adams, C.P.; Biglang-Awa, I.M.; Patel, A.B.; Vincent, H.; Haas-Stapleton, E.J.; Weers, P.M. Apolipoprotein A-I binding to anionic vesicles and lipopolysaccharides: Role for lysine residues in antimicrobial properties. Biochim. Biophys. Acta 2013, 1828, 1503–1510. [CrossRef] [PubMed]
59. Ontsuka, K.; Kotobuki, Y.; Shiraishi, H.; Serada, S.; Ohta, S.; Tanemura, A.; Yang, L.; Fujimoto, M.; Arima, K.; Suzuki, S.;et al. Periostin, a matricellular protein, accelerates cutaneous wound repair by activating dermal fibroblasts. Exp. Dermatol.2012, 21, 331–336. [CrossRef]
60. Evdokiou, A.; Kanisicak, O.; Gierek, S.; Barry, A.; Ivey, M.J.; Zhang, X.; Bodnar, R.J.; Satish, L. Characterization of Burn Eschar Pericytes. J. Clin. Med. 2020, 9, 606. [CrossRef] [PubMed]
61. Yin, H.L. Gelsolin: Calcium- and polyphosphoinositide-regulated actin-modulating protein. Bioessays 1987, 7, 176–179. [CrossRef]
62. Vaid, B.; Chopra, B.S.; Raut, S.; Sagar, A.; Badmalia, M.D.; Ashish; Khatri, N. Antioxidant and Wound Healing Property of Gelsolin in 3T3-L1 Cells. Oxid. Med. Cell Longev. 2020, 2020, 4045365. [CrossRef] [PubMed]
63. Xianhui, L.; Pinglian, L.; Xiaojuan,W.;Wei, C.; Yong, Y.; Feng, R.; Peng, S.; Gang, X. The association between plasma gelsolin level and prognosis of burn patients. Burn. J. Int. Soc. Burn. Inj. 2014, 40, 1552–1555. [CrossRef]